Alma Mater Studiorum - Università di Bologna

DOTTORATO DI RICERCA IN

INGEGNERIA CIVILE, CHIMICA, AMBIENTALE E DEI MATERIALI

Ciclo 34

Settore Concorsuale: 08/A3 - INFRASTRUTTURE E SISTEMI DI TRASPORTO, ESTIMO E VALUTAZIONE

Settore Scientifico Disciplinare: ICAR/04 - STRADE, FERROVIE ED AEROPORTI

WASTE MINERAL FILLER RECYCLING IN NEW PAVEMENT SOLUTIONS

Presentata da: Abbas Solouki

Coordinatore Dottorato

Alessandro Tugnoli

Supervisore

Riccardo Lamperti

Co-supervisore

Cesare Sangiorgi

Esame finale anno 2022

DECLARATION

The content of the thesis is the result of work which has been carried out as part of the Horizon 2020 – Marie Skłodowska-Curie Actions – ITN project "SAFERUP! - Sustainable, Accessible, Safe, Resilient and Smart Urban Pavements".

To Maryam

تقدیم به همسر عزیزم، مریم

You are a treasure if the gems are your aim
No more than a grain if a loaf is your claim!
-

Recall this secret, when you play this game:
Whatever you pursued, is what you became!

Rumi (13th Century-Persian Poet)-Translation: Maryam Dilmaghani

در طلب گوهر کانی کانی – تا در هوس لقمهٔ نانی نانی

این نکتهٔ رمز اگر بدانی دانی – هر چیزی که در جستن آنی آنی

مولانا

ACKNOWLEDGEMENT

ABSTRACT

With a rapid increase in construction of roads, buildings and infrastructures the demand for aggregates has substantially increased. These natural materials are mainly obtained from riverbeds, local quarries and mines. Recycling of waste material has been considered as a good solution, where researchers have applied different types of solid waste for construction purposes. Società Azionaria Prodotti Asfaltico Bituminosi Affini (S.A.P.A.B.A. s.r.l.) is an asphalt/aggregate production plant located in Bologna, Italy. The aggregate plants mainly process and produce high quality limestone aggregates obtained from local quarries. The raw limestone aggregates are crushed, sieved, washed and stockpiled into different batches. The resulting dirt and mud from the washing process is stored at specific sedimentation lakes close to the plant. The materials filling up the sedimentation lakes are mainly silt and clay particles originating from the washed limestone aggregates. These kinds of materials, also referred to as waste mineral fillers or quarry dust have gained interest over the years and have been recycled in different civil engineering applications. The recycling of waste mineral fillers and quarry dust could help to reduce natural aggregate demand and improve the sustainability of aggregate production plant. Furthermore, the reuse of the by-products such as waste silt could convert the linear economy to a circular economy, where a second chance is given to by-products of hidden value. Moreover, due to limited capacity of SAPABA's sedimentation lakes, it is critical to seek and implement practical waste management and recycling techniques to promote sustainability. The initiative and motivation of the current research follows the 12th objective of the sustainable development goals, "responsible consumption and production", proposed by the United Nations. As a result, the overall aim of the current study was to reduce the impact of waste mineral fillers

through recycling in new paving solutions. Considering three paving types of cement-bound, geopolymer-bound and asphalt pavements the following objectives were set: 1) To investigate the possibility of recycling waste silt in cement-bound paving solution; 2) To explore the feasibility of producing geopolymer-bound paving solutions containing waste silt; 3) To study the potential of using waste silt as fillers in different asphalt pavements. The first objective was achieved by utilizing waste silt into cement-bound materials. For this purpose, the by-product was introduced to cement mortars and was partially replaced (20%) with the natural sand. The silt was further used to produce concrete paving blocks and were characterized according to the EN 1338 standard. Different Design of Experiments (DOE) approaches were used to optimize the mixture design of the cement mortars and concrete paving blocks. The second objective was pursued by studying the feasibility of using the waste silt as a filler in geopolymer cement products. The data on geopolymer cements produced with waste mineral filler were thoroughly summarized and indicated the need of thermal treatment of the waste silt. Thus, A DOE was produced, and the optimum calcination conditions of the waste silt was obtained. Geopolymer cement mixtures were made with sodium or potassium alkali solutions and were tested for compressive strength and leaching. Higher calcination temperatures showed better compressive strength, regardless of liquid type. By considering the compressive strength, leaching, and X-ray diffraction (XRD) analysis, the optimum calcination temperature and time was selected as 750 °C for 2 h. Having determined the optimum calcination condition, geopolymer-based paving blocks were designed and produced. Initially, Geopolymer cement was produced and its mechanical, thermal and microstructure properties were investigated. The thermogravimetric analysis indicated a phase change for the geopolymer samples

at 750 °C. The Scanning Electron Microscopy imaging confirmed the formation of the geopolymer structure. The geopolymer cement was mixed with predefined proportion of sand and gravel to produce geopolymer concrete paving blocks. The physical and mechanical properties of the final prototype bricks were investigated following the EN 1338 standard. The third objective was achieved by evaluating the rheological and mechanical performance of hot mix, porous and semi-flexible asphalt containing waste silt. The limestone filler of a hot mix asphalt was replaced with thermally and untreated waste silt. The rheological properties were studied using frequency sweep and Multiple Stress Creep Recovery (MSCR) tests, whereas the mechanical characteristics were investigated by means of Marshall stability, air voids content, and Indirect Tensile Strength (ITS) tests. Samples produced with thermally treated silt showed to have the highest stiffness compared to the other samples and demonstrated similar behavior to the control sample in terms of rheological properties. The results indicated that the 100% substitution of common filler with thermally treated waste silt does not have any adverse effect on the performance of HMA and their mastic. In this regard, an additional study was conducted, and a porous asphalt skeleton was grouted with a geopolymer cement containing waste silt. A control sample was also produced and was grouted with a cement-based grouting material obtained from a local company. The mechanical properties of the final semi-flexible pavement were compared. Regardless of mixture type, both semi-flexible pavements fulfilled the suggested mechanical performance requirements by the Italian specifications. To sum up, different paving blocks and asphalt pavements mixtures containing waste silt were proposed that presented acceptable performance when compared to different national and European standards.

TABLE OF CONTENTS

LIST OF FIGURES

LIST OF TABLES

Chapter 1: Introduction

1.1 General background

With a rapid increase in construction of roads, buildings and infrastructures the demand for aggregates has substantially increased [1]. These natural materials are mainly obtained from riverbeds, local quarries and mines and as all natural supplies are limited. Considering sustainability as a critical design parameter, engineers, stakeholders and policy makers have sought for alternative materials and approaches. Recycling of waste material has been considered as a good solution, where researchers have applied different types of solid waste for construction purposes. For instance, construction and demolition (C&D) waste has been successfully used in the production of asphalt pavements [2–4], concrete [5,6] and geopolymers [7,8]. Several different types of waste materials have been considered as a replacement for natural aggregates such as crumb rubber tire [9], artificial aggregates [10], ceramic waste [11], etc.

During the aggregate production, the materials are crushed using different mechanical crushers depending on the type and size of the aggregates. The crushed materials are then sieved and screened to meet consumers requirements. The final stage and before stockpiling of the stones and aggregates, the materials are washed, and unwanted soil and dirt is removed. The dirt is separated from the used water in special precipitation tanks and the unwanted material is then pumped out into sedimentation lakes located close to the aggregate plants. The stored material in the sedimentation lakes is directly related to the type of the mineral processed at the plants. These materials, also referred to as waste mineral

fillers or quarry dust have gained interest over the years and have been recycled in different civil engineering applications.

Waste mineral fillers have been used in cement-bound materials to produce cement mortar and concrete cement [12]. This sustainable approach could reduce the adverse impact of the waste material on the environment. For instance, waste materials produced from manufactured sand units were used in different percentages ranging from 0 to 60% to produce concrete building blocks [12]. The results indicated that the substitution of 30% of the sand with quarry dust improved different parameters of the concrete blocks including Abrasion resistance, acoustic absorption and sorptivity properties. In a different approach, recycled marine sediments were used to produce concrete paving blocks [13]. The ingredients used consisted of silt (74%), lime, glass powder and cement. The preliminary results showed promising, and the authors suggested that the blocks could be used as building materials.

Geopolymer consist of two different parts, the highly reactive precursor rich in Al and Si and a sodium or potassium-based alkali solution. When mixed, a 3D network of Si-O-Al is formed presenting several properties such as high compressive strength, durability, heat and fire resistance, etc. [14]. The literature available regarding the application of quarry dust and waste mineral fillers in geopolymer cement and binder is moderate [15,16]. For instance, lightweight aggregates were produced from waste silt and oil palm fuel ash [17]. The materials were mixed with a sodium-based alkali solution resulting in geopolymer cement. The results indicated high crushing value for samples produced with 60% of silt. Loose silty soil was stabilized using fly-ash geopolymer containing recycled concrete aggregates. Various mechanical

properties such as compressive strength, resilient modulus and indirect tensile strength of the geopolymer stabilized silt was compared to those stabilized with ordinary Portland cement. The authors stated that higher mechanical properties were reported for geopolymer stabilized samples [18].

In addition to concrete and geopolymers, quarry dust and waste fillers have also been used in asphalt pavements. Waste lime was substituted with conventional asphalt fillers at different ratios of 25 to 100% and various engineering properties such as Marshall stability, resilient modulus and indirect tensile strength of the asphalt pavement specimens were evaluated [18]. The results indicated higher moisture damage resistance when compared to samples produced with convenient fillers. By considering the results of several tests, the authors concluded the possibility of using waste lime as filler in asphalt pavements. Another study evaluated the effect of several quarry dusts and by-products on various mechanical properties of asphalt pavements [18]. The by-products were used as filler in the pavement. The results indicated that when blast furnace slag or recycled concrete were used, superior results were obtained. It was also stated that mixing quarry dust with cement could reduce the hydrophilic characteristics of the fillers.

1.2 Problem identification

Società Azionaria Prodotti Asfaltico Bituminosi Affini (S.A.P.A.B.A. s.r.l.) is an asphalt/aggregate production plant located in Bologna, Italy. The aggregate plants mainly process and produce high quality limestone aggregates obtained from local quarries. The raw limestone aggregates are crushed, sieved, washed and stockpiled into different batches. The resulting dirt and mud from the washing process is stored at specific sedimentation lakes close to the plant. The

materials filling up the sedimentation lakes are mainly silt and clay particles originating from the washed limestone aggregates. Figure 1.1 illustrates the geographical location of S.A.P.A.B.A. and its sedimentation lakes (a and b).
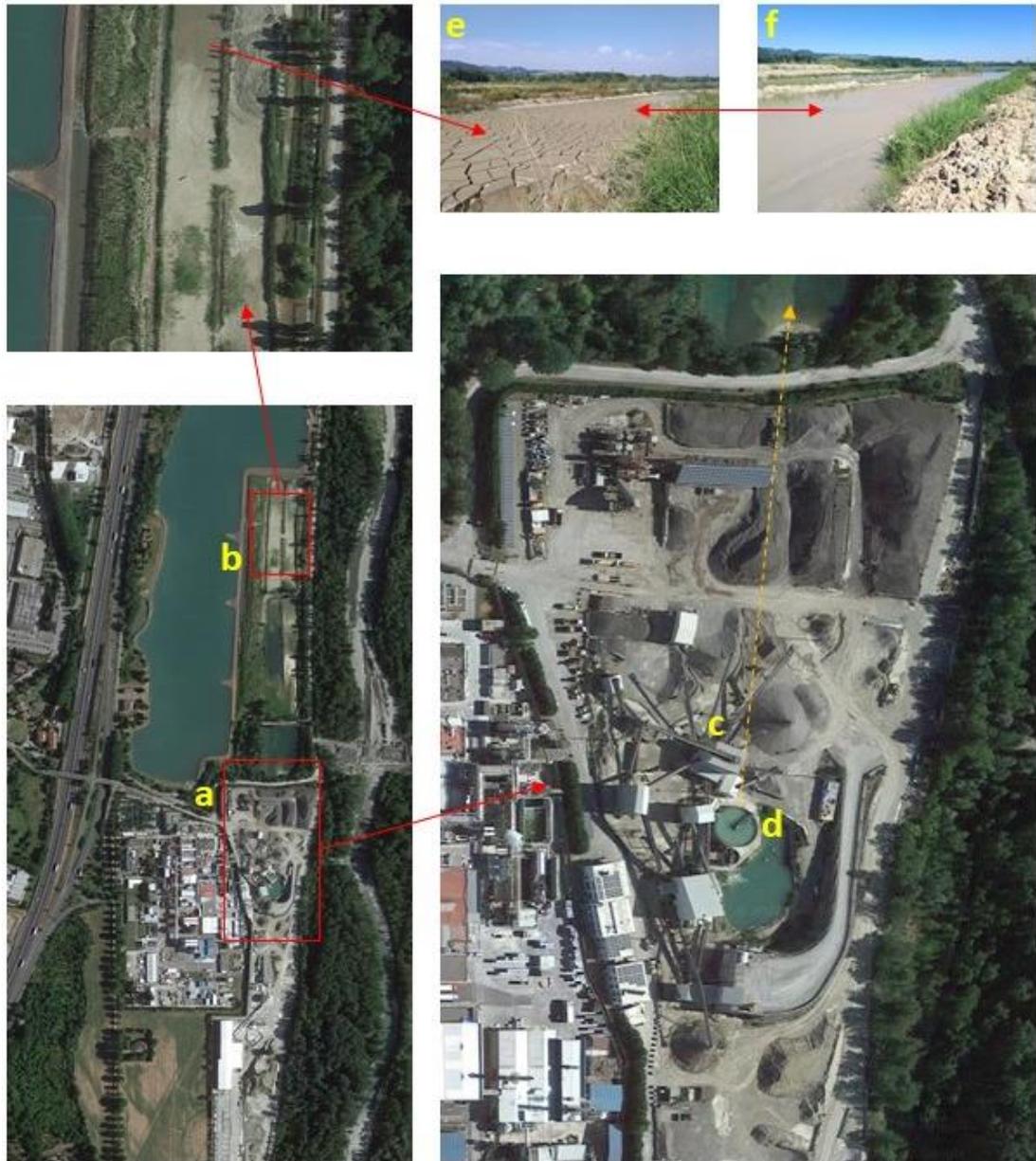
Figure 1.1. S.A.P.A.B.A. aggregate production plant, Bologna, Italy. Aggregate plant, a; sedimentation lakes, b; aggregate plant, c; precipitation tank, d; sedimentation lakes at different filling stages, e and f.

In summary, the raw limestone is processed at the plants (c), and the silt and dirt collected at the bottom of the precipitation tank (d) is pumped out towards the sedimentation lakes indicated by the orange dashed line. There are a total of three sedimentation lakes present at the company's site, which are flooded with the waste materials consecutively (e and f).

The recycling of waste mineral fillers and quarry dust could help to reduce natural aggregate demand and improve the sustainability of aggregate production plant. Furthermore, the reuse of the by-products such as waste silt could convert the linear economy to a circular economy, where a second chance is given to by-products of hidden value. Moreover, due to limited capacity of SAPABA's sedimentation lakes, it is critical to seek and implement practical waste management and recycling techniques to promote sustainability.

1.3 Waste silt

The limestone aggregates are usually obtained from local quarries and are crushed, washed and processed by the company's aggregate production facility. The waste silt used for the current project was obtained from the sedimentation lakes (Figure 1.2). The raw material was extracted and stored in small stockpiles allowing the excess water to evaporate. The unwanted material such as crushed stones, wood, plant roots, etc. were separated from the stockpile. The samples were then oven dried at 120 °C for 48 hours, crushed using a Los Angeles machine. The silt was stored in a dry place for further use.

Figure 1.2. Obtained silt from sedimentation lakes. During aggregate production (A) the produced silt is pumped to the sedimentation lakes (B). The material is oven dried and finely crushed prior to final use (C).

The elemental and compound analysis of the waste silt was examined using X-ray fluorescence (XRF) (Shimadzu, Kyoto, Japan) and X-ray powder diffraction (XRD) (Rigaku, Tokyo, Japan), respectively. The raw silt, with a pH of 7.0, met all the requirements of the Italian legal limits regarding the amount of hazardous material (Table 1.1). The mineralogical evaluation revealed the presence of quartz (32%), calcite (28%), illite/micas (21%), and chlorite (5%), with traces of dolomite and feldspars (Figure 1.3).

Table 1.1. Chemical oxides present in waste silt.

Parameter	Value (%)
SiO_2	43.5
TiO_2	0.6
Al_2O_3	12.5
Fe_2O_3	6.1
MnO	0.2
CaO	15.8
Na_2O	1.0
K_2O	1.9
P_2O_5	0.1
MgO	3.0
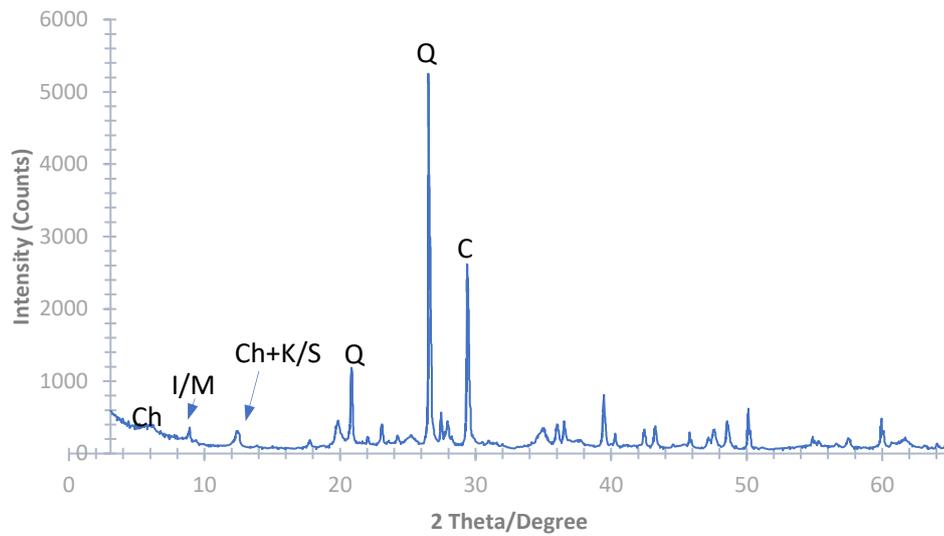
Figure 1.3. Waste silt XRD analysis reveals a crystalline structure observed as sharp peaks in the diagram. Q = quartz, I/M = illite–mica, Ch = chlorite, K/S = kaolinite/serpentine.

Chapters 2 to 8 have used the same raw silt. Thus, the provided engineering properties presented herein applies to all chapters.

1.4 Aims and objectives

The initiative and motivation of the current research follows the 12th objective of the Sustainable Development Goals, "responsible consumption and production", proposed by the United Nations, focusing on consumption and productions patterns which consider and ensure sustainability. As a result, the overall aim of the current study was to reduce the impact of waste mineral fillers through recycling it in new paving solutions. Considering three paving types of cement-bound, geopolymer-bound and asphalt pavements the following objectives were set.

- To investigate the possibility of recycling waste silt in cement-bound paving solution

- To explore the feasibility of producing geopolymer-bound paving solutions containing waste silt

- To study the potential of using waste silt as fillers in different asphalt pavements.

1.5 Significance of research

The current study aimed at proposing various recycling techniques and presented novel paving solutions that included waste silt. Moreover, the presented work is a case study dedicated to providing a circular economy for S.A.P.A.B.A. Accordingly, the significance of the research is as follows:

- Three different approaches of recycling waste silt have been proposed.

- Calcined silt was successfully used in geopolymer cement and demonstrated no environmental hazards according to Horizontal Dynamic Surface Leaching Test.

- Geopolymer paving blocks containing waste silt were produced.

- The inclusion of calcined silt in asphalt pavements were proposed for the first time.

- The capacity and potential of using geopolymer grouts containing waste silt has been investigated.

1.6 Organization of thesis

The current paper-based thesis consists of 9 chapters, which has been organized in 3 parts according to its context.

PART I consists of Chapters 2 and 3, where the feasibility of recycling the waste silt in cement-bound mixtures are discussed. Natural sand was partially replaced with the raw silt, where cement mortars and concrete paving blocks were produced.

PART II including Chapters 4, 5 and 6, focuses on the production and characterization of geopolymer cement/concrete produced with waste silt. The application of waste mineral fillers in geopolymers were reviewed. Afterwards, the mineralogical, mechanical and environmental properties of geopolymer cements containing silt were investigated. Having understood the behavior of the produced geopolymer, the final section examined the mechanical properties of geopolymer paving blocks according to EN 1338 standard.

PART III consisting of Chapters 7 and 8 investigates the potential of recycling waste silt into asphalt pavements. For this purpose, untreated and thermally treated silt were used as mineral fillers in Hot Mix Asphalt and porous asphalt samples. The second section demonstrated the potential application of geopolymer-based grouts for semi-flexible (grouted macadam) pavements.

Chapter 9 summarizes the overall findings of this study and discusses potential challenges and limitations of recycling waste silt.

PART I: CEMENT-BOUND

Part I, consisting of chapters 2 and 3, investigates the possibility of using waste silt in cement-bound materials.

The studies presented in this section have been published as follows:

1. Solouki, A.; Viscomi, G.; Tataranni, P.; Sangiorgi, C. Preliminary Evaluation of Cement Mortars Containing Waste Silt Optimized with the Design of Experiments Method. *Mater.* 2021, *14*.

2. Solouki, A.; Tataranni, P. Mixture Optimization of Concrete Paving Blocks Containing Waste Silt. 2022, 1–15.

A third paper titled "Strength Estimation of Cement Mortars Containing Waste Silt Using Machine Learning Techniques" (Danial Rezazadeh Eidgahee, Hashem Jahangir, Abbas Solouki[*], Cesare Sangiorgi, and Piergiorgio Tataranni) has been submitted. The paper further discussed the possibility of optimizing concrete paving blocks mixture through Machine Learning Techniques. The paper is an outcome of the PhD research. However, it has not been included in the dissertation.

Chapter 2: Preliminary evaluation of cement mortars containing waste silt optimized with the Design of Experiments method

2.1 Introduction

The first step in every quarrying process starts with the stripping stage, where the unwanted materials are removed from the Earth's surface. Based on the quality and type of the rocks, up to three different crushing stages could be applied during aggregate production. At the final step, the crushed aggregates go through the washing and screening stage, which is vital for quality and gradation control of the materials. The water used during the washing process is directed to precipitation tanks for further processing. The resulting residues which mainly consist of dirt and very fine powdery substances are piped out into artificial lakes and ponds called tailing mines or sedimentation lakes. These materials, mostly mineral fillers from plant processes, could become an environmental issue due to the landfilling limitations and strict legislation on their disposal [19]. Every year, up to 3 billion tons of non-renewable natural aggregates are demanded worldwide by the construction sector [20] and approximately 623 million tons of waste (mining and quarrying) were produced in 2018 [1]. Global efforts have been made to reduce the number of virgin aggregates used for construction and infrastructure sectors. For instance, based on the revised waste framework directive in Europe recycling of at least 70% of construction and demolition waste materials by 2020 was obligatory for all member states [20]. Nonetheless, quarries must work at full capacity to keep up with the demand for raw materials. Therefore, quarry/mining waste management has become an important aspect

during the past decades and various methods have been proposed for reducing its impacts on the environment.

Quarry waste has been used in various applications such as geopolymer production [21], soil stabilization [22], pavements [23,24] and production of artificial aggregates [25]. Studies and experimental applications have also highlighted the possibility of using quarry waste in cementitious materials. For instance, Cavaleri et al. (2018) partially substituted sand with quarry dust to produce concrete. The results indicated that the substitution of 13% of sand with limestone quarry dust could improve the mechanistic properties of the cement, whereas 26% of quarry dust led to lower mechanical properties [26]. The inclusion of quarry dust in cement bound materials and its effect on various properties of cement such as transport, dimensional stability, alkali–silica reaction, the heat of hydration and color were investigated. Medina et al. [27] found no adverse effects from the addition of quarry dust into the mixture and suggested its use in the design of new type II/A conventional as well as type II/A special low heat cement. These alternative applications could potentially reduce the environmental impact of using raw materials and of course decrease the impact of landfilling industrial waste fillers. Felekoglu (2007) incorporated quarry dust limestone powder in Self-Compacting Concrete (SCC) and paste applications with the aim of reducing the environmental impact of the waste quarry powder [28]. Various physical and mechanical properties of the cement paste were examined, and the performance of the mixture indicated the possibility of using up to 10% of limestone quarry dust in normal-strength self-compacting cement. Similar work on self-compacting concrete was carried on by Uysal et al. [29], where Portland cement was partially replaced with different quarry dust including limestone, basalt, and marble. The results were similar to

previous studies which suggested the economic feasibility of using the mentioned powders in SCC production [28,29]. In a different attempt to manage mine waste, a study was conducted aiming to investigate the possibility of using gold waste rocks as construction materials [30]. The waste materials were collected from an open-mine site located in the Abitibi-Temiscamingue region (QC, Quebec, Canada) and the material was used for concrete production. The obtained compressive strength for concretes made with waste rocks and natural sand and gravel were comparable after 28 and 56 days of curing [30]. In a separate study, limestone dust was substituted by 30% of the total concrete weight to produce lightweight concrete. The mechanical properties of the synthetic material were tested and the result showed acceptable performance [31]. However, the authors indicated that further work and tests regarding the mechanical properties of the lightweight concrete are required.

Concrete and mortars are produced using different design methods. For instance, various common approaches have been reviewed for the production of self-compacting cement [32]. The mixture could be designed based on empirical methods. Compressive strength or rheological properties of the paste could also determine the mixture design. However, an approach that has not been fully exploited is the use of statistical models for concrete mixture design. For instance, the effect of different ingredients such as glass fiber, metakaolin (MK), paste and silica sand on the flexural and compressive strength of glass fiber (GF)-reinforced concrete (GRC) was studied [33]. The authors also applied the Taguchi method to optimize the final mix design based on four factors including aggregate (SS)-to-cement ratio (A/C), GF, W/C and MK contents. The data indicated that SS, MK, GF and CP contents significantly affected the final strength of the concrete mixtures. However, most statistical approaches are

limited to factorial designs [34,35] and response surface methods [36,37] and less attention has been paid to mixture-design of experiments methods. It is by the use of a mixture-design approach that one could simultaneously study the effects of all the components and their interactions. The effect of including fly ash (FA), nano-silica (nS), and recycled plastic on the mechanical properties and cost of concrete was investigated by applying two different mixture design approaches [38]. The first model was produced from a screening model and the results were then used as an input for the sequential optimization. Based on the models, the authors suggested that by adding 2.5% of nS and 10% of FA about 44% of coarse aggregates could be substituted by plastic. A simple lattice mixture design having three factors and five levels was applied to study the effect of three different sand types on self-compacting cement properties [39]. The models indicated an increase in compressive strength with an increase in crushed sand proportions. However, when dune sand was used, the resulting strength values dropped.

Transforming quarry dust/waste into secondary materials could give a second chance to waste materials, contribute to waste management, balance natural resource utilization and produce a circular economy for the construction sector [40–43]. Thus, the current research focused on producing cement mortars by substituting natural sand with the waste silt obtained from limestone aggregate production S.A.P.A.B.A. s.r.l. (Pontecchio Marconi, Italy).

2.2 Materials

Waste silt and natural limestone sand (0–4 mm) were used to produce cement mortars. The raw silt was obtained from S.A.P.A.B.A. Please refer to section 1.3 for further details. The gradation curve of the sand is shown in Figure 2.1. The obtained values for bulk density (g/cm3) (UNI 1097-6), sand equivalent (uni 933-

8) and harmful fines (gMB/KG) (UNI 933-9) were reported as 2.658, 90 and 0.5, respectively. The light organic impurities were reported as 0.07 which was well below the 0.5 limits. Finally, a 42.5 R white Portland cement (Buzzi Unicem, Casale Monferrato, Italy) and a specially designed additive that allows the use of swelling clays or aggregates with very high fines were used.
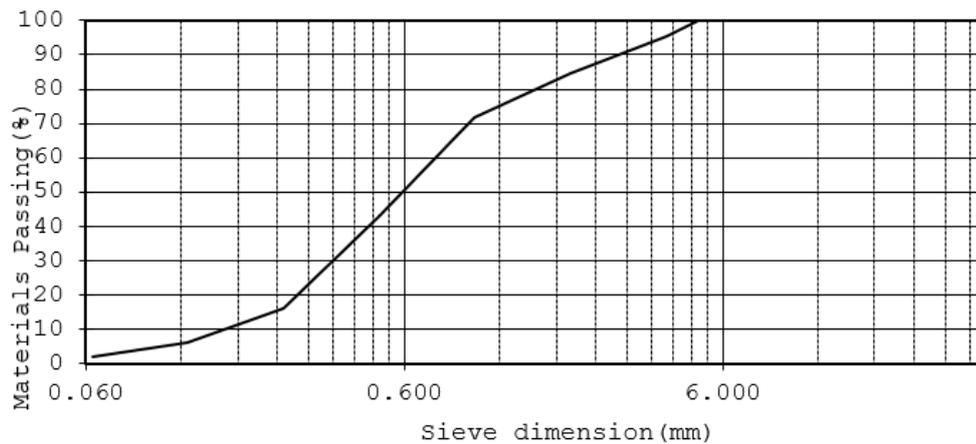
Figure 2.1. Limestone sand gradation curve.

2.3 Methods

2.3.1 Design of Experiments

As for the first step in any Design of Experiments (DOE), the purpose of the experiment should be determined. In some cases, optimization of a process or response(s) is the main goal, whereas in some studies the effect of certain factors and their levels on the outcome is the focus. Therefore, each experiment and DOE will have a specific purpose and need to be tackled differently. The boundaries of an experiment are defined and restrained based on selected ranges of the variables. For instance, selecting a testing temperature between 20 to 80 °C for a specific experiment will define its experimental region. The design will be finalized by determining the number of levels for the corresponding factors.

A Response Surface Methodology (RSM) [44] is a statistical tool, which investigates the relationship between variables of an experiment with the produced outcomes. Compared to a full factorial design, RSM can significantly reduce the number of required experimental runs. In many studies, the aim is to select the ingredient's proportion of a blend. In such cases, the implementation of a mixture design (a special type of RSM) could effectively determine the dependent variables' proportions that will produce the desired response. In a mixture design experiment, the dependent factors are proportions of different components of a blend and the total sum of all factors for each run will be equal to 1 or 100% (Equation (1)). The mixture DOE allows studying the effects of different ingredients/factors on different responses such as compressive and flexural strength of the mortar specimens. However, in such cases, applying standard design will require a higher number of experiments to find the final mix design. An n-component mixture is presented in Equation (1).

$$0 \leq x_i \leq 1 \quad i = 1, 2, 3, \dots, n \quad \sum_{i=1}^{n} x_i = 1 \quad \text{Equation (1)}$$

where the proportion of the ith ingredient/factor is represented by xi.

Two of the most widely used mixture designs are the simplex lattice and simplex centroid designs. The former design is applied when the components/ingredients are equally spaced within the design. Furthermore, in such cases, a full cubic analysis could be applied. However, only special cubic estimates could be conducted for centroid design. In both cases, no constraints or boundary limits are set. On the other hand, an extreme vertex design could only be used when linear or boundary constraints are set for the components. In such cases, the mixture design will only cover a small proportion within the simplex design and usually occurs when components have upper and lower boundaries.

Each DOE has its specific requirements and inputs. For the current study, a mixture DOE having 5 different components including cement, water, sand, silt and additive was proposed. Due to the high number of factors, the extreme vertices design was used rather than the simplex centroid design. Extreme vertices design only covers small spaces in the simplex design and could be adapted when the design space is not linear. However, not much literature has been found regarding extreme vertices design for cement bound materials [33,38].

To produce the mixture DOE, the five components and their corresponding boundaries were inputted into JMP® software. The determined upper and lower boundaries (total weight of mixture) for cement, water, sand, silt and additive were as 22–28%, 12–20%, 43–61%, 2–20% and 0.17–0.35%, respectively. As mentioned above extreme vertices design was selected. Consequently, a DOE having 49 randomized runs was produced, where for each run 3 specimens from the same batch were produced. The average value for the corresponding strength (compressive or flexural) was used as inputs to produce the models. Therefore, after inputting the flexural strength (FS) and Unconfined Compressive Strength (UCS) values in the DOE, two corresponding models were produced. The data analysis was also carried out in JMP® software (Version 14.0. SAS Institute Inc., Cary, NC, 1989-2019). Up to five levels of interactions were chosen and the forward selection with Akaike Information Criteria (AIC) was applied to determine the significance of the models. The model was produced, and the optimum results were indicated using the prediction profiler tool for both compressive and flexural strength measurements. The desirability factor was based on the maximum usage of silt in the mixture. Therefore, the value of the

silt was set to 20% and the corresponding values for the remaining components were calculated according to the obtained models.

2.3.2 Sample Preparation

The samples were prepared by mixing Cement, sand and silt before adding water and the additive (Figure 2.2). The mortar was poured into metal molds ($4 \times 4 \times 16$ cm) and was cured at room temperature for 28 days. The samples were first tested for flexural strength resulting in each beam to be broken into half. Each half was then tested for compressive strength. The whole procedure was based on EN 1015-11:2019 (E) standard.
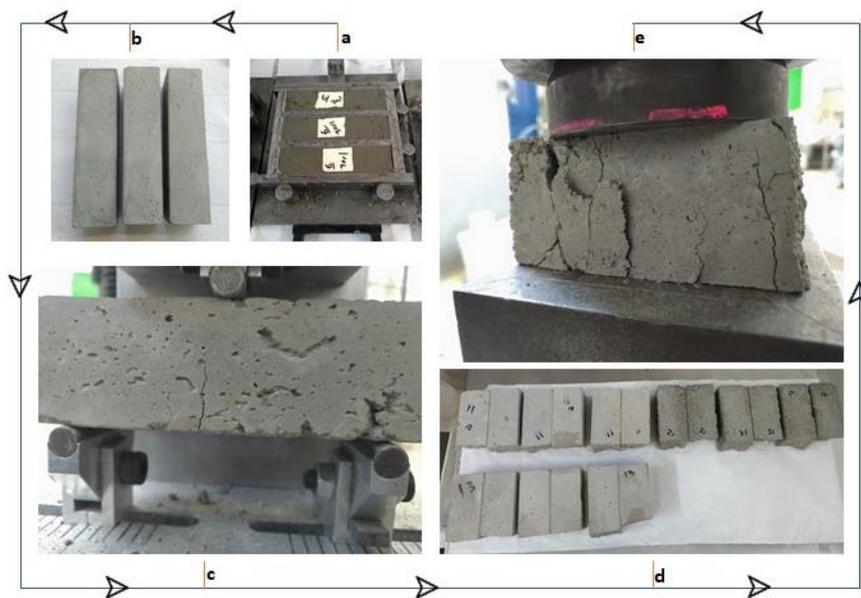
Figure 2.2. Cement mortar sample production and strength (flexural and compressive) testing procedure.

The overall workflow for cement mortar production is shown in Figure 2.3.
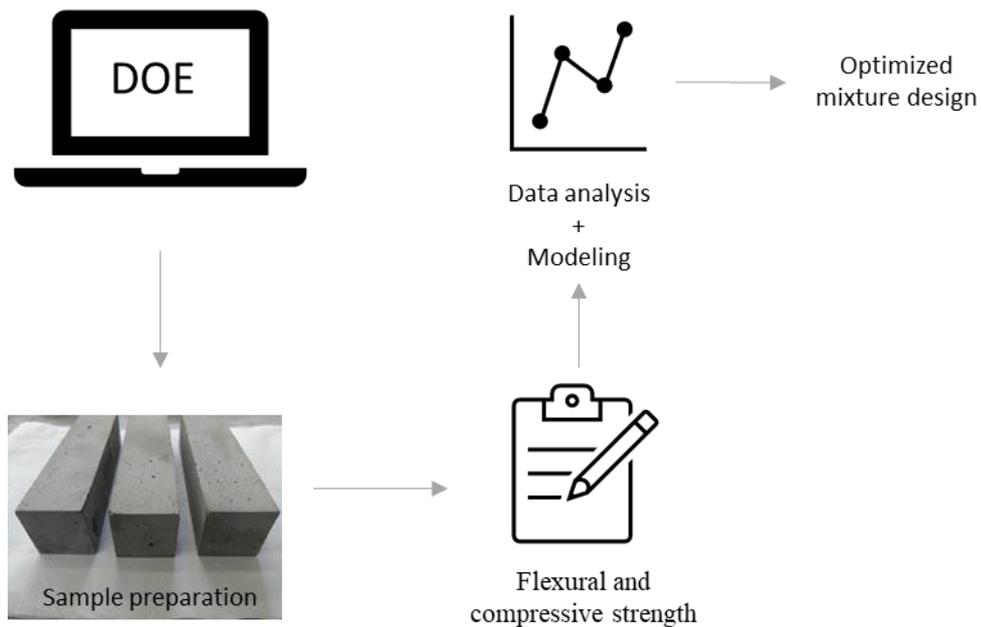
Figure 2.3. Flow chart for cement mortar production.

2.4 Results and Discussion

An efficient way of studying a mixture in which all components sum to 1 (100%) is to use the mixture design approach. With this method, the changes in the ingredients of a mixture or blend and the resulting effects on the responses could be explored. Thus, by applying the mixture design concept, the effect of cement, water, sand, silt and the additive on the responses including compressive and flexural strength were investigated.

The initial model was constructed based on 49 randomized runs. The order of the tests was randomized to reduce the chance of bias in the results that could have occurred due to differences in materials or experimental conditions. However, to improve the accuracy of the models and based on the residual plots, a total of 10 runs were identified as outliers and were eliminated from the model [45].

Consequently, the second attempt improved the overall accuracy of the models up to 20%. The summary of fit and the residual plots for the models are presented in Table 2.1 and Table 2.2 and Figure 2.4 and Figure 2.5. The results indicated an R2 value of 95.5 and 91.2% for the models related to UCS and FS, respectively.

Table 2.1. Summary of fit. Effect of components on Unconfined Compressive Strength (UCS).

Indicator	Value
R Square	0.955208
R Square Adj	0.925996
Root Mean Square Error	3.106147
Mean of Response	25.78675
Observations (or Sum Wgts)	39

Table 2.2. Summary of fit. Effect of components on flexural strength.

Indicator	Value
R Square	0.911509
R Square Adj	0.879905
Root Mean Square Error	0.795718
Mean of Response	5.679888
Observations (or Sum Wgts)	39
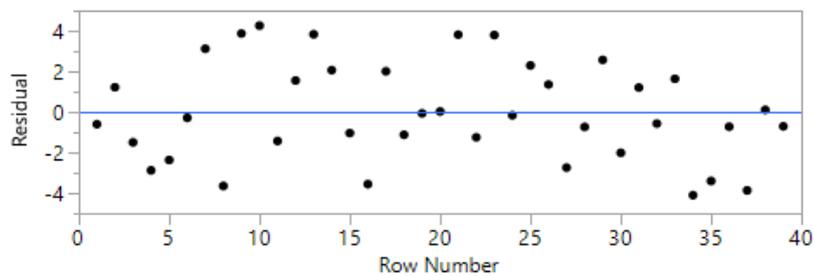
Figure 2.4. Residual plot for UCS model.
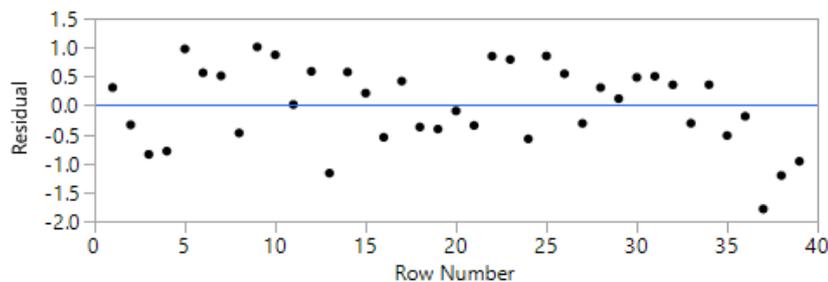
Figure 2.5. Residual plot for the flexural strength model.

The design of experiments consisting of 39 randomized runs is presented in Table 2.3. The flexural and UCS were inputted into the DOE resulting in a model (equation). For each of the 39 runs, the obtained model was used to calculate the FS and UCS, which are also included in the table as predicted FS and predicted UCS. The actual versus the predicted values for flexural and UCS are also depicted in Figure 2.6, where the blue line indicates the average value for both UCS and FS. The graphs indicate a linear relationship between actual and predicted values which is also backed up by the high reliability of the models (R^2). The calculated models for UCS and FS are presented as supplementary data.
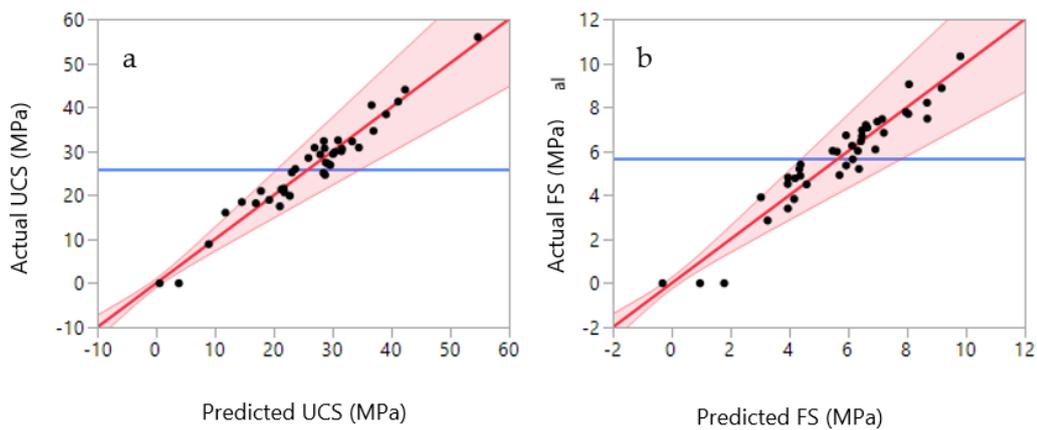
Figure 2.6. Actual versus predicted values for: (a) compressive; (b) flexural strength.

Table 2.3. Design of experiments data.

	Cement (%)	Water (%)	Sand (%)	Silt (%)	Additive (%)	FS (MPa)	UCS (MPa)	Pred. FS (MPa)	Pred. UCS (MPa)
1	22.00	20.00	55.65	2.00	0.35	0.00	0.00	−0.31	0.60
2	22.00	14.65	43.00	20.00	0.35	3.83	18.17	4.16	16.95
3	24.64	13.56	55.79	5.79	0.215	6.08	30.01	6.92	31.50
4	28.00	20.00	43.00	8.83	0.17	4.91	19.86	5.70	22.73
5	24.83	12.00	61.00	2.00	0.17	9.04	34.59	8.06	36.96
6	22.00	14.83	43.00	20.00	0.17	4.51	18.94	3.94	19.23
7	22.00	12.00	45.65	20.00	0.35	4.88	20.95	4.37	17.83
8	22.00	12.00	61.00	4.65	0.35	8.20	30.82	8.68	34.47
9	28.00	20.00	43.00	8.65	0.35	5.39	18.45	4.38	14.57
10	28.00	20.00	49.83	2.00	0.17	3.91	16.05	3.03	11.78
11	23.23	13.56	48.21	14.79	0.215	6.45	27.41	6.43	28.84

	Cement (%)	Water (%)	Sand (%)	Silt (%)	Additive (%)	FS (MPa)	UCS (MPa)	Pred. FS (MPa)	Pred. UCS (MPa)
12	22.00	14.83	61.00	2.00	0.17	7.19	32.48	6.60	30.93
13	24.55	13.56	46.79	14.79	0.305	5.20	30.78	6.36	26.95
14	23.23	17.56	53.12	5.79	0.305	4.77	25.15	4.19	23.09
15	26.23	17.56	46.79	9.21	0.215	6.68	30.55	6.47	31.59
16	22.00	12.00	45.83	20.00	0.17	3.40	17.48	3.95	21.04
17	23.23	13.56	48.12	14.79	0.305	7.07	30.66	6.65	28.65
18	26.23	13.56	46.79	13.12	0.305	6.84	32.21	7.21	33.33
19	28.00	12.00	43.00	16.83	0.17	2.85	8.89	3.26	8.95
20	22.00	20.00	43.00	14.65	0.35	4.49	21.32	4.59	21.30
21	22.00	12.00	61.00	4.83	0.17	7.70	40.45	8.04	36.64
22	28.00	12.00	43.00	16.65	0.35	4.80	20.59	3.95	21.84
23	23.23	14.98	55.79	5.79	0.215	6.72	32.31	5.93	28.51
24	22.00	20.00	43.00	14.83	0.17	5.35	21.53	5.93	21.70
25	23.23	17.56	53.21	5.79	0.215	5.20	25.96	4.34	23.66
26	26.23	17.56	50.12	5.79	0.305	6.02	29.26	5.47	27.90
27	23.23	14.98	46.79	14.79	0.215	6.02	26.86	6.33	29.60
28	22.00	14.65	61.00	2.00	0.35	7.46	29.35	7.15	30.08
29	24.64	13.56	46.79	14.79	0.215	6.25	28.46	6.13	25.89
30	23.23	14.89	46.79	14.79	0.305	6.95	27.17	6.47	29.18
31	28.00	12.00	57.65	2.00	0.35	10.31	55.91	9.81	54.70
32	23.23	13.56	55.79	7.12	0.305	7.34	29.80	6.99	30.37
33	28.00	12.00	57.83	2.00	0.17	8.87	43.96	9.17	42.33
34	26.23	17.56	50.21	5.79	0.215	5.98	24.62	5.62	28.73
35	23.23	14.89	55.79	5.79	0.305	5.63	25.05	6.15	28.45
36	26.23	13.56	54.12	5.79	0.305	7.77	38.37	7.96	39.10
37	28.00	20.00	49.65	2.00	0.35	0.00	0.00	1.79	3.86
38	24.65	12.00	61.00	2.00	0.35	7.48	41.25	8.69	41.14
39	22.00	20.00	55.83	2.00	0.17	0.00	0.00	0.96	0.70

FS: flexural strength; UCS: unconfined compressive strength; pred flex: predicted values for flexural strength; pred UCS: predicted values for UCS.

2.4.1 Compressive Strength

The analysis of variance for the UCS predicted model is shown in Table 2.4. Based on the analysis, a change in the amounts of components (cement, water, sand, silt, additives) significantly ($p < 0.0001$) affects the compressive strength of the cement mortars. The t-ratio reported in Table 2.5 indicates the influence of each component on the resulting compressive strength values. Compared to other main components, the sand has the highest effect on UCS followed by cement and silt. Thus, the maximized value for the responses will be obtained by maximizing the sand component in the mixture. On the other hand, an increase in water amount could decrease the UCS value which is shown as a negative ratio of -1.63 in Table 2.5. The water and additive did not show a significant effect on

the compressive strength ($p \nleq 0.05$). However, despite their insignificance, the water and additive were not deleted from the model. It must be noted that components/ingredients could not be deleted in a mixture design process since the resulting mixture will be different than the initial one. For instance, if cement is removed from the mix, the resulting product will no longer be a cement mortar. It is also noteworthy to mention that the main components in Table 2.5 and Table 2.7 were coded as pseudo-components. This approach simplifies design construction and model fitting and makes parameter estimates more meaningful.

The relationship between silt, sand, cement, water and additives with compressive strength are shown in Figure 2.7. The highest value for compressive strength is only achieved when the silt amount is minimum (2%). However, the addition of 20% silt and 22% cement could produce mortars with approximately 20 MPa compressive strength (Figure 2.7a). The silt and sand showed a negative correlation, where a decrease in silt content increased the amount of sand in the mixture. In addition, an increase in sand content led to an increase in compressive strength (Figure 2.7b). The effect of sand and cement on the compressive strength is also shown in the ternary plots (Figure 2.8a), where an increase in sand and cement content increases the final compressive strength. The highest UCS values were observed when the sand ratio was between 56 to 58% of the total weight of the mortar. The interaction between silt and the additive was not as significant as the interactions between silt and other components. For instance, based on Figure 2.7c, in a few regions, the decrease or increase of additives did not dramatically affect the overall UCS. An increase in water content (12 to 20%) led to a decrease in the compressive strength of the samples (Figure 2.7d). This was also confirmed in Figure 2.8b and is a well-known phenomenon since an increase in water

content reduces the compaction rate of the cement/concrete mixtures leading to lower compressive strength.

Table 2.4. Analysis of variance for the UCS model.

Source	DF	Sum of Squares	Mean Square	F Ratio
Model	15	4732.2927	315.486	32.6991
Error	23	221.9074	9.648	Prob > F
U. Total	38	4954.2001	-	<.0001*

Table 2.5. Effect summary/parameter estimates for compressive strength values.

Term	Estimate	Std Error	t Ratio	Prob > |t|
(Cement-0.22)/0.2083	85.702806	17.88592	4.79	<0.0001 *
(Water-0.12)/0.2083	−62.6514	38.50179	−1.63	0.1173
(Sand-0.43)/0.2083	48.611973	4.193305	11.59	<0.0001 *
(Silt-0.02)/0.2083	9.0094789	3.948727	2.28	0.0321 *
(Additive-0.0017)/0.2083	−282.3226	278.2153	−1.01	0.3208
Cement * Water	−11.66381	88.82965	−0.13	0.8967
Water * Sand	−21.87772	67.99387	−0.32	0.7505
Water * Silt	169.97529	66.1488	2.57	0.0171 *
Sand * Silt	0.2183764	21.45658	0.01	0.9920
Cement * Additive	5901.5652	1620.775	3.64	0.0014 *
Water*Additive	808.67954	1254.483	0.64	0.5255
Cement * Sand * (Cement-Sand)	195.20254	62.03723	3.15	0.0045 *
Cement * Silt * (Cement-Silt)	254.78546	63.84024	3.99	0.0006 *
Water * Sand * Silt	409.27446	187.3776	2.18	0.0394 *
Sand * Silt * (Sand-Silt)	−77.41989	18.82222	−4.11	0.0004 *
Cement * Water * Additive	−23724.89	6424.449	−3.69	0.0012 *

Statistically significant parameters are indicated by *

One of the aims of conducting a DOE is to benefit from its optimization capabilities. During an optimization process, one could aim for maximizing or minimizing a certain response. Moreover, the optimization could be achieved by defining a certain range or limits. During the optimization process, it is also possible to select the best mixture based on a desirable dependent variable. For instance, the profiler option in JMP software was used and the amount of silt was set to 20%. As illustrated in Figure 2.9, a compressive strength of 22 MPa could be achieved when the mixture contains 22% cement, 13% water, 44 sand, 0.17% additive and 20% of silt. Decreasing the amount of silt to 16% could increase the compressive strength to 26 MPa. However, since the focus of the study was to

maximize the use of waste silt, the model was optimized based on the highest amount of silt in the mixture. The real mean values obtained for a different amount of silt is depicted in Figure 2.10, where the maximum strength was obtained when only 5% of waste silt was introduced into the mixture.
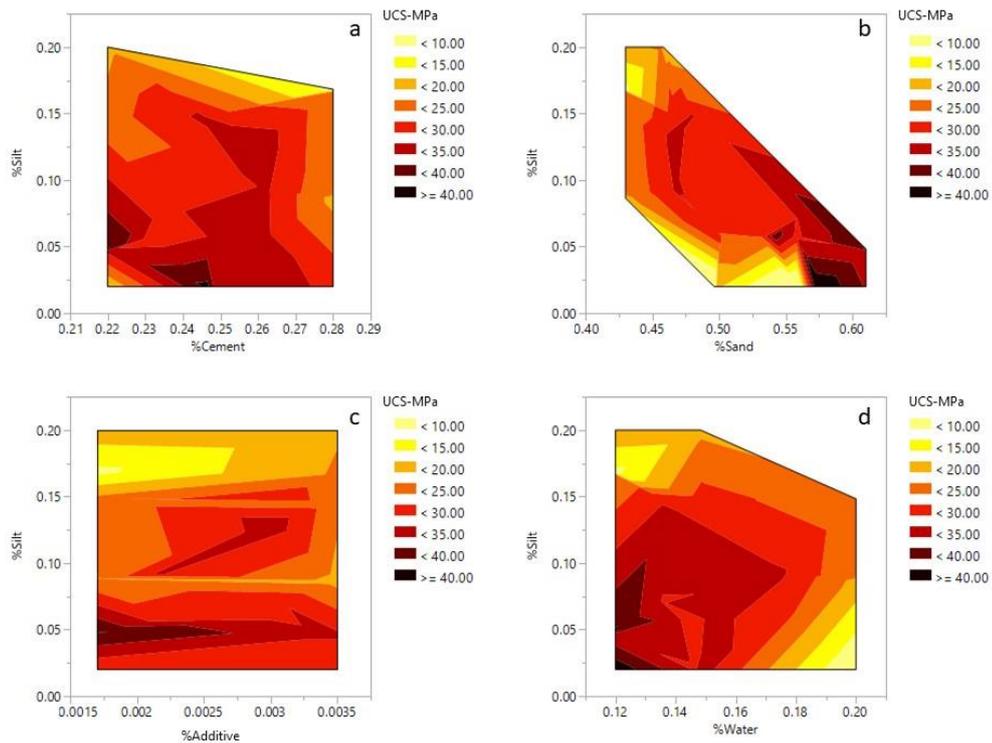
Figure 2.7. Contour plots for 28 days compressive strength: (a) silt–cement; (b) silt–sand; (c) silt–admixture; (d) silt–water.
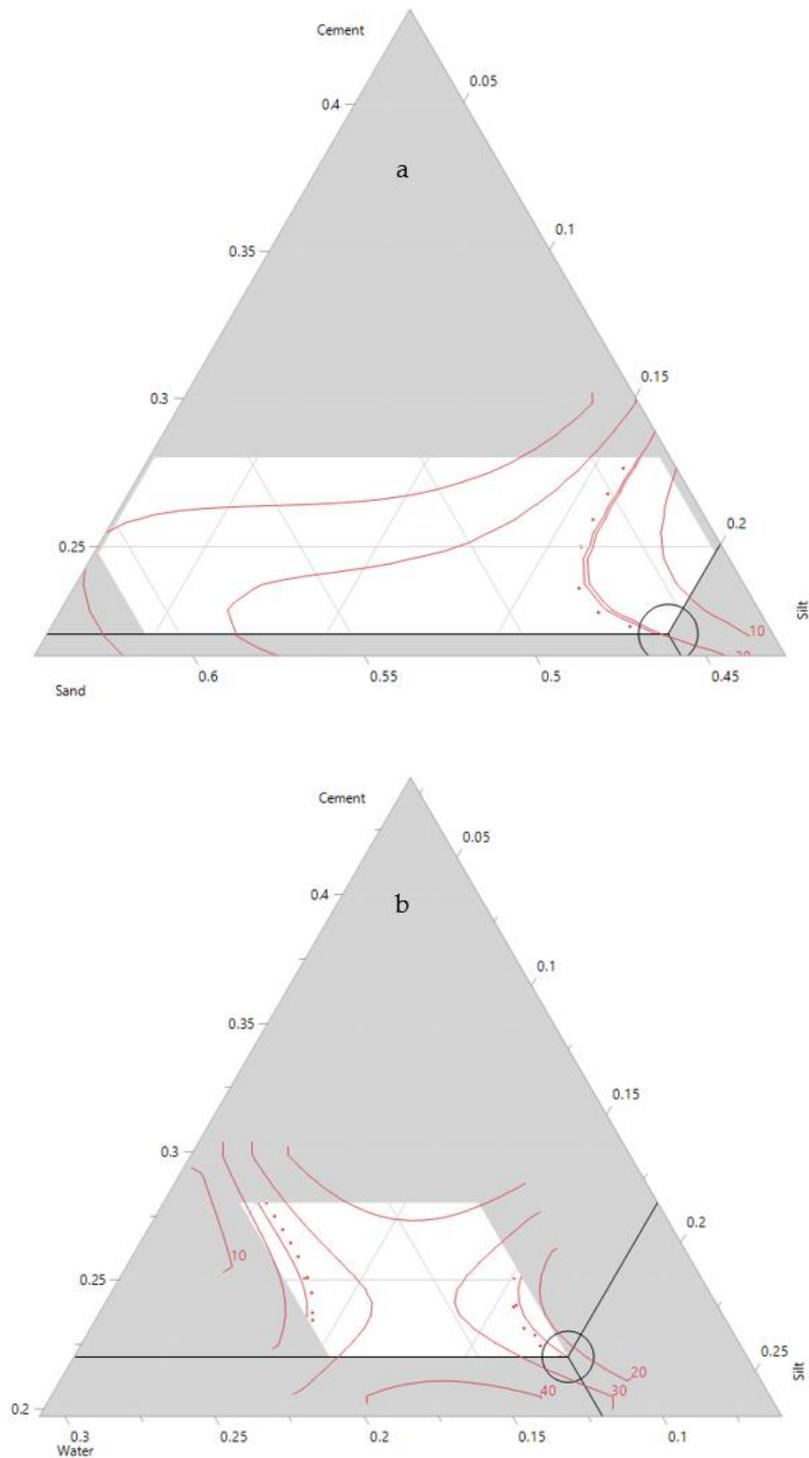
Figure 2.8. Ternary contour plots for 28 days compressive strength comparing component ratios: (a) cement–silt–sand; (b) cement–silt–water.
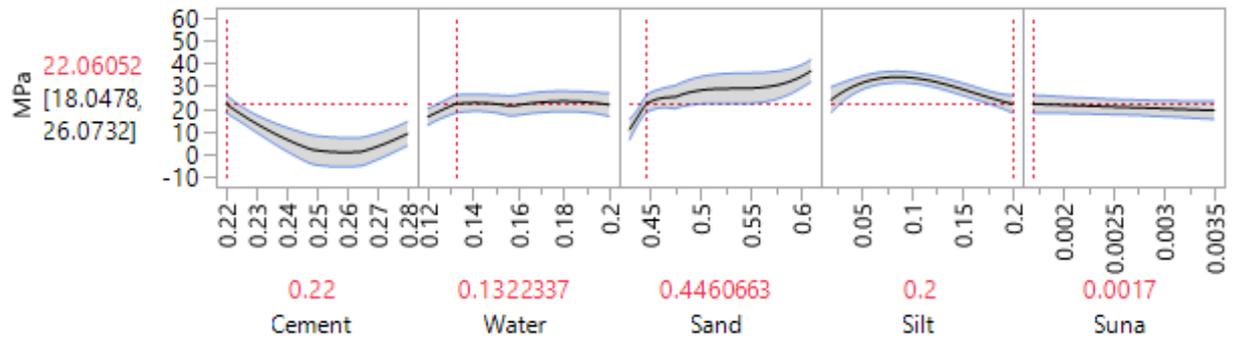
Figure 2.9. Optimization of 28 days compressive strength based on maximized silt content.
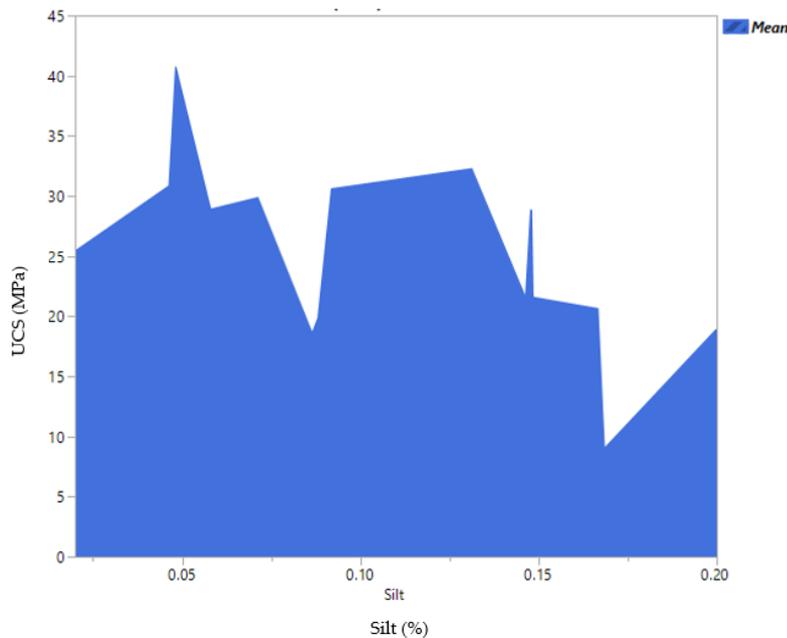
Figure 2.10. Mean values for 28 days UCS (MPa) versus silt content (%).

2.4.2 Flexural Strength

Based on the ANOVA analysis, a change in the components including cement, water, sand, silt and additive significantly affected the flexural strength of the cement mortars ($p < 0.0001$) (Table 2.6). The t-ratio reported in Table 2.7 indicates the influence of each component on the resulting flexural strength values. Compared to other main components, the sand has the highest effect on

27

the mechanical properties, followed by cement. Water had a high and negative

correlation with flexural strength. Silt and additive do not have a significant effect

on the final response. However, the interaction between water-silt is high and

comparable to the effect of sand. Thus, the maximized value for the response will

be obtained by maximizing the sand component in the mixture. As mentioned

before, despite their insignificance, the silt and additive could not be deleted from

the model because of the nature of the mixture design.

Table 2.6. Analysis of variance for flexural strength model.

Source	DF	Sum of Squares	Mean Square	F Ratio
Model	10	182.61511	18.2615	28.8415
Error	28	17.72870	0.6332	Prob > F
U. Total	38	200.34381	-	<.0001*

Table 2.7. Effect summary/parameter estimates for flexural strength values.

Term	Estimate	Std Error	t Ratio	Prob > |t|
(Cement-0.22)/0.2083	17.270749	1.904416	9.07	<0.0001 *
(Water-0.12)/0.2083	−13.02035	1.903995	−6.84	<0.0001 *
(Sand-0.43)/0.2083	9.6833449	0.748193	12.94	<0.0001 *
(Silt-0.02)/0.2083	0.5155091	0.79756	0.65	0.5233
(Additive-0.0017)/0.2083	73.118157	45.426	1.61	0.1187
Water * Silt	44.859904	4.34842	10.32	<0.0001 *
Sand * Silt	7.619343	2.810101	2.71	0.0113 *
Cement * Sand * (Cement-Sand)	31.001789	10.3192	3.00	0.0056 *
Cement * Silt * (Cement-Silt)	23.954223	10.01144	2.39	0.0237 *
Sand * Silt * (Sand-Silt)	−15.11265	4.698824	−3.22	0.0033 *
Water * Additive * (Water-Additive)	−1462.162	549.0786	−2.66	0.0127 *

Statistically significant parameters are indicated by *

The relationship between silt, sand, cement, water and additive with the flexural

strength are shown in Figure 2.11. Like the compressive strength, the highest

value for flexural strength is only achieved when the silt amount is set to a

minimum (2%). However, the addition of 20% silt and 22% cement could

produce mortars withstanding approximately 4.0 MPa of flexural strength

(Figure 2.11a).
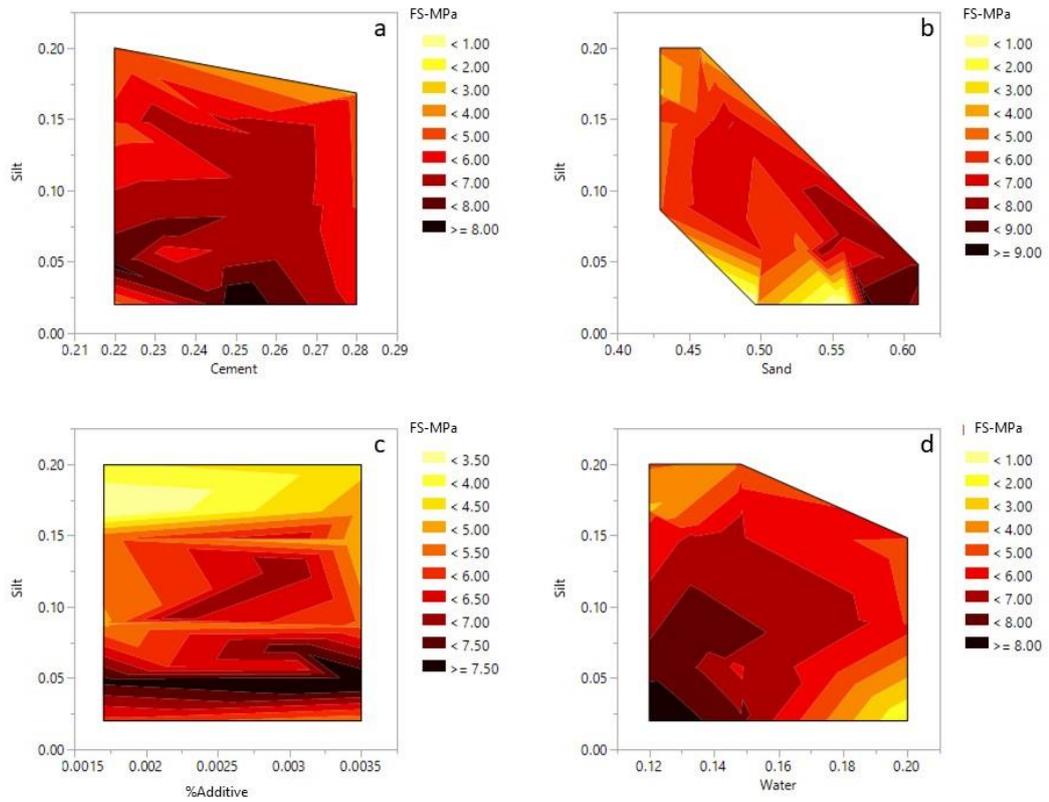
Figure 2.11. Contour plots for 28 days flexural strength: (a) silt–cement; (b) silt–sand; (c) silt–admixture; (d) silt–water.

With the silt content fixed at 2%, the flexural strength decreased when the sand content increased from 50 to 55%. This could be due to the higher content of cement in the mixture (Figure 2.11b). However, when the amount of silt is increased to 10% or higher, an increase of sand content in the mortar mixtures improves the flexural strength. An increase in the additive content improved the flexural strength, which is visible in the contour plot (Figure 2.11c). Regardless of silt content, the flexural values improve with higher additive values. However, this trend reverses and the flexural strength starts to decrease for additive values higher than 0.3%. Similar trends were observable for the model constructed for the compressive strength. The effects of water, sand and silt on the flexural strength are also observable in the ternary plot (Figure 2.12). The increase of silt

follows a similar trend to water and decreases the flexural strength of the mixture. However, it is only the sand that improves the final strength of the mixture.
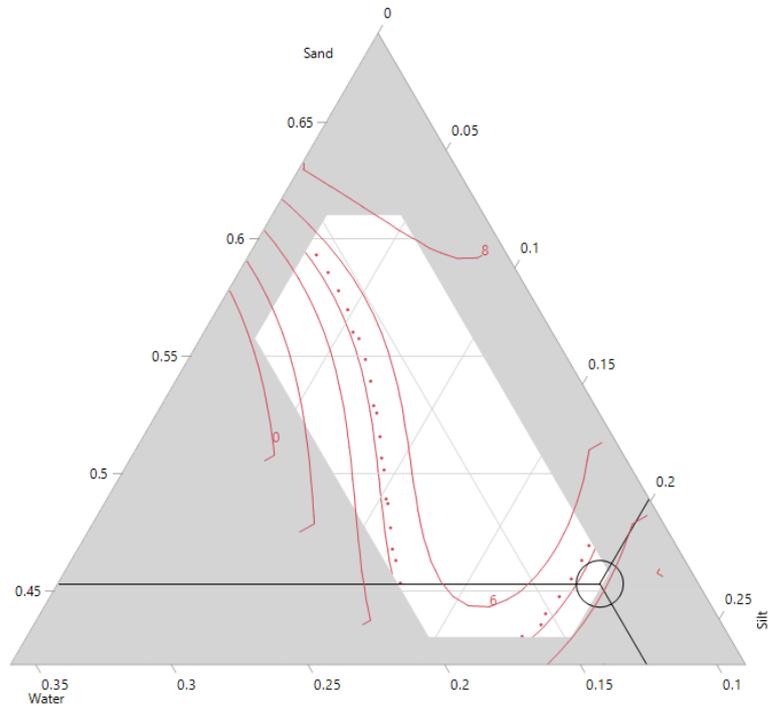
Figure 2.12. Ternary contour plot for 28 days flexural strength.

The profiler option in JMP software was used and the silt was set to 20 percent. As illustrated in Figure 2.13, a flexural strength of 4.0 MPa could be achieved when the mixture contains 22% cement, 13% water, 44.83% sand, 0.17% additive and 20% of silt. Decreasing the amount of silt to 16% could increase the strength to 6 MPa. However, as highlighted before, the current work aimed to improve the silt content without compromising the cement mortar performances. Water to cement ratios for both responses was approximately 0.59 which is slightly higher than the normal values (W/C = 0.5). Due to the nature of silt/clay particles extra water is required to increase the workability of the cement mortar mixtures [46]. The real mean values obtained for different amounts of silt is

depicted in Figure 2.14, where the maximum strength was obtained when only

5% of waste silt was introduced into the mixture.
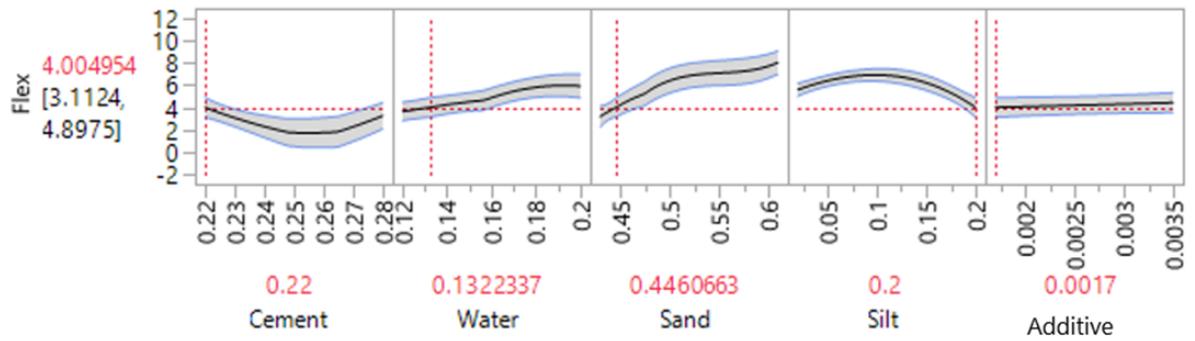
Figure 2.13. Optimization of 28 days flexural strength (MPa) based on maximized silt content.

The overall trend indicates and confirms a decrease in the strength with an

increase of silt content in the mortar mixtures.
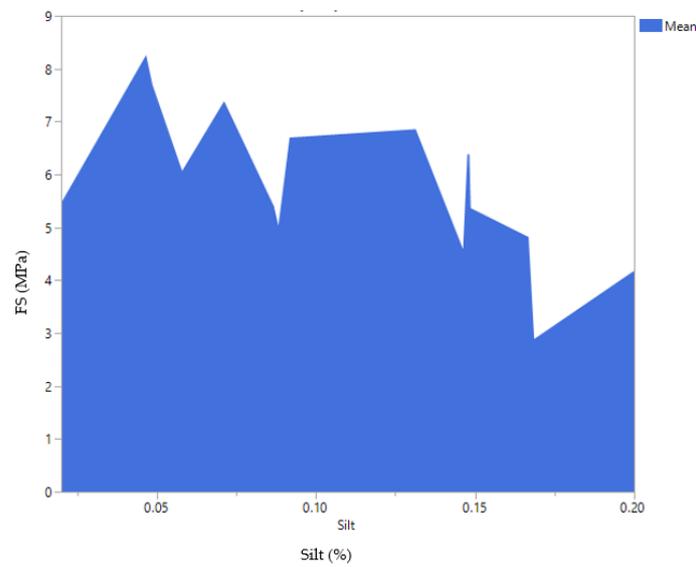
Figure 2.14. Mean values for 28 days flexural strength (FS) (MPa) versus silt content (%).

2.5 Conclusions

The current research focused on producing cement mortars by partially substituting natural sand with the waste silt obtained from the limestone aggregate production in S.A.P.A.B.A. s.r.l. (Italy). Thus, a DOE method was proposed to define the optimum mix design, aiming to include waste silt without affecting the final performance of the cement mortar. Three cement mortar beams were produced and tested for each of the 49 randomized mixtures defined by the DOE method. The obtained results validate the design approach and suggest the possibility of substituting up to 20% of natural sand with waste silt (by weight) in cement mortar mixtures. The corresponding maximum compressive and flexural strength were reported as 22 MPa and 4.0 MPa, respectively. However, by reducing the silt amount to 16%, the compressive and flexural strength will increase to approximately 30 and 6.5 MPa, respectively. The silt particles are larger than natural sand and shorter than clay minerals. When silt and clay particles are introduced into cement/concrete mixtures, more water is required for producing a homogenized mixture. However, the addition of too much water could decrease the compaction of the mixture and reduce the final strength of the mixture. The addition of a special admixture improved the mixing process of the mixture even though it showed no significant effects on the models. Recycling a high amount of washed silt into cement-bound materials could dramatically help with the recycling process of such material and decrease its adverse impact on the environment.

Chapter 3: Mixture Optimization of Concrete Paving Blocks Containing Waste Silt

3.1 Introduction

As time has passed, sustainability has gained more and more interest amongst researchers, authorities, and politicians and has shifted far away from just being a concept. Nowadays, millions of contexts are available that discuss sustainability from different viewpoints. The construction sector, for instance, has been focusing on various aspects of sustainability and many efforts have been put into producing eco-friendly and sustainable infrastructure. Out of the several examples and approaches, one could point out the recycling of waste or by-products into construction materials.

Most of the waste materials are secondary products of various manufacturing processes, such as the aggregate washing process, stone quarries, etc. Recycling such material is of paramount importance since it could reduce the adverse environmental impacts due to landfills. These kinds of materials have been used in the production of several products, such as geopolymers, cement mortars, artificial aggregates, and pavements [9,21,43,47–50].

Concrete paving blocks are building elements being used in roads, pedestrian walks, driveways, and parking lots. Various studies have attempted to build paving blocks containing waste products [51,52]. This would decrease the use of natural aggregates, where approximately up to 3 billion tons of non-renewable natural aggregates are demanded by the construction sector [20].

For instance, both conventional construction and demolition (C&D) and waste material from concrete and ceramic precast production was reused as a source of aggregates to produce new concrete floor blocks. It was claimed that the latter waste material outperformed C&D waste adopted for the same application [53]. The specification of the produced floor blocks was in line with the European standards even at 100% replacement. Similar results were obtained when 100% recycled concrete aggregates (RCA) were used for the manufacturing of new paving blocks [54]. The authors indicated a slight decrease in the strength of the produced samples. However, the experimental paving blocks fulfilled the accepted limits. A different approach was adopted by Penteado et al. (2016), who used ceramic polishing waste and ceramic tile waste as a partial replacement for cement and sand, respectively, for the production of paving blocks [55]. The findings suggested that the replacement of 30% fine aggregate or 20% cement with ceramic tile wastes to produce paving blocks is suitable for heavy vehicle traffic. Similar methods of replacing waste material with cement to produce concrete paving blocks have been investigated by various researchers [56–58].

Natural aggregate production includes a washing process that cleans the aggregates from dirt and mud. During limestone aggregate production, the water used could be contaminated with silt particles. By nature, silt particles are bigger than clay and are formed from two main crystal layers of silica (tetrahedral) and alumina (octahedral). Similar to clay materials, silt is not a favorable material, and its application in infrastructure requires special attention [46]. Several studies have investigated the feasibility of using clay materials in various applications [59]. For instance, a study aimed to investigate the inclusion of RCA and crushed clay bricks (CCB) on the mechanical properties of recycled concrete [60]. The results indicated that 50% of CCB decreased the workability of the concrete

samples, making them hard to compact and mix. CCB influenced the compressive and splitting tensile strength the most.

Partition and paving blocks were produced from recycled marine sediments consisting of gravel, sand, silt, and clay [61]. The paving blocks produced with raw sediment had the highest profit based on the cost–benefit assessment. As a similar concept, the sedimentation of a mud dam was extracted and efforts were made to produce bricks and building materials [13]. The extracted sediments were composed of 74% of silt. To ensure better performance, lime, cement, and glass powder and fiber were also included in the brick mixtures and the compressive strength and flexural strength of the samples were studied. Overall, it was concluded that some of the mixtures had the potential to be used as building materials.

Soil containing gravel, sand, silt, and clay was stabilized with cement to produce mud-based paving blocks [62]. The splitting tensile strength of the mud blocks was suitable for pedestrian footpaths. The final composition of the mud paving blocks suggested that soil containing 5% fine particles could be used.

In a different approach, waste brick powder (WBP) was added to stabilize silt with high plasticity properties [63]. The WBP ranged between 6 and 30% of the dry soil weight. The authors concluded that the addition of WBP increased the compressive strength, California Bearing Ratio, and density of the silt, whereas various parameters such as Atterberg limits, linear shrinkage, and free swelling decreased.

The feasibility of using limestone dust and cement to produce masonry blocks was investigated by Galetakis et al. (2004) [64]. The cylindrical samples

presented compressive strengths above 7 MPa, indicating the suitability of using quarry waste and cement mixtures to produce bricks.

To control and manage stormwater, efforts were made to produce porous clay paving blocks containing rice bran [65]. The clay soil constituted about 14% silt and clay particles. Interestingly, the porous bricks were able to meet the requirements of the WHO standard in terms of wastewater reuse application. It was further indicated that the application of rice bran below 10% could provide sufficient strength and drainage, allowing the bricks to be used in lightweight pedestrian areas.

Various studies have benefitted from the mixture design method for optimizing their mixtures and blends. For instance, the DOE method was used to predict the compressive strength of concrete samples from early aged mixtures. A total of 114 samples were tested and the ACI stepwise method was applied. The authors indicated that the suggested models were capable of predicting the 28th day compressive strength of the concrete samples [66]. A mixture design was applied by [67], where different combinations of polymer concretes including resin, aggregates and microfiller were studied. The mentioned components were also limited through upper and lower values. Various mechanical properties such as compressive, flexural, tensile, and splitting tensile strength were tested and included in the model as the responses. The authors suggested an overall mixture being optimized based on the maximized desirability of all responses [67]. Defining upper and lower limits for variable components and limiting the sum of two or three variables to a certain value is common and results in producing an irregular experimental region [68]. In some cases, researchers benefit from multiple optimization methods and combine various numerical methods with

DOE. For instance, both a numerical method and a DOE were used to optimize the thermal performance of lightweight concrete building blocks [69]. The authors optimized the blocks for the best thermal insulation, keeping the manufacturing cost at a minimum.

The available data on concrete paving blocks containing waste silt are quite scarce. Thus, the present study aimed to investigate the feasibility of including high amounts of silt in concrete paving blocks. For this purpose, two objectives were set: the optimization of paving-block mix design through the Design of Experiments (DOE) approach and the physical and mechanical characterization of the obtained paving blocks based on the EN 1338 standard.

3.2 Materials and Methods

The production of paving blocks was divided into two different sections. In the first section (Phase I), a total of 12 different aggregate combinations were defined by the Design of Experiments model. Consequently, a total of 12 mixtures with different aggregate blends were produced and the tensile splitting strength of each sample was applied to the DOE model. JMP software was used to optimize the mathematical model and an optimized model was proposed to identify the best aggregate blend. In Phase II, a total of 9 samples were produced using the proposed aggregate blend, which were characterized based on the EN 1338 standard.

3.2.1 Materials

The aggregates including gravel (4–8 mm), sand (0–4 mm), and silt were provided by S.A.P.A.B.A. The chemical and mineralogical properties of the silt is fully described in Section 1.3. The recorded values for bulk density (EN 1097-6), sand equivalent (EN 933-8), and harmful fines (EN 933-9) of the sand and

gravel are presented in Table 3.1. A 42.5 R cement was used for the paving blocks (Buzzi Unicem, Casale Monferrato, Italy). In addition, a specific additive that allows the use of swelling clays or aggregates with very high fines was used.

Table 3.1. Sand and gravel physical properties.

Material	Bulk Density (g/cm3) EN 1097-6	Sand Equivalent (%) EN 933-8	Harmful Fines (gMB/Kg) EN 933-9
Sand (0–4 mm)	2.616	92	0.5
Gravel (4–8 mm)	2.667	-	-

3.2.2 Design of Experiments and Mixture Optimization

For the current study, JMP® software (Version 14.0. SAS Institute Inc., Cary, NC, USA, 1989–2019) was used to produce the mixture designs. The three main components (input variables) were selected as gravel, sand, and silt, and the response output was selected as the tensile splitting strength (T). Producing pure mixtures only containing one component was not in favor of the research. Thus, the components were limited to lower (0) and upper boundaries (1) corresponding to 0 and 100%, respectively (Table 3.2).

Table 3.2. Mix design components: upper and lower boundaries.

Indicator	Upper	Lower
Gravel	0.00	0.65
Sand	0.00	0.65
Silt	0.00	0.40

The DOE produced a total of 12 randomized runs. More specifically, the second-degree model was produced by selecting the forward stepwise approach. Furthermore, minimum BIC (Sawa Bayesian information criterion) was selected over AICc (corrected Akaike information criterion) due to having a lower value. The BIC and AICc are information criteria methods used to assess model fit while

penalizing the number of estimated parameters. The mixture suggested for each run was used to produce the concrete paving block tested in terms of tensile splitting strength. The model was further analyzed using JMP software and the profiler tool was benefitted to optimize the final aggregate gradation. Concrete Paving-Block Preparation

A total of 12 concrete mixtures each with three replicas were created based on the DOE model design. To produce each set, cement and proportioned aggregates were mixed. Water and the special additive were added to the mixture. For each mixture, the aggregate-to-cement ratio (A/C) was fixed at 4.62 and enough water was added to reach a slump value of 0. The A/C ratio was recommended by a local paving-block producer. The material was then transferred to special plastic molds. The samples were demolded after 24 h and were cured for 28 days before testing. Figure 3.1 illustrates the mixing process and the final demolded samples.

Figure 3.1. Concrete paving block specimen. Each set of blocks contains 3 repeats and are numbered from right to left. The mixture design of each block is presented in Table 3.3.

2.4. Concrete Paving-Block Characterization

Once the optimized mix design from the DOE analysis was achieved, the suggested blend was adopted to produce paving blocks for the following characterization based on the EN 1338 standard:

- Shape and dimensions;

- Weathering resistance in terms of water absorption;

- Tensile splitting strength (T);

- Abrasion resistance;

- Slip/skid resistance.

This European standard is specific to concrete paving blocks and classifies concrete bricks into various categories based on their performance.

3.3 Results and discussion

3.3.1 Phase I: Mix Design Optimization through the Design of Experiments Approach

Cement concrete mixtures are composed of various ingredients, such as cement, aggregates, additives, and water, where all components add up to 100%. The composition of aggregates including coarse, fine, and fillers of concrete mixtures also follows the same principle, i.e., the sum of the components equals 1 (100%). An effective method of studying such blends, where changes in the mixture composition could affect various outcomes (responses), is by applying the mixture design method. Consequently, the effect of various aggregate compositions (gravel, sand, and silt) on the splitting tensile strength (T) of cement concrete paving blocks was studied using the DOE method.

In this study, the input variables were gravel, sand, and silt (%), and the T of the resulting mixtures was selected as the response. To provide a model, the Design of Experiments indicated 12 randomized runs each with a different aggregate gradation. T was obtained based on the EN 1338 standard for each mixture and the average values were included in the DOE (Table 3.3).

Table 3.3. Design of experimental data.

Run		Gravel (%)	Sand (%)	Silt (%)	T (MPa)
A	1	0.3	0.3	0.4	0.4
F	2	0	0.6	0.4	0.91
I	3	0.5	0.5	0	1.87
D	4	0.625	0	0.375	0.67
G	5	0.65	0.175	0.175	1.24
E	6	0	0.65	0.35	0.83
B	7	0.65	0	0.35	0.47
J	8	0.65	0.35	0	1.91
K	9	0.35	0.65	0	2.8
C	10	0.6	0	0.4	0.52
H	11	0.175	0.65	0.175	1.26
B	12	0	0.625	0.375	0.47

The highest value for T was obtained for the ninth sample with 0% silt (2.8 MPa), whereas the lowest value (0.4 MPa) was related to the first mixture with 40% silt. Furthermore, the usage of a higher amount of silt increased the water-to-cement ratio of the mixture, limiting the compaction rate. Low T values were also observed for samples lacking coarse aggregates (gravel), such as samples 2, 6, and 12. A good gradation curve is vital to having desirable strength. A very dense or gapped gradation could tamper with the final compaction, resulting in lower mechanical values.

The summary of fit for the produced model is presented in Table 3.4, indicating an R2 value of 90.55. The produced model was then used to predict the corresponding T value for each of the 12 mixtures. The actual versus the predicted T values are depicted in Figure 3.2, where the blue line indicates an

average T of approximately 1.1 MPa. Table 3.6 shows the significance of adding a term to a model given that the other terms are already entered. For instance, sand added the highest significance to the model, followed by gravel. On the other hand, the silt parameter did not have a significant effect on the model ($p < 0.05$). In such cases, one could eliminate the insignificant parameter from the model, improving the overall accuracy. However, the elimination of insignificant parameters is not possible for the mixture design approach. A concrete mixture is composed of different ingredients, such as cement, water, and aggregates. By removing any of these components from the design, the produced outcome will no longer be a concrete mixture. Thus, the silt parameter was kept in the model. Moreover, the coefficient of the factors (gravel, sand, and silt) is indicated in the T ratio column of Table 3.6. It is observable that silt had a negative value of -0.61, indicating that an increase in the silt content decreased the overall strength of the concrete bricks. This occurred because a high amount of silt increases the need for water in the mixture, which results in lower strength values. Overall, the produced model showed a very high significance value ($p < 0.0002$), as indicated by the analysis of variance Table 3.6).

Table 3.4. Summary of fit.

Indicator	Value
RSquare	0.91
RSquare Adj	0.87
Root mean square error	0.27
Mean of response	1.11
Observations (or sum wgts)	12
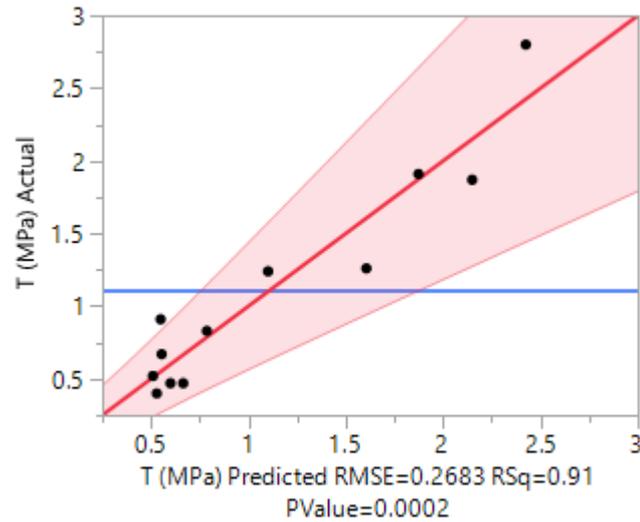
Figure 3.2. Actual vs. predicted T values.

Table 3.5. Parameter estimates.

Term	Estimate	Std Error	T Ratio	Prob > |t|
Gravel (%) (Mixture)	1.2302425	0.475316	2.59	0.0322
Sand (%) (Mixture)	3.068301	0.502842	6.10	0.0003
Silt (%) (Mixture)	−0.570944	0.916089	−0.62	0.5505
Sand (%) * Silt (%)	−4.43013	2.750201	−1.61	0.1459

The main components of the DOE include the term "(Mixture)". These components cannot be deleted during model optimization even if they show insignificant differences.

Table 3.6. Analysis of variance for the produced model.

Source	DF	Sum of Squares	Mean Square	F Ratio
Model	3	5.5204633	1.84015	25.5594
Error	8	0.5759617	0.07200	Prob > F
U. total	11	6.0964250		0.0002

The relationship between aggregate composition and T was studied by producing contour plots (Figure 3.3). The final percentages of silt, sand, and gravel directly affected the final strength of the brick samples. In both cases (Figure 3.3a, b), the highest value for T was obtained when the percentage of silt was below 5% (total aggregate weight). Moreover, to reach the maximum strength (T > 2.5 MPa), the amount of sand and gravel need to be approximately between 60 and 65% and 33 and 38%, respectively. The silt had a negative interaction with both sand and

43

gravel, i.e., an increase in silt content resulted in lower T results. This is also observable in the contour plots, where the application of more than 30% of silt dramatically decreased the strength.
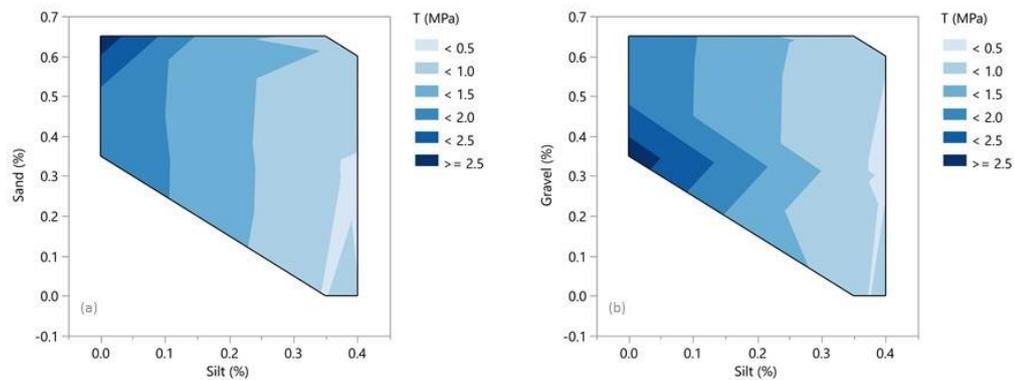
Figure 3.3. Contour plots for splitting tensile strength: (a) silt-sand and (b) silt-gravel.

One of the most important goals when conducting a Design of Experiments through JMP software is to benefit from its powerful optimization tools. The profiler option provides a cross-section of the model, where the curve of each factor shows the relationship with the response based on the levels of other factors. In model optimization, various factors could be considered. One approach is to use the profiler to maximize or minimize the desirability, that is, by simultaneously changing each available variable factor to achieve the target value. However, some design blends may have costly ingredients, or, on the contrary, may include waste/by-products that need to be recycled into certain products. In such scenarios, the variable factor could be fixed at a desired value and the corresponding outcome or response would be optimized accordingly. The current research aimed to maximize the amount of recycled silt in the production of concrete paving blocks. Thus, the profiler tool in the JMP software was used

to optimize the concrete mixture accordingly (Figure 3.4). The optimum blend had an approximate T of 1.49 MPa, resulting from a mixture consisting of 15, 65, and 20% gravel, sand, and silt, respectively. The amount of silt was fixed at 20% and the remaining parameters were calculated accordingly. In Figure 3.4, the values presented in the brackets (1.2112, 1.76643) are the 95% confidence intervals for the tensile splitting strength values. The dotted red lines indicate the selected value for each parameter and the resulting outcome (T) of the model. The slope of the factors represents the coefficient of the parameters, which is also tabulated in Table 3.6. Figure 3.4 also includes the graphs related to the desirability factor of the mathematical model. The desirability function normalizes the responses from the lowest (0) to the highest obtainable value (1). From the desirability graphs (Figure 3.4) it is concluded that by using the 20% silt in the mixture, only 45.5% of the possible T values were obtained.
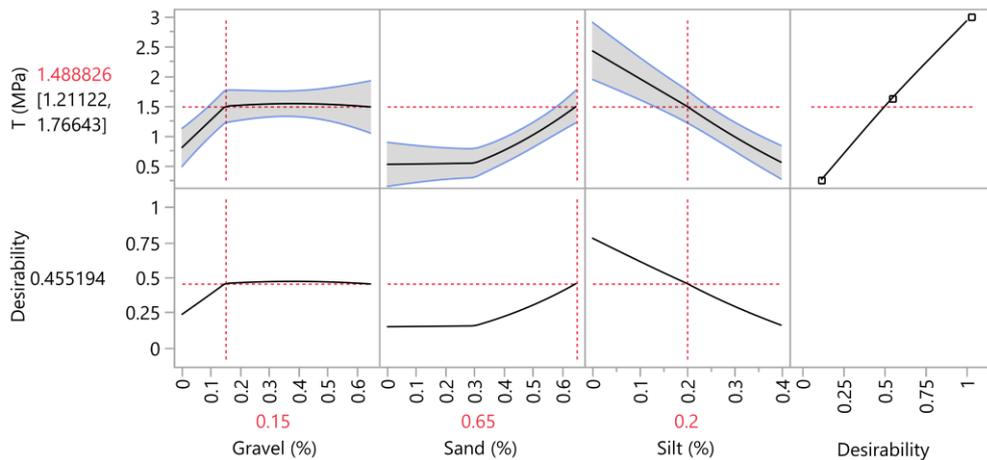
Figure 3.4. Model optimization using the profiler tool in the JMP software.

To further understand the model and study the relationship between different variables and their effect on the final strength, a ternary plot was produced (Figure 3.5).
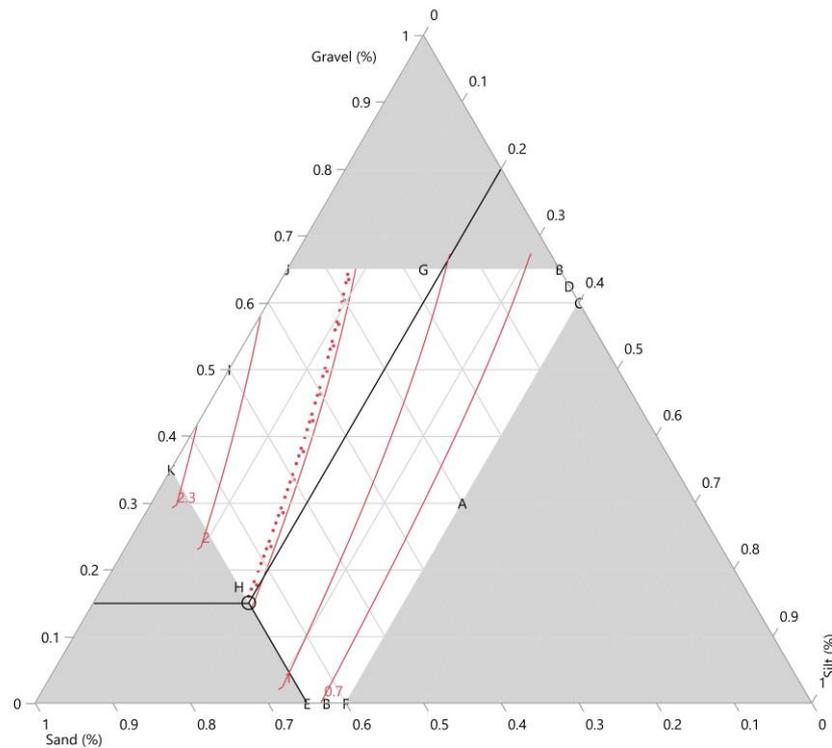
Figure 3.5. Ternary plot. The alphanumerical labels refer to the corresponding runs shown Table 3.3.

The white section represents the model area. However, the constraints applied to the variable parameters are shown in the grayed-out section of the plot. The splitting tensile strength obtained through the mechanical test for each sample (run) is designated in alphanumerical labels in the ternary plot. The labels are also included in Table 3.3. The marker indicates the area in the plot where the optimum mixture was achieved. In addition, the red-dotted line corresponds to a strength equal to 1.489 MPa, as obtained in Figure 3.4. The ternary plot also shows that a decrease in silt content and an increase in sand content increased the overall strength of the samples. The plot shows that the same value of 1.489 MPa was achievable using less silt, that is, 8.5% instead of 20%. However, this would lead to recycling less silt into concrete paving blocks.

All in all, according to the profiler optimization, the final values selected for gravel, sand, and silt were calculated as 15, 65, and 20%, respectively. The final mixture was conducted based on the optimized aggregate gradation, keeping the aggregate-to-cement ratio at 4.62. Similar to the production of the first mixtures, enough water was added to achieve slump values close to 0.

3.3.2 Phase II: Concrete Block Characterization

The optimized mixture design from the DOE method was used, considering an aggregate-to-cement ratio of 4.62 and a water-to-cement (W/C) ratio of 0.58 to achieve slump values close to 0. The high W/C ratio was due to the presence of silt and clay materials that have a larger surface area compared to sand and gravel, resulting in higher absorption power.

A total of nine concrete paving blocks were produced and tested following the specifications of the EN 1338 standard. In the following sections, the results related to the tests specified in the standard are presented.

3.3.2.1 Measurements

The consistency of the paving blocks was verified through geometrical measurements, making it a compulsory test based on Annex C of the EN 1338 standard. A total of nine blocks were produced and the measurements were recorded to the nearest millimeter. The dimensions, deviation, and permissible deviations are reported in Table 3.7. The obtained results indicate that the produced blocks were in line with the suggested requirements proposed by the standard. Therefore, the addition of silt to the concrete paving blocks did not have any adverse effects on the final produced materials in terms of geometrical properties. The standard also classifies the bricks based on their weight per square meter. The average value obtained for the concrete paving blocks was 121.04

kg/m2, which is within the 120–180 kg/m2 range noted for common concrete paving blocks.

Table 3.7. Concrete paving block average measurements and deviations.

Measurement	Length (mm)	Width (mm)	Height (mm)
Concrete blocks	200	100	60
Deviation	±1	±2	±2
Permissible deviation	±2	±2	±3

3.3.2.2 Water Absorption

Among the two methods defined by Annex E of the EN 1338 standard, the water absorption approach was selected to determine the weathering resistance of the paving blocks. The average data obtained for three samples regarding the water absorption are presented in Table 3.8.

Table 3.8. Average water absorption data and limits.

Paving Block	Water Absorption (%)
Concrete block	7.78 ± 1
EN 1338 limit	<6% (class 1-Mark B)

This test is of paramount importance for paving blocks to be used in pedestrian areas. Since the porosity of a material is directly responsible for its saturation level, the water absorption test could indirectly provide insight into the air-void content of the paving blocks. The standard suggests values lower than 6% for moisture content, whereas the concrete paving blocks showed a water absorption rate of 7.78%. Since no pressure was applied during the paving-block production, lower compaction rates were obtained. Studies have provided different methods for decreasing the water absorption of silt, such as applying pressure and vibration at high frequencies [25] or by adding lime to concrete mixtures [70].

3.3.2.3 Tensile Splitting Strength

The only mechanical test specified by the EN 1338 standard is the tensile splitting strength test. Table 3.10 presents the obtained average value of T and failure load

(F) for three identical concrete paving-block samples. The standard states that the obtained values should not be lower than 3.6 MPa and 250 N/mm, respectively. None of the paving blocks reached such requirements. The average of the three samples tested equaled 1.7 MPa, which is about half of the required strength. Applying pressure during molding of the samples will most likely increase the final strength of the samples. Furthermore, the amount of water used to produce the paving blocks containing silt was higher than the normal water-to-cement ratios of common paving blocks. Thus, water could have limited the compaction rate, resulting in a low tensile splitting strength for the samples.

Moreover, the adopted casting method could be responsible for the formation of air voids, suggested by the high water absorption and low mechanical properties. The adoption of vibration at high frequencies and pressure during the molding procedure could decrease the porosity of the material, improving both properties.

Table 3.9. Tensile splitting strength of concrete paving blocks after 28 days.

Paving Block	T(MPa)	F (N/mm)
Concrete block	1.7 ± 0.2	183.83 ± 3.0
EN 1338 limit	>3.6	>250

3.3.2.4 Abrasion Resistance

The ability to withstand friction is defined as the abrasion resistance of a surface, which correlates directly to its durability. The wide wheel abrasion test was used to evaluate the abrasion resistance of the paving blocks based on the EN 1338 standard (Figure 3.6).

Figure 3.6. Wide wheel abrasion test on concrete paving blocks.

The obtained results and classification of the bricks are provided in Table 3.10. The average of three experimental bricks had an abrasion of 25.48 mm, classifying the bricks as Class 1-Mark F based on the standard. The curing conditions, mix design, and final surface of the paving blocks can directly affect the abrasion value [43]. Thus, improved resistance in terms of abrasion could be achieved through better curing of the bricks or by the inclusion of various materials such as waste rubber [71,72].

Table 3.10. Abrasion resistance for the concrete paving blocks.

Paving Block	Groove Dimension (mm)	Classification (EN 1338)
1	26.26	-
2	24.27	-
3	25.90	-
Average	25.48	Class 1-Mark F

3.3.2.5 Skid Resistance

The safety of pedestrians is an important parameter that should be considered during the production of paving blocks. One of the most important functional characteristics could be the unpolished slip-resistance value (USRV), as indicated in Annex I of the EN 1338 standard. The USRV indicates the suitability of paving blocks' finishing surface for pedestrians. The USRV of three identical

paving blocks is shown in Table 3.11. The concrete paving blocks showed considerable skid resistance and fell within the lower and upper limits suggested by some guidelines. However, no limitations or suggestions are given by the EN 1338 standard. The inclusion of silt did not affect the slip/skid resistance of the material and the produced concrete paving blocks showed acceptable USRV values.

Table 3.11. Skid resistance of paving blocks.

Paving Block	USRV
1	73.4
2	71.4
3	72.2
Average	72.3

3.4 Conclusions

A Design of Experiments (mixture design) was applied to investigate the feasibility of including waste silt in concrete paving blocks. Based on the DOE, a total of 12 different aggregate blends consisting of gravel, sand, and silt were produced. Each of the 12 blends were tested for tensile splitting strength based on the EN 1338 standard. The produced model was then optimized using JMP software, resulting in the final blend having 15% gravel, 65% sand, and 20% of silt. The second phase of the study focused on the physical and mechanical properties of the concrete paving blocks produced with the optimized mix design. Based on the EN 1338 standard, shape and dimension measurements and various tests, including weathering resistance in terms of water absorption, tensile splitting strength, abrasion resistance, and slip/skid resistance, were conducted. The summary of the findings are as follows:

- The DOE method proved to be suitable for mixture optimization of the experimental concrete paving blocks.

- The samples produced with the optimum mixture showed consistency in terms of physical measurements, implying that the addition of silt did not negatively affect the workability of the concrete.

- The water absorption of the paving blocks was calculated as 7.78%, which is higher than the recommended values. This phenomenon could be related to the casting procedures, which allowed the formation of water-accessible voids.

- The recorded T values were lower compared to the required values for paving blocks.

- In terms of abrasion resistance, the experimental paving blocks fell in the lowest class foreseen in the EN 1338 standard. Improved curing methods or including specific materials in the mix design could improve the performance of the concrete blocks.

- The skid resistance fell within the recommended range, showing sufficient friction. This will assure the safety of pedestrians.

All in all, this preliminary laboratory characterization showed promising results to produce concrete paving blocks containing waste silt. However, improvements are needed to validate the application of this experimental material for the construction of paving areas.

PART II: GEOPOLYMER CEMENT

PART II consists of Chapters 4, 5 and discusses the recycling of the waste silt into geopolymer-based materials. The First chapter summarizes the literature surrounding geopolymer production using waste mineral fillers. The second section determines the optimum calcination conditions of the waste silt. Finally, geopolymer paving blocks are produced and characterized according to EN 1338 standard.

The studies presented in this section have been published as follows:

1. Solouki, A.; Viscomi, G.; Lamperti, R.; Tataranni, P. Quarry Waste as Precursors in Geopolymers for Civil Engineering Applications: A Decade in Review. *Materials (Basel).* 2020, *13*, 3146, doi:10.3390/ma13143146.

2. Solouki, A.; Fathollahi, A.; Viscomi, G.; Tataranni, P.; Valdrè, G.; Coupe, S.J.; Sangiorgi, C. Thermally treated waste silt as filler in geopolymer cement. Materials (Basel). 2021, 14, doi:10.3390/ma14175102.

3. Mechanical, thermal and microstructure properties of silt-based geopolymer paving blocks. (under review)

4. Moro, D.; Fabbri, R.; Romano, J.; Ulian, G.; Calafato, A.; Solouki, A.; Sangiorgi, C.; Valdrè, G. Thermal, X-ray Diffraction and Oedometric Analyses of Silt-Waste/NaOH-Activated Metakaolin Geopolymer Composite. J. Compos. Sci. 2021, 5, 269, doi:10.3390/jcs5100269. (The paper is an outcome of the PhD. However, it is not included in the dissertation)

Chapter 4: Quarry Waste as Precursors in Geopolymers for Civil Engineering Applications: A Decade in Review

4.1 Introduction

Road and construction sectors are practicing greener solutions where aggregate recycling has become an essential principle for most authorities. Various studies have investigated the feasibility of recycling 100% of asphalt pavements [73–75] or have tried to produce concrete using construction and demolition waste [76]. Nevertheless, aggregate quarries still must keep up with the global demand for virgin aggregates. The aggregates are transported to the processing plants where they are first crushed into smaller and manageable sizes. The crushing and milling stages are usually followed by screening and washing of aggregates prior to final stockpiling. The water used during the washing process is directed to precipitation tanks for further processing. The resulting residue, which is mainly consisted of dirt and very fine powdery substances, are piped out into artificial lakes and ponds called tailing mines. These materials, mostly mineral fillers from plant processes, could become an environmental issue because of the landfilling limitations and strict legislation on their disposal.

Over the past decades, various techniques and methods have been employed as solutions for recycling mining waste. For instance, tungsten mining waste has been processed and used as a filler in asphalt pavements. The study substituted the mining waste with the typical limestone filler in asphalt pavement. The results did not indicate any adverse effects of the waste filler on the performance of tested hot mix asphalts [77]. With a similar concept, magnetite was used as a

filler in various mastic mixtures with the aim of providing a solution for recycling mining waste and microwave healing of asphalt pavements [78]. Other approaches to recycling waste mineral fillers include the application of mining waste in cement paste backfill [79], recovery of valuable metals [8,9], paint production [80], carbon capture and storage [81], and concrete production [82]. All methods follow one aim, which is to reduce the impact of mineral waste on the environment [83].

Alternatively, some quarry wastes are both rich in aluminosilicates and have the proper mineralogy, which allows their application as precursors to produce geopolymer cement and similar synthetic materials. Geopolymers are alternative binders which have diverse applications in various fields such as coatings and adhesives [84], fiber composite production [85], decorative stone artifacts [14], thermal insulations [86], building materials, low-energy ceramic tiles [87], waste encapsulation [88], thermal shock refractories [14], biotechnologies [88], etc. Geopolymers were first introduced by Joseph Davidovits in the early 1970s, where his primary aim was producing nonflammable and noncombustible plastics. During his studies he discovered that the synthesis of some organic plastics in alkali solutions as well as mineral zeolites and feldspathoids were driven by the same hydrothermal conditions. Through further reviewing of zeolites synthesis-related patents and literature he realized a gap, which had not been investigated before. Afterwards, he developed materials rich in aluminosilicates with a three-dimensional amorphous to a semi-crystalline structure and coined it as geopolymers [14,89]. In other words, geopolymers are mineral polymers produced through geochemistry or geosynthesis and their discovery has increased the scientific interests and application of a new class of inorganic polymers over the past decades. For instance, kaolinitic clays were wet

mud and were only processable through compression or extrusion. However, in 1975, a geopolymer in the form of a liquid binder was discovered and patented, which included metakaolin and soluble alkali silicates [14]. The mineral resin (metakaolin + Na-silicate + NaOH) had an exothermic reaction, which was advantageous since it helped the hardening of thick materials. In addition, the sodium silicate (SS) increased the hardening speed of the liquid binder.

Geopolymer cement and concrete have been widely used in different civil engineering application. They are produced with low processed natural materials or industrial by-products, minimizing carbon footprint. The presence of calcium cations mainly obtained from GGBFS provides room temperature hardening for geopolymer. In addition, the setting time of geopolymers are faster compared to normal concrete yet slow enough to allow plant to site transportations [14]. Geopolymers are not affected by common durability issues related with conventional concrete and could outperform conventional concrete in many aspects. For instance, the maximum reported compressive strength for geopolymer samples produced with loess and fly ash was reported as 113.8 MPa, which is much higher than those obtained by ordinary Portland cement (OPC) [15]. High performance Portland cement (HPC) was compared to geopolymer concrete in terms of mechanical and thermal behavior and microstructure properties [16]. Regarding compressive strength, geopolymer concrete showed faster setting times up to 15 MPa just after two hours. However, the strength of both mixtures became similar after 7 days of curing and maxed at about 60 MPa after 2 years. In terms of porosity and microcracks, geopolymer concrete had formed a denser structure compared to HPC. Lastly, thermal analyses by Differential scanning calorimetry (DSC) and Thermogravimetric analysis (TGA) indicated fire resistance of geopolymer concrete compared to HPC.

Geopolymer cement is categorized into four different types including slag, fly ash, ferro-sialate, and rock-based geopolymer cements [14,90]. Each type is composed of different materials, mix design, and consequently different curing/processing procedures. Regardless of the type, most systems use alkali solutions consisting of NaOH and soluble sodium silicates. The very first geopolymer containing slag was produced in the early 1980s. This type of geopolymer consisted of metakaolin, ground granulated blast furnace slag, and alkali silicate solution [90]. Fly ash geopolymers are mainly produced by two different methods. The first group contains fly ash and a very strong alkaline solution. This system requires heat curing of up to 48 h at temperatures ranging from 60 to 85 °C. On the other hand, geopolymers made with fly ash and blast furnace slag do not require heat curing and use a user-friendly alkaline solution [88,91,92]. Rock-based geopolymer cement allows the utilization of volcanic tuffs and mine tailings within the geopolymer system. These geopolymers have lower CO_2 footprint and better properties compared to the normal slag-based geopolymers.

Mine waste management has become an important aspect during the past decades and various methods have been proposed for reducing its impacts on the environment. In this regard, geopolymer cement has become an interesting and alternative method for mine tailing management [77,93,94]. The number of published articles on geopolymers has increased dramatically. Thus, the aim of this paper is to review and summarize published data related to geopolymer cement and concrete containing waste mine tailings and quarry dust.

4.2 Geopolymer Composition

In general, a geopolymer consists of two essential parts including precursors and hardeners/activators. The precursors are raw materials rich in alumino-silicate oxides with high reactivity. The precursors are mixed with liquid hardeners to form a geopolymeric gel, which consequently hardens because of geopolymer condensation. Different precursors have been used in various research studies such as fly ash [95–97], metakaolin [98–100], and blast furnace slag [101–104]. In most cases, the reviewed studies have investigated the feasibility of using quarry dust, mine tailings, or industrial waste as precursors in geopolymer cements and binders [105–114]. Since quarry dust and mining by-products are the focus of the current paper, a separate section has been dedicated to them.

4.2.1 Precursors

4.2.1.1 Metakaolin

Calcined kaolinitic clays otherwise known as metakaolin (MK) were one of the first precursors used in geopolymer research. The initial application of MK was mainly in paper and plastic industries where it was used as filler. However, about four decades ago, a flash calciner technology was used instead of a normal rotary kiln furnace to produce a new type of metakaolin named Argical® [115]. Today, various chemical companies have produced different types of metakaolin, which are suitable for different applications. The composition of metakaolin is mainly made of SiO_2 and Al_2O_3 with a small percentage of metal oxides. Davidovits (2019) investigated the exothermicity data of several metakaolin and indicated the minimum time required for each metakaolin to reach its highest thermal peak in an alkaline solution [115].

By reviewing various studies during the past decade, it becomes evident that metakaolin has kept its popularity as the main precursor among different researchers. However, in recent years, with the aim of recycling as much industrial waste as possible, the popularity of metakaolin has decreased. For example, recently in an attempt of reducing inorganic waste, up to 70% of tungsten waste, along with only 10% of metakaolin were used as precursors in an alkaline-activated foam mix design [98]. In addition, the authors used aluminum powder as the foaming agent and claimed that the strength of the final product was equal or even higher than samples made with only MK and fly ash. In a different approach, vanadium mine residues were used with metakaolin for geopolymer production [110]. Chemical and mineralogical studies indicated that part of the mining waste favorably reacted with the soluble silicon and the unreacted section acted as aggregates in the mixture.

4.2.1.2 Fly Ash

Coal power stations are still one of the main solutions for providing electricity worldwide. At electricity power plants, finely powdered coal is injected with air into a combustion furnace where it immediately burns at very high temperatures. Consequently, the shales and clay inside the suspended coal that are rich in silica, aluminum, and iron melt. Upon rapid cooling, the material solidifies into spherical material commonly known as fly ash. Fly ash has been used as a precursor in geopolymer cement and binder production throughout the world. Based on plant type and combustion temperatures (ranging from 800 to 1800 °C), the final chemical composition of fly ash may differ (Table 4.1). Therefore, an X-ray diffraction (XRD) analysis could aid the selection of appropriate fly ash for geopolymer production. In this regard, the properties of appropriate fly ash for alkali-activation has been suggested [116,117]. The papers indicate that to

ensure a proper alkalization, the fly ash should have a Si/Al ratio between 2 and 3.5. In addition, the percentage of Fe_2O_3 should be lower than 10% while the percentage of unburnt material should be as low as 5%. Furthermore, fly ash should have a high vitreous rate and the percentage of active silica such as glass should be above 40%. Regarding particle size, it has been suggested that between 80 and 90% of the particles should be smaller than 45 µm. The mentioned characteristics could improve the final geopolymer product. However, high calcium, quartz, and mullite content should be avoided. The reactivity of Si/Al in the fly ash would be affected by high quartz and mullite (>5%) content, whereas high CaO could initiate a fast setting of geopolymer paste during preparation [118].

Table 4.1. Coal composition before and after combustion, adapted from [14].

Coal Minerals	Phase After Combustion Process		
	850 °C	1500 °C	1800 °C
Quartz	Quartz	Cristobalite	Glass
Kaolinite	Metakaolin	Glass + mullite	Glass
Illite	Illite	Glass + mullite	Glass
Pyrite FeS2	FeS/FeO	Hematite + glass Magnetite + glass	Glass
Calcite	CaO	Glass	Glass

Geopolymer cements and binders have various applications in building and construction projects. For instance, in an attempt to recycle quarry dust, geopolymer adhesive mortars were made using fly ash, crushed stone dust with different NaOH molarity and ratios [112]. Considering energy levels, waste and raw material usage, a maximum amount of 67% of quarry dust was proposed as the most efficient quantity during geopolymer production. Moreover, the authors suggested that fly ash and the quarry dust formed a homogenous mixture. In a separate attempt, the potential of recycling marble quarry dust into a geopolymer system was investigated [119]. In this regard, the geopolymer mixture consisted of fly ash, blast furnace slag, clay, gypsum, concrete, and marble sludge. The

results indicated that the mixture containing no clay and gypsum had shown the highest compressive strength rate of 52 MPa. This is interesting since Davidovits [14] has claimed that the addition of gypsum inhibits the geopolymer chain reaction and may lead to adverse results. The applications of geopolymers are vast and are not only limited to mortars and cements. For example, in a study conducted by Yliniemi et al. (2017), gold, copper, and zinc tailings were incorporated into the fly ash geopolymer system to produce artificial aggregates. The aggregates were then used in mortars and concrete specimens, which showed enhanced mechanical properties compared to LECAs (light expanded clay aggregates) [120]. The application of fine materials into aggregate systems and unbound materials has been given negative feedback through the works conducted in the soil mechanics field, which usually result in reduced resilient modulus and increased permanent deformation. Therefore, in some cases, geopolymers have been employed as a greener solution for soil stabilization. Loess is formed from clay and silt particles, which provides for bearing capacity. However, the material will deteriorate and eventually collapse in case of direct water contact. An experimental study evaluated the possibility of loess stabilization through fly ash-based geopolymerization [96]. The authors claimed that the fly ash geopolymer binder bonds with the loess and provides a stable structure. A conceptual microstructure model regarding loess stabilization using geopolymer is shown in Figure 4.1.
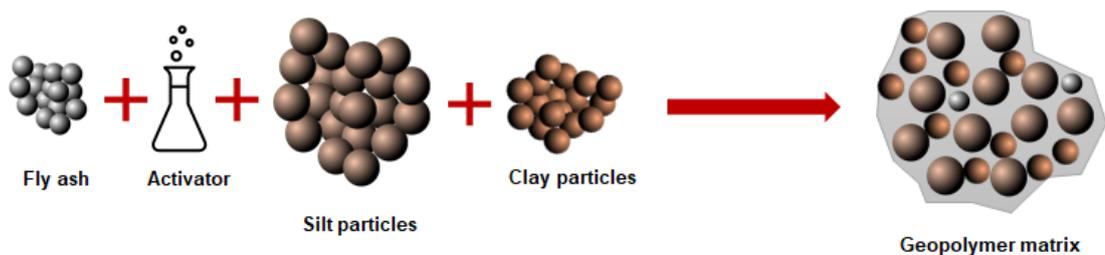
Figure 4.1. Loess stabilization using geopolymer binder [96].

4.2.1.3 Ground Granulated Blast Furnace Slag

During iron manufacturing process fluxing agents are added to the molten iron to produce molten slag. The molten slag is immediately quenched, which initiates the granulating process. The granulated slag is then dried and ground to produce ground granulated blast furnace slag (GGBFS). The slag is rich in aluminum, magnesium, and calcium-silicates with a semi-crystalline glass-like structure. In general, the composition of slag consists of SiO_2, Al_2O_3, CaO, MgO and between 44 to 47% of the total composition is made up of SiO_2,$+Al_2O_3$ [14]. Slow cooling procedures such as air-cooling method would not produce hydraulic or pozzolanic phase. Consequently, air-cooled slags will not be appropriate for geopolymer production.

Various papers have included blast furnace slag as a precursor for producing geopolymers containing quarry waste [30,34,35,37,38,44,54–60]. The potential of using geopolymers consisting of copper mine tailings and slag for pavement construction was investigated [101]. The addition of 50% GGBFS increased the unconfined compressive strength (UCS) by 20 MPa compared to samples produced with 0% GGBFS. The increase in the UCS was related to large surface area and higher chemical reactivity, high smelting temperatures and the amorphous structure of the GGBFS. In addition, the water to solid ratio dropped by 15% with the addition of 50% GGBFS compared to the control sample. The reduction of the water content decreased the required NaOH and sodium silicate in the mixture, which could be a benefit in terms of production costs.

Ambient temperature curing for geopolymer mixtures containing GGBFS could be applicable because of the presence of calcium cations. In most scenarios, this would eliminate the need for elevated temperature curing and could facilitate

industrial implementations. For instance, the addition of slag to alkali activated fly ash was investigated [121]. In addition to room temperature curing, two fly ash samples were also cured at 60 °C. The latter showed higher UCS compared to same samples cured at ambient temperature. However, the mixture containing 15% slag showed a maximum strength of 47.5 MPa, which was very similar to the USC of samples merely made with fly ash and cured at 60 °C. Special attention should be given to the working time (pot-life) of such mixes since high amounts of GGBFS could lead to flash settings. The fast hardening of geopolymers dramatically affects field work by limiting the transportation opportunity window (plant to site).

4.2.2 Activators/Hardeners

To successfully produce a geopolymer network, in addition to precursors, an alkaline solution is essential for bonding aggregates and materials together through a specific chemical reaction. Moreover, despite their lower popularity compared to alkaline solutions, an acidic medium (e.g., phosphate) could also be used for geopolymer production [14,122]. The typical alkaline solution includes sodium or potassium hydroxide and soluble silicates. The hydroxide helps with the dissolution of the aluminosilicates available in the mixture and the soluble silicates act as the main binding source in geopolymer mixtures [123]. Based on the literature, different activator-related variables could affect the final properties of geopolymer cements and binders. These parameters include alkali cation type (Na+, K+), soluble silicate alkalinity, the molarity of the activators, and hydroxide to silicate ratio. In addition, the solid to liquid ratio, Si/Al and (Na+, K+)/Al ratio also influence mixtures' final properties [124–126].

The most common alkali cations used during geopolymer preparation are sodium and potassium. It is indicated by the literature that Na+ cations are better in regards of promoting aluminosilicates than K+ cations [14]. The ease of handling or workability is an important factor in geopolymer applications, which is determined by molecular ratio, density, and temperature of soluble silicates. For instance, the viscosity of Na+ silicates increase with an increase in molecular ratio. However, potassium-based alkaline solutions are much less viscous compared to the Na+ hydroxide solutions. Moreover, despite it being less effective for the dissolution process, potassium-based activators could achieve higher compressive strength value compared to sodium-based activators. Higher compressive strength and lower viscosity of potassium mixtures compared to sodium solutions are observable in literature [96,105]. For instance, it was indicated that the compressive strength of samples made with fly ash and loess increased from 29.5 to 113.8 MPa when KOH was used instead of NaOH as the activator. [96].

The soluble silicates act as binders for the geopolymer matrix and its history dates to 1640 where it was introduced by Van Helmont. However, the term waterglass was first coined by Johann Nepomuk Von Fuchs in 1818 when he mixed silica with caustic soda potash (i.e., potassium compounds and potassium-bearing materials). The waterglass was used as glue, cement, paints, detergents, and hardening materials in artificial stone production [14]. Currently, the soluble silicates are used as detergents, chemical applications, and as adhesives. Various studies have evaluated the effect of sodium or potassium silicates on geopolymer mixtures. For instance, it was claimed that its addition to the solution could approximately double the compressive strength of the fly ash-based geopolymer samples [117,127]. The soluble silicates used in different studies vary in terms of

molecular weight and chemical structure (Table 4.2). The molar ratio is also an important factor since it is directly related to the corrosiveness of the solutions. In general, the molar ratio (MR) $(SiO_2/Na_2O) < 1.45$ is known to be corrosive which may cause problems during handling for the workers. Furthermore, higher MR will lead to longer setting values. A study conducted by Kastiukas et al. (2017) investigated the effects of different SiO_2-Na_2O ratios by varying sodium silicate (SS) to sodium hydroxide (SH) ratios [128]. The authors suggested 3.6% for Na_2O concentration when proportioning SS/SH. In addition, the study used up to 40% of waste glass, which led to a reduction of 22.5% in sodium silicate usage. In a different study, Manjarrez et al. (2019), varied the ratio of sodium silicate to sodium hydroxide from 0.0 to 1.5 in an attempt to understand its effect on compressive strength of geopolymer samples [101]. The maximum strength of 23.5 MPa was observed for 10 M at SS/NaOH = 1.0.

Table 4.2. Commercial silicates, adapted from [14].

Silicate type	MR (SiO_2:Na_2O)
Sodium orthosilicate Na_4SiO_4	0.5
Sodium metasilicate Na_2SiO_3	1.0
Sodium disilicate $Na_2Si_2O_5$	2.0
Sodium polysilicate $Na_2O._3.3SiO_2$	3.3

The molar ratio of different soluble silicates is also important in terms of free metal cations and (NA^+, K^+)/Al ratios. To have a chemically stable structure, the Na/Al ratio should be equal to 1. Furthermore, the Si/Al ratio depends mainly on the type of geopolymers application. A ratio lower than three is suggested in the literature for geopolymer cement and concrete production [125,129]. In most cases, the ratios are calculated regarding the molar ratios of each element. However, the reactivity of used materials may differ, and the final leaching of Si and Al elements is related to both the chemical composition and mineralogy of precursors. Therefore, a simple method for determining geopolymer reactivity

has been proposed by Davidovits [14], where the same amount of activator is used with different amounts of precursors. The hardness of the mixture is measured with a penetrometer after 1 and 2 h. Lower penetration values are an indication of higher mixture reactivity. This method is also appropriate for identifying the flash setting time that could be identified as a mix hardening time less than 30 min. Finally, the minimum amount of required precursors could be determined.

The amount of activator has a great influence on the geopolymer properties considering the solid–liquid ratio. Scanning electron microscopy was used to study the microstructure development in geopolymer pastes. It was concluded that a solid to liquid ratio of 4 showed higher mechanical strength, cohesiveness, and lower micro-crack and micropores compared to lower ratios [105]. Water makes the movement of the particles within the geopolymer gel possible, where the chemical reactions take place. In each reaction cycle, part of the water is reintroduced into the mixture. Thus, it is essential to prevent any water (evaporation) during mixing and curing stages [130]. High liquid to solid ratios could show adverse effects on the final compressive strength of geopolymer samples. For instance, the strength of vanadium geopolymer samples reduced from 23.89 to 5.23 MPa when water to binder ratio was increased from 0.28 to 0.44 in the mixture [110]. Excessive addition of water could decrease the alkalinity of the liquid hardeners and therefore, less dissolution of Si and Al element will occur. Consequently, the compressive strength will reduce significantly [123].

4.3 Quarry Dust and Mine Tailings as Precursors

Bedrocks and unconsolidated deposits are the main sources for most of the obtained aggregates worldwide. In this regard, most of the mineral aggregates are collected from surface-mined stone quarries or from sand and gravel pits. The first step in every quarrying process starts with the stripping stage [131]. This step is critical for improving the overall quality of the products since the unwanted material will be removed from the mining surface minimizing the variations of materials passing n. 200 sieve size. The mineral fillers either obtained through quarry blasting or from excavating gravel deposits are then prepared for the crushing stage. The aggregates go through a stage called scalping which is primarily used for diverting and separating fines from coarse aggregates during the first crushing stage. This is very important since the fines can be removed from the production process if the specifications are not met. The unwanted materials can be piled as waste or used as lower quality aggregates. Depending on the type of rock being processed, the material can undergo up to three crushing stages, which usually uses jaw or gyratory crusher. The crushed aggregates usually have long and thin shapes that are not suitable for asphalt pavement production. Consequently, the impact crushers are preferable. The materials are then gathered in a surge pile and stocked for further processing as required. The second and third crushing stages usually use cone and roll crushers. At the final step, the crushed aggregates go through the screening stage which is vital for quality and gradation control of the materials. Annually, aggregate production process produces huge amounts of by-products which are referred to as mine tailing, quarry dust, or waste mineral fillers by various researchers. These by-products can consist of water, heavy metals, and toxic substances depending on their origin [132]. Different methods have been undertaken for recycling

quarry and mine tailings. As for one approach, the production of geopolymer cement and binder using quarry waste has gained attention. Various types of tailings from quarries and mines have been studied which include silt, tungsten, vanadium, iron, gold, copper, zinc, granite, marble, lithium, and phosphate. In this section, the production of geopolymers using different mine tailings IS summarized.

4.3.1 Silt

Lampris et al. [133] collected waste silt from five different aggregate washing plants in the United Kingdom for the production of artificial aggregates through geopolymerization. The geopolymers were constructed using silt and mixes containing metakaolin or fly ash. The latter showed a higher compressive strength of about 30.5 MPa which is more than the mechanical properties generally required for aggregates for building materials. It must be mentioned that the varying chemical composition of waste silt can adversely affect the final quality of the products. This paper is one of the very few which have investigated the recycling of waste silt into geopolymer applications. In one of the most recent attempts, Coode Island silt was improved using fly ash and slag with different proportions of sodium and potassium liquid activators [134]. The authors suggested that the resulting geopolymers could be appropriate for deep soil mixing projects. Interestingly, silt obtained from the Yellow River was used in a geopolymer binder for the production of an artificial flood-preventing stone [135]. It was claimed that the addition of slag had dramatically increased the final compressive strength of the samples. Loess particles which include silt and clay were utilized in a fly ash geopolymer [96]. The loess samples were stabilized successfully using different alkaline activator types including sodium and potassium hydroxides. In a similar work, a case study was conducted in a

reservoir located in southern Italy [136]. The aim of the paper was to deal with the loss of water storage capacity of the lakes through alkaline activation of silt residues. The results indicated that the clay and silt could be calcined and reused in applications such as binder, precast, and bricks through alkaline activation.

4.3.2 Tungsten Ore

Tungsten was one of the most popular mine tailings waste investigated during the past decade, where different studies have tried to increase its reactivity by means of different methods. For instance, calcination of mud waste obtained from tungsten mining process with sodium carbonate was investigated by Pacheco-Torgal et al. (2010) [137]. The authors observed high efflorescence of sodium after water immersion (Figure 4.2). Despite achieving high strength values, this method did not achieve favorable thermal reactivity rates. The activation of tungsten mining waste was also investigated through the addition of waste glass [98]. For instance, the addition of 40% of waste glass provided additional silica in the geopolymeric mixture and thus improved the overall strength of the samples by 127% compared to samples containing zero percent of waste glass [128]. Higher silica rates produced 3D structural networks (Si/Al of 2:1).

(a)   (b)

Figure 4.2. Right: mine waste calcinated at 950. Left: mine waste calcinated with sodium carbonate after water immersion, reproduced with permission from [137].

The durability of the geopolymer has also been tested against acid resistance, where higher acid and abrasion resistance for samples made with tungsten mine waste compared to ordinary Portland cement was observed [138,139]. In a different approach, tungsten mine waste has been used in grouted pavements [140]. The samples made with geopolymer grout presented the lowest compressive strength compared to typical mixtures. It was also concluded that the curing conditions of the mixtures containing geopolymers required further evaluation. Tungsten ore and waste has also been used in different types of pavement applications. For instance, Sangiorgi et al. [93] investigated different recycling scenarios of the waste aggregates and powders obtained from the Panasqueira mine located in Portugal. Additionally, the economic and social impact of the potential recycling techniques were estimated for the local communities. The authors recommended various methods for recycling the tailings of the Panasqueira mine such as its incorporation in the road construction field. However, the focus of the study was to produce alkali-activated composites from mining and quarrying waste based on the available and demanding requirements of authorities. It was suggested that the production of such material could be a competitive and viable solution, which could lead to the manufacturing of aggregates for road paving materials. Similar studies related to the same project verified that artificial aggregates can be produced through the geopomymerization of tungsten mine tailings [106,141].

4.3.3 Vanadium Ore

The demand for vanadium extraction has risen significantly and therefore, the mine tailings could turn to possible threats for the environment. The papers reviewed have used vanadium tailings as precursors in geopolymer production. Different methods have been used to reactivate the inert tailing mines such as

mechanical activation. For instance, planetary mill ball was used to crush vanadium tailings to smaller particles for a maximum duration of 5.5 h [142]. As shown in Figure 4.3, an increase in milling time increased Si and Al elements during leaching tests. The authors concluded that the mechanical activation had destroyed the crystalline structure of the material, which led to higher compressive time and faster setting duration.
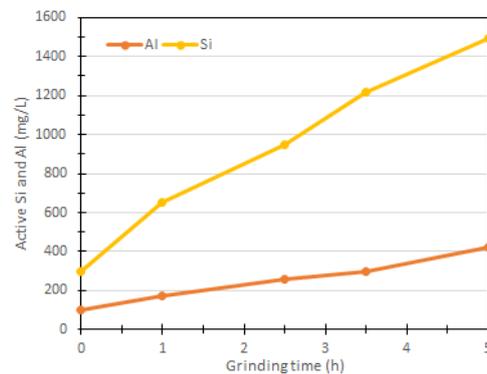
Figure 4.3. Mechanical activation of vanadium mine tailing, reproduced with permission from [142].

A different approach was considered to increase the reactivity of vanadium mine tailings. In a study conducted by Jiao et al. (2011), solid NaOH was roasted with the vanadium tailing for 1 h at 450 °C. After cooling down, the mixture was mixed with metakaolin and distilled water. The highest compressive strength was obtained with the addition of 30% metakaolin and curing temperature of 60 °C [100].

4.3.4 Marble

During quarrying and different processing methods, huge amounts of marble waste are produced worldwide. Mable stone is the result of metamorphism of sedimentary carbonate rocks such as limestone or dolomite rocks. Like other mine tailings and quarry dust, studies have considered using marble stone waste

as precursors in geopolymer production. In a study from Thakur et al. (2019), different molarities of NaOH (2 and 4 M) and sodium metasilicate were used in the production of fly ash-based geopolymer containing marble stone waste [143]. Marble waste and fly ash were initially mixed prior to the addition of the alkaline solution. The mixture was mixed and molded into rectangular casts (Figure 4.4). The highest compressive strength was related to the mixtures made with 4 M NaOH. The authors highlighted that both chemical properties and mineralogy of the precursors used (fly ash and marble waste) are of paramount importance during geopolymer manufacturing. The amount of reactive Si and Al leached during the chemical reactions may differ from the values obtained during XRF analysis. Therefore, regardless of geopolymer precursor type, it was recommended that the mixing procedure of geopolymers should begin with the preparation of geopolymer paste (e.g., fly ash and liquid hardener/activator). The next step should be the addition of less active precursors or fillers such as marble waste. Otherwise, the silicate present in the activators will not fully engage in the chemical reaction and will remain inside the mixture. This will result in glossy surfaces after the curing process since the unreacted silicates will move to the surface of the sample [14].
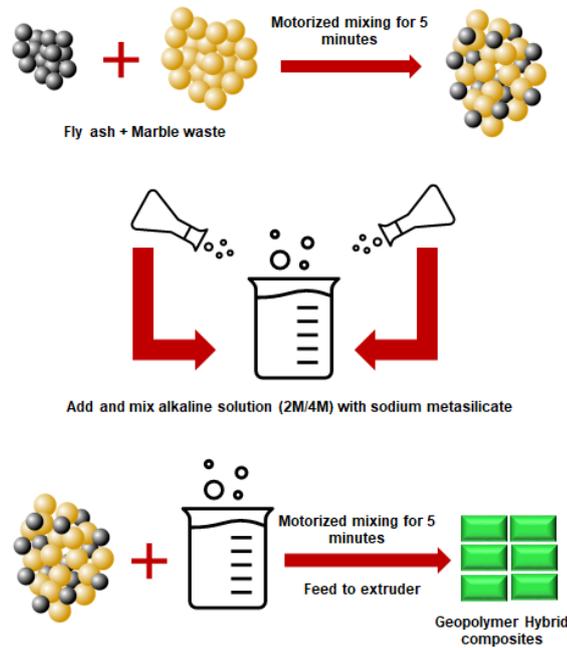
Figure 4.4. Mixing procedure for marble-based geopolymer cement, reproduced with permission from [143].

4.3.5 Iron Ore

Iron ore tailings are produced in vast amounts during iron extraction and mining process. Studies have proposed different methods for incorporating mine tailings into geopolymer binders and cements. For instance, the application of iron ore tailing as fine aggregates into mortar made with fly ash was investigated. The maximum compressive strength obtained was 8.27 MPa after 28 days of curing [144]. The production of geopolymer bricks using iron ore tailings was also investigated by different researchers [103,145]. One of the major advantages of producing geopolymer bricks is the avoidance of using high-temperature kiln firing used during traditional production procedures. For instance, geopolymer bricks achieved high compressive strength of 50.53 MPa when cured at 80 °C for 7 days [145]. The authors stated that the produced bricks met ASTM and Australian standard requirements set for bricks. In addition to geopolymer bricks,

the possibility of producing lightweight aggregates using iron ore and foam-gel casting technique was investigated [146]. The behavior of iron ore tailing geopolymer samples exposed to different heat-cooling cycles of up to 800 °C was monitored [147]. The samples were made by replacing 10, 20, and 30% (IOT10, IOT20, IOT30) of the fly ash with iron ore mine tailings. The authors stated that the addition of more than 20% of iron ore tailing could significantly increase the setting time of the geopolymer cement. In addition, the loss of compressive strength at different thermal cycles were lower in sample made with iron ore tailings compared to those of the control samples (Figure 4.5).
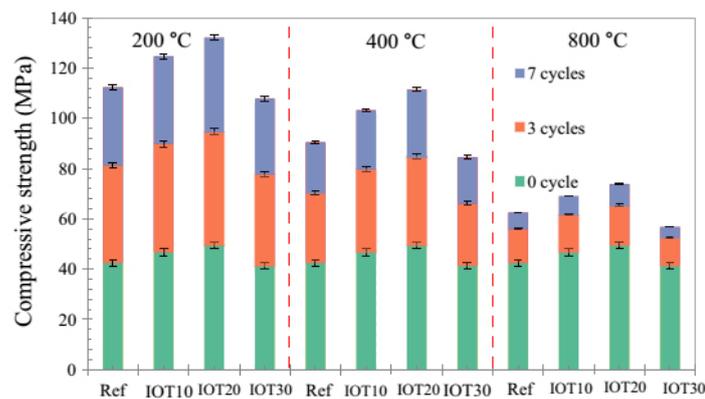
Figure 4.5. Compressive strength of iron ore tailing based geopolymers exposed to different heat cycles, reproduced with permission from [147].

4.3.6 Gold and Copper Ore

The immobilization of heavy metals is one of the major priorities in gold mine waste management. Because of its effective capability, geopolymers are widely used as a tool to reduce the impact of heavy metal leaching on the environment. Therefore, various studies have used geopolymers to encapsulate gold mine wastes [148–150]. A recent study evaluated the possibility of using gold mine tailing obtained from Finland as a precursor [151]. The Si/Al and the Na/Al ratios ranged between 2.5–3.5 and 0.8–1.5, respectively. The authors investigated

leaching values after 7, and 28 days and 18 months. The geopolymer leaching values for the most problematic elements including As, Sb, B, and V were reported to be very low after 18 months of curing. The addition of slag to gold mine tailings allowed for room temperature curing which is in accordance with similar studies [148]. The studies on heavy metal leaching have been followed up by applying a response surface method to better understand the properties of samples made with gold tailings [152].

Copper mine tailings have been used in different applications. Ahmari et al. (2012), mixed NaOH with copper tailings [153]. The aim was to produce suitable alkaline activated material to be used as base layer in pavement construction. The results indicated that the correct amount of NaOH could increase the unconfined compressive strength of the samples compared to the reference material. The findings were similar to a work conducted by Manjarrez et al. (2018) [114]. It was suggested that using appropriate moisture content and NaOH concentration could produce geopolymers, which could satisfy the strength requirements for cement treated-base specified by various road agencies in the United States. The potential of using copper tailings in different applications was examined through different literature. Cement kiln dust (CKD) was added to bricks made with NaOH and copper tailings [154]. It was shown that the addition of CKD significantly improved the durability and mechanical properties of the mixtures. Another application of copper tailing was to produce lightweight aggregates where it was used in cement and mortar mixtures. Compared to LECAs, the lightweight aggregates showed higher mechanical properties and density [120]. The Si/Al and Na/Al ratio of copper waste geopolymers were enhanced by the addition of aluminum sludge [155]. As expected, the addition of aluminum and

optimum amount of NaOH significantly increased the compressive strength of the samples.

4.3.7 Phosphate, Lithium, and Basalt

Most of the tailing mines may be rich in Si and Al elements. However, the reactivity of the material used as precursors is also an essential parameter. One method of increasing the reactivity of the precursors is to calcine the mine tailings. For instance, the effect of thermal treatment on phosphate, kaolinite, and lithium mine tailings was investigated [156]. Regarding lithium tailings, even calcination did not result in a proper dissolution of material and therefore, the authors were not able to examine the mechanical properties (Figure 4.6).
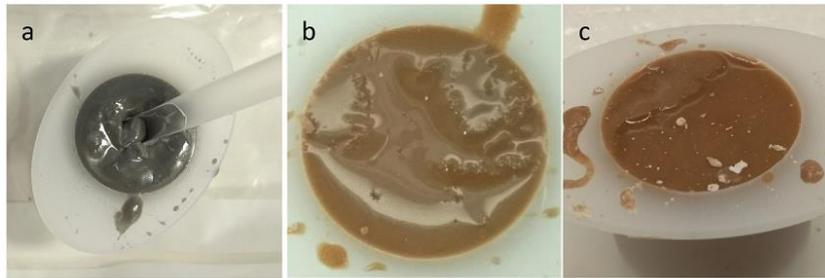
Figure 4.6. Lithium geopolymer calcination at different temperatures (a) not calcined, (b) calcined at 750 °C, (c) calcined at 900 °C, reproduced with permission from [156].

On the other hand, the best results were observed at calcination temperature of 700 °C for both kaolinite and phosphate mine tailings [156]. Currently, efforts are being made to better understand and evaluate the most determinant and critical parameter that affects the mechanical and chemical properties of geopolymers. For example, statistical analysis is being more frequently applied to aid the identification of important parameters. In this line, the results of the response surface method study indicated that curing temperature was the most critical factor related to the strength of material [157].

Basalt is an igneous rock widely available in the earth's crust, where its high recyclability and low impurities have allowed it to be used in various applications [158]. Because of its high alumina and silica content, geopolymers containing basalt precursors have become an interesting topic for various researchers. However, in most cases, the focus has been on basalt fibers and less attention has been paid to basalt powders. It is obvious that the using basalt waste would be much more cost-effective than using raw and virgin material. Waste basalt powder has been used for producing geopolymer bricks and artificial lightweight aggregates. Different ratios of sodium hydroxide and silicates were mixed with MK and basalt powder [43]. A liquid to solid ratio of 0.75 and curing of 24 h at 70 °C achieved the highest compressive strength of 64 MPa. Regardless of precursor type and amount, the activators have either contained sodium hydroxide and sodium silicate or they have only contained one type of hardener. For instance, other studies were conducted on geopolymer-containing basalt and only sodium hydroxide was used as an activator at different activator/precursor ratio from 0.1 to 0.5 [159]. In addition, basalt was obtained as raw material and was milled to a very fine powder. Curing conditions similar to the previous works were applied. The Si/Al ratio of the samples were fixed at 2.8, which produced the maximum compressive strength of 57 MPa. Comparing the results from the two studies suggests that the reduction in mechanical properties could be related to the difference between the alkaline solutions of the studies, where the latter had only used NaOH for its activator rather than a combination of sodium silicate and NaOH. A separate study investigated the possibility of producing novel low impact porous pavement layers using synthetic aggregates [94]. The aggregates were made of geopolymer paste containing 10 M NaOH, sodium silicate, waste

basalt powder, and metakaolin. The curing time and temperature were 12 h at 60 °C, which returned the highest compressive strength of 65 MPa.

4.4 Precursor Pre-Treatment and Calcination

Because of the crystalline nature of various tailings, calcination or thermal treatments have been widely used as a step toward achieving high-performance geopolymer cements and binders [137,138,156,160–162]. Three major calcination methods are used at industrial stage which include rotary furnace, multiple earth furnace and flash calcination plants. The methodology behind each method is different. However, the flash calcination plants have gained favorable attention due to their efficiency and relatively lower energy consumption. The overall process of the flash calcination method for MK production is illustrated in Figure 4.7.
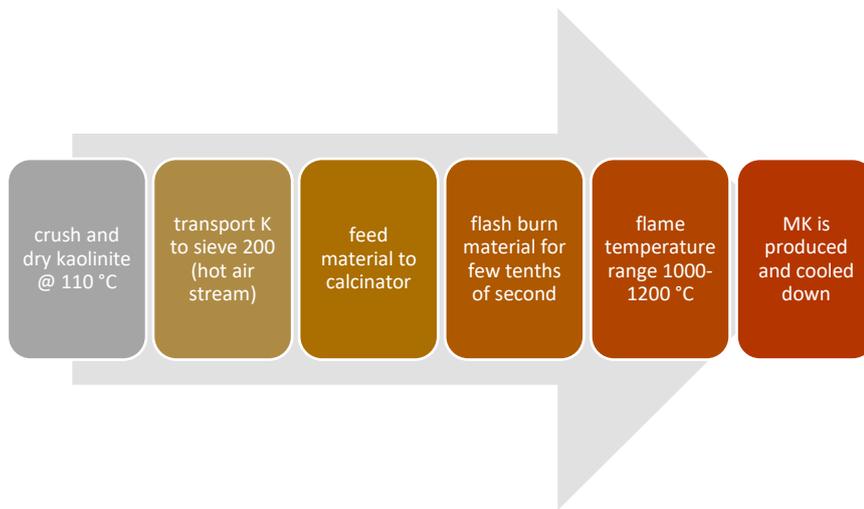
Figure 4.7. Flash calcination of MK, adapted from [163].

However, the calcination process at the laboratory stage is mostly done with the aid of static furnaces, which can normally heat materials up to 1200 °C. In some cases, the heating rate during calcination is reported. Therefore, at least three important parameters could affect the laboratory calcination of materials, which

include the temperature of calcination, heating rate, and calcination duration. It has to be noted that overcalcination could decrease the reactivity of the materials due to the formation of inert crystalline structure. Fast cooling of calcined material is suggested since it could avoid crystallization of the raw material during the thermal treatment. It was for this reason that the calcination of mining waste was quenched in water after being exposed to high temperatures for a certain amount of time (Figure 4.8) [137]. In most calcination procedures, small details could help with the reproducibility of the test for future studies. For instance, one method is to put the samples inside the furnace and then start the calcination process. In this case, a certain time is required to pass for the furnace to reach the target temperature. Then the sample is calcined for a desired duration. Finally, the sample will remain inside to reach room temperatures. However, if the sample is placed in the oven only when the target temperature is reached and is immediately taken out after the desired calcination period has finished, the duration for which the sample is calcined would be significantly different compared to the first method [115].
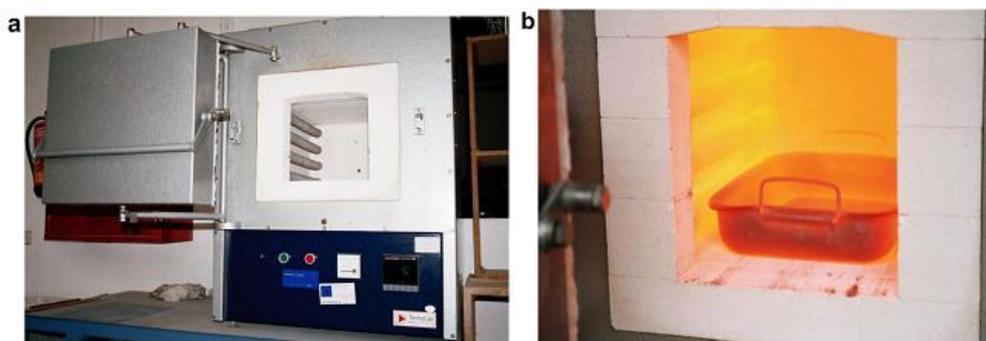
Figure 4.8. Calcination method for tungsten mine tailing, (a) furnace, (b) quenching of material, reproduced with permission from [137].

The production of geopolymers containing clay and silt is highly dependent on the reactivity of the clayey material in question. Therefore, various researchers

have attempted to calcine the clay sediments at different times and temperatures to achieve durable geopolymer cement [162–166]. An increase of calcination temperature from 400 to 750 °C resulted in higher leaching of Si and Al. Consequently, enhanced mechanical properties were observed [162]. In most cases, the effective calcination temperature ranged from 600 to 800 °C.

The calcination is not only limited to the precursors. In some cases, attempts have been made to calcine the solid part of activators such as NaOH with different precursors such as copper [167], gold [152], phosphate [122], quarry stone dust [108], and vanadium [100,168]. This method is referred to as alkaline fusion where the NaOH pellets are added to the precursors at different weight ratios. Usually, liquid sodium silicate or water is then added to the mixture to start the geopolymer reaction. The fusion temperature for the reviewed papers ranged from 450 to 800 °C for a maximum of 2 h.

4.5 Curing Conditions

Heat curing for an appropriate time and temperature is highly suggested for geopolymers containing low-calcium content. The heat treatment aids the chemical reaction occurring in geopolymer paste and increases geopolymerization process. For instance, the durability of geopolymer mixtures produced with calcinated tungsten waste mud were evaluated at different curing conditions. In the first stage, the samples were either cured at room or elevated temperature of 130 °C between 7 and 28 days. The samples were then placed in water baths for different durations ranging from 0 to 91 days. The study revealed that all samples disintegrated when introduced to water. However, samples cured at 130 °C or cured for longer period showed higher durability. In addition, a significant loss in strength was observed within the first 4 week of water

immersion, where the UCS decreased to 1–3 MPa. The low durability in all cases were possibly related to an incomplete geopolymer process/reaction. Moreover, the reactivity of the materials in use may not have been efficient for geopolymer production. Lastly, it was suggested that higher curing temperatures could speed up the initial reactions in geopolymer network, since samples cured at 130 °C showed better durability than room temperature-cured samples [169]. Curing can be achieved through a steam or dry heating system. However, it was noted that the dry curing method showed 15% higher compressive strength than that of steam-cured geopolymer concrete [170]. Figure 4.9 demonstrates the effect of both curing days and temperature on the compressive strength of vanadium-based geopolymers [110]. The samples were cured in an oven for 24 h. Higher curing time and temperature resulted in higher compressive strength.
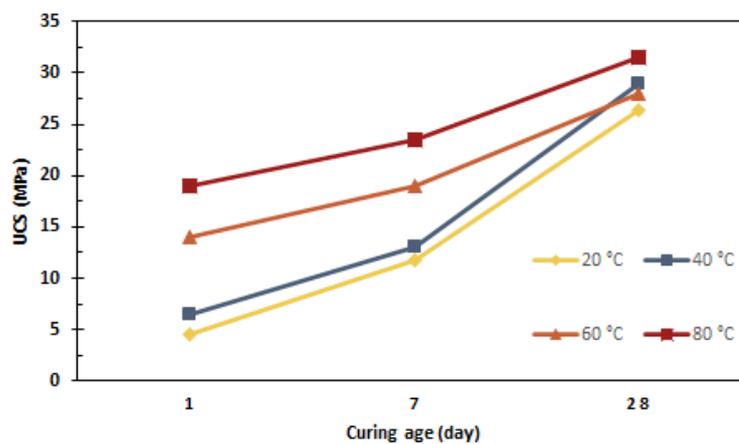
Figure 4.9. Effect of curing days and temperature on the compressive strength of vanadium mine tailing based geopolymers [110].

Different curing times and temperatures have been used in various studies. For instance, curing was used prior to and after the demolding of geopolymer samples. The geopolymer paste was prepared and cured in an oven for 40 or 60 °C for 24 h. The de-molded samples were then subjected to the same curing

temperature for a duration of 7, 14, and 28 days. It was indicated that higher curing temperature and duration resulted in higher compressive strength of the material, where the highest UCS of 14.78 and 20.49 were reported for samples cured for 28 days at 40 and 60 °C, respectively [171]. In some cases, the effect of different curing duration was observed. For example, the curing temperature was kept constant and the effect of different curing durations of 1, 3, and 5 h was investigated on the performance of fly ash geopolymers [112]. The authors found the curing temperature of more than three hours challenging for its implementation in a real construction site. A higher curing temperature of 80 °C for 5 h was suggested to have the best effect on geopolymer compressive strength reaching to 19.2 MPa. Curing duration of more than 24 h decreased the overall geopolymer compressive strength [124]. It is evident from the literature that both curing time and temperature could directly affect the mechanical properties of geopolymers. In a different attempt, samples were cured both in water and at room temperature for different durations [172]. The samples underwent three different curing conditions that included curing at room temperature, the curing in an oven at 45 and 75 °C for 24 h. The samples were then de-molded and half of them were cured inside water for 90 days. The authors indicated that temperatures up to 75 °C can increase the hardening process of the samples. However, wet curing method was excluded because of high efflorescence (Figure 4.10).
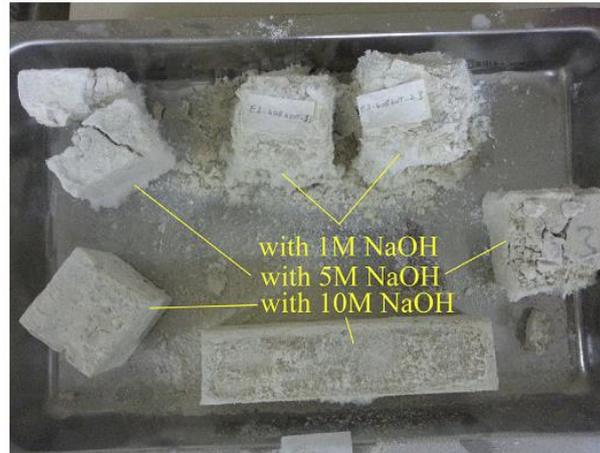
Figure 4.10. Wet-curing of marble geopolymer cement, reproduced with permission from [172].

Achieving the highest compressive strength as possible could be the main goal for most studies and projects. However, the sustainability and cost-efficiency of any proposed approach should also be taken into consideration. Based on the literature, it was indicated that temperature and curing conditions could increase the ultimate strength of the geopolymers. Unfortunately, higher temperatures and longer curing conditions consume much more fuel and energy compared to those samples which are cured at room temperature. Consequently, the overall cost of projects and research applying these methodologies will inevitably increase. In addition, the implementation of different curing conditions may not be applicable on a real scale in most project sites.

4.6 Mechanical and Chemical Properties

Engineering properties such as compressive strength, density, durability and acid resistance, water absorption, and abrasion of geopolymers containing mining waste were investigated by different studies. Unconfined compressive strength (UCS) is the most common mechanical property that has been investigated in the literature. The impact of different parameters involved in geopolymer production

on UCS has been reported by various authors. This includes the effect of precursor type and ratio [31,34,45,46,83,111], calcination [137,162,163,165,166], activator blends [96,99,124,136,173], liquid to solid ratio [104,105,110,174], Si/Al and Na/Al [155,175,176], and curing conditions [135,169,177]. For geopolymerization, Si/Al lower than 3 is suggested since higher ratios would create linear structures rather than a 3D structure. In addition, one of the most important methods of controlling the leaching of geopolymers is to have a chemically stable structure. This is achieved by reaching a Na/Al of 1 in the geopolymer mix.

Different types of mine tailings waste can provide unique physical strength and properties to geopolymers when combined with the common precursors such as metakaolin, blast furnace slag, and fly ash. Studies on geopolymer produced with copper highlighted that the compressive strength of the samples varied significantly when metakaolin was added as a precursor in the mix design. The maximum compressive strength of 23 MPa was obtained substituting 38% of the total weight with MK. With similar curing conditions, the compressive strength dropped to 18 MPa when the exact amount of MK (38%) was replaced with the blast furnace slag [111]. However, in a separate study, only copper tailings were used [171]. In this case, the highest achieved strength was reported to be 15.70 MPa for samples cured at 60 °C. The difference between the compressive strength of the mentioned studies could be related to the presence of MK and the difference in activator content. Only sodium silicate with different concentrations was used by Falah et al. [171], whereas Paiva et al. [111] used a combination of sodium silicate and 10 M sodium hydroxide as activators. Similar activator content of SS and 10 M NaOH was used for producing lightweight aggregates and paving blocks using basalt powders and MK as precursors [43,94]. With very

similar curing conditions, only basalt was activated using NaOH for the production of microcrystalline particles [159]. Samples that benefitted from MK and a combination of both SS and SH [43,94] presented higher compressive strength.

The density of geopolymer made with quarry dust and waste glass was investigated [178], where the addition of geopolymer cement to the soil was able to increase the maximum dry density of the final mixture. In a separate work on the bulk density of fly ash geopolymer [112], the highest obtained value was related to samples made with NaOH (12 M) and sodium silicate, which were cured for 1 h (Figure 4.11).
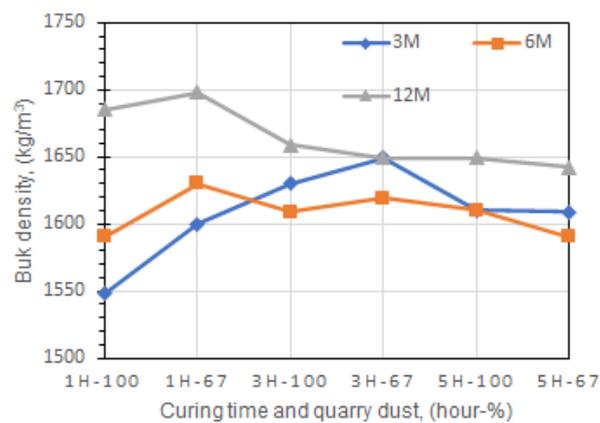
Figure 4.11. Bulk density-curing time waste glass-based geopolymers, reproduced with permission from [112].

Durability is an important aspect of geopolymer science, which has been studied by various researchers [141,145,169,179,180]. One method of studying the durability of geopolymers is for example to immerse the samples in water for a period of 24 h. Doing so would give an overall view of the effect of water immersion on the physical properties of the sample. It was understood that most

of the partially alkali-activated specimens were disintegrated after being submerged in water for a period between 0 and 90 days [169]. The key to obtaining a geopolymer structure that would behave similarly to ordinary Portland cement during wet curing conditions is to achieve a chemically stable state. This is obtained by satisfying the required Si/Al and Na/Al ratios [14]. The durability of geopolymers in terms of resistance against sulfide and acidic attacks was also covered by the reviewed literature [138,139]. In this regard, 50 mm cube samples were cured in sulfuric, hydrochloric, and nitric acid solutions for 28 days [139]. The results indicated that both acid and precursor type affected the overall outcome. Acid attacks are observable as weight loss of samples.

Among the reviewed context, less attention was paid to the abrasion and thermal resistance properties of geopolymer samples. The abrasion for geopolymer samples was assessed by calculation of weight loss of samples subjected to 1000 cycles in the Los Angeles Machine [138]. The obtained data indicated higher abrasion resistance of geopolymer samples made with tungsten mining waste than those of ordinary Portland cement. Regarding the resistance of geopolymer specimens against intense thermal cycles, it was shown that the compressive strength of all samples was significantly dropped [147]. However, the experimental data showed that the addition of iron ore tailing had increased the thermal resistance of the samples compared to the sample made with fly ash.

It is noteworthy, that every mine tailing has its own unique mineralogy and reactivity rate, which differs from source to source and type to type. XRF (X-ray fluorescence) and X-ray powder diffraction (XRD) has been frequently used by various studies to determine chemical oxidation and mineralogy (crystalline phase) of geopolymers, respectively. The obtained data are of paramount

importance since they could indicate Si/Al and Na/Al of the final geopolymer mixture. For instance, XRD analysis for tungsten mud waste showed that the crystalline phase (quartz and muscovite) was not changed after the polycondensation process [17]. Furthermore, the XRF analysis indicated a decrease of Na_2O concentrations for samples submerged in water (7–91 days). Since Na^+ cations did not fully react within the geopolymer network and the excess NaOH activator was dissolved in water (Na/Al $\neq$ 1) and because of the presence of crystalline phase after the addition of alkaline solution, the authors suggested that the geopolymer reaction was not fully completed. The outcome was excessive leachate of Na^+ cations freely interacting with water.

The addition of 20% iron ore tailing to fly ash-based geopolymer decreased the porosity and microcracking of samples [18]. Thus, the denser microstructure provided better thermal resistance compared to samples with no iron ore tailings. Scanning electron microscope (SEM) was used to evaluate the microstructure of tungsten mining waste-based hybrid alkaline materials [19]. The optimum mixture containing 10 M sodium silicate and potassium hydroxide as alkaline solution showed a maximum UCS of 29.2 MPa. The compact structure showed the presence of gehlenite hydrates and small cracks were observed because of rapid synthesis of the binder. The outcome suggested that the microstructure of the mixture could be influenced by the molarity and type of activators used for geopolymer production. Adesanya (2020) investigated the effects of mechanical activation on phyllite's chemical and microstructure properties [20]. The mechanical milling was conducted for 9 and 15 min. The XRD analysis indicated a continuous breakdown of the crystalline phase related to muscovite and chamosite. However, Albite and quartz had no significant change in terms of their crystalline structure after the milling process. It was noted that the amorphous

phase had increased by 47% wt. The study concluded that the mechanical activation had led to higher solubility of Si and Al in alkaline solutions.

4.7 Conclusions

The applications of various quarry and mine waste for geopolymer production in the past ten years have been reviewed. The extracted data including authors, publication year, type of precursors, activators, activator to precursor ratio, curing conditions, Si/Al, (Na, K)/Al, UCS, and the mineralogy of the mine tailings are presented in Table 4.3. The following conclusions could be drawn from the reviewed literature:

- The type of precursor has a direct impact on various mechanical and chemical properties of geopolymers. Inert waste dust could act as a filler/aggregate in the geopolymer structure, whereas reactive quarry waste could act as a precursor in the geopolymer matrix. Therefore, the mineralogy of the precursor being used must be studied.

- The mineral waste was used as a precursor to produce geopolymers. In addition, some studies used the waste-based geopolymers to create artificial aggregates. In both cases, promising results were observed.

- The addition of Mk, GGBFS, and fly ash to quarry/mine waste could improve the geopolymer network by satisfying Si/Al and Na/Al ratios.

- Thermal treatment of mineral waste has proven to increase the amorphous phase and reactivity of the material providing better dissolution of Si and Al in alkali mediums. For instance, some silt and clay materials are rich in quartz and have less reactivity due to their crystalline structure. Calcination could modify the structure and provide a better source of reactive material.

- Based on the literature, different activator-related variables could affect the final properties of geopolymer cements and binders. These parameters include alkali cation type (Na+, K+), soluble silicate alkalinity, the molarity of the activators and hydroxide to silicate ratio. In addition, the solid to liquid ratio, Si/Al and (Na+, K+)/Al ratio also influence the final mixture properties.

- Potassium silicates are less viscous and provide higher compressive strength compared to the more common sodium silicates.

- Curing samples at elevated temperatures increases the reaction rate of geopolymers. Ambient temperature curing has also been practiced in different studies, which have shown acceptable outcomes. Room curing temperature could be aided by including GGBFS in the mixture.

- Water-curing of geopolymer samples has shown adverse effect on the mechanical properties and durability of produced samples. Backed up by various studies, excessive leaching has been related to incomplete polycondensation of the geopolymer network. Excess alkali solution interacts with water and appear as white powder on the surface of products.

- The microstructure of geopolymers could be affected by molarity and type of alkali solution. In addition, mechanical and thermal treatments have shown to change porosity and chemical structure of geopolymers.

- The following recommendations have been proposed:

- A standard method for geopolymer production including step-by-step procedures on selecting proper precursors could be proposed. Geopolymer specific standards for leachate tests as well as in-depth chemical analysis (NRM, FTIR, and XRD) could be included.

- Since various parameters affect the overall performance of geopolymers, acquiring a full understanding of all the involved parameters is very difficult. In this regard, applying statistical methods such as design of experiments (DOE) could reduce the overall time required for understanding the relations between various factors. Moreover, statistical analysis could also provide mathematical modeling that could fine-tune geopolymer mix design and enhance the final performance.

- Using ambient temperature curing systems will facilitate industrial implementations. Most of the proposed mix designs for geopolymers can only be conducted at laboratory scale and industrial aspects have not been foreseen. For instance, heat curing is being widely used in almost every study related to geopolymers. However, curing every produced geopolymer sample at manufacturing plants would dramatically increase the final production costs of geopolymers.

- Considering the cost of metakaolin and alkaline solutions, every effort should be considered to reduce the final cost of geopolymers. Thus, it would be more appropriate to select local raw/waste material which will eliminate transportation and material costs giving geopolymers a more competitive market.

- User-friendly alkaline solutions should be used more frequently.

- The mixing procedure should start with creating the binder. The binder consists of reactive precursor such as MK and the hardener/activator. The mixing should then continue with the addition of less reactive materials such as mineral waste and mine tailings.

Table 4.3. Summary of reviewed studies on geopolymer cement and binders containing mine tailings.

Ref.	Year	Precursors	Activators/Mix Design	A/P	Curing	Si/Al, Na, K/Al	UCS MPa	Mineralogy/Chemical Composition
[177]	2018	Antigorite	SiO_2/Na_2O = 2.25	0.25	24 h @RT 1, 7, 28 d	N/A	49 15-wet cure	Serpentine, talc, olivne, pyroxenes, amphiboles, magnetite
[94]	2019	Basalt, MK	SS, SH 10 M, SiO_2/Na_2O = 1.99, SS/SH = 4	0.75	12 h @ 60 °C	N/A	65	N/A
[43]	2019	Basalt, MK	SS, SH 10 M, SiO_2/Na_2O = 1.99, SS/SH = 4	0.75	24 h @ 70 °C +3–28 d	N/A	64	N/A
[159]	2017	Basalt	NaOH	0.1–0.5	24 h @ 80 °C	Si/Al = 2.8	57	Plagioclase, clinopyroxene, olivine, and magnetite
[181]	2019	Boron, calcined	Sodium silicate consisted of 8% Na_2O, 27% SiO_2, and 65% H_2O by mass NaOH	~0.40	Heat treatment cycle	N/A	38	Colemanite, hydroboracite, illite, montmorillonite, calcite, and quartz
[171]	2019	Copper	SiO_2/Na_2O = 3.2 6 M	0.23	7, 14, 28 @ 40, 60 °C	10–38 Si/Al 0.45–2.80 Al/Na	6.44–15.70	Tremolite, chlorite, quartz, talc, magnesium silicate hydrate, dolomite, and calcite
[111]	2019	Copper, slag, MK	SS, SH 10 M	0.1 + water	7 d @ 20 °C	Si/Al = 2 Na/Al = 1	4–45	Piryte, anhydrite, caldecahydrite, quartz
[101]	2019	Copper	NaOH 5, 10, 15 M, SS/SH 0, 0.5, 1.0, 1.5	0.158	45–85 °C, 7 d	~3–5 Si/Al	23.5	Quartz, gypsum, and albite
[114]	2018	Copper	NaOH, 0, 3, 5, 7, 11 M	11–19% water	7 d @ 35 °C	Na/Al 0.3–1.1	5.32	Quartz, gypsum, albite, sanidine
[167]	2017	Copper, calcined	NaOH @ 550–650 °C	N/A	N/A	Leaching test	N/A	Quartz, albite, chlorite, dolomite
[120]	2017	Copper, zinc, fly ash, gold	SS, SH, SiO_2/Na_2O = 2.5	W/c 57–63	28 d @ RT	N/A	~30	N/A
[182]	2015	Copper, slag	NaOH 15 M	16% water	7 d @ 60, 75, 90, and 105 °C	1.8–3.2 Na/Al	75	Quartz, albite, sanidine, gypsum
[155]	2015	Copper, aluminum sludge	SH	0.8–1.3	7 d @ 90 °C	0.08–6.75 Si/Al 0.34–1.3 Na/Al	~45	Quartz, albite
[154]	2013	Copper, ckd	NaOH 15 M	12–20%	7 d @ 90 °C	3–14 Si/Al 0.8–3.0 Na/Al	~50	Albite, gypsum, quartz, sanidine
[179]	2013	Copper	NaOH 15 M	16% water	7 d @ 90 °C	7.76 Si/Al 0.86 Na/Al	~35	Albite, gypsum, quartz, sanidine

Ref.	Year	Precursors	Activators/Mix Design	A/P	Curing	Si/Al, Na, K/Al	UCS MPa	Mineralogy/Chemical Composition
[127]	2012	Copper	(SiO2/Na2O) of 3.22 NaOH 5, 10, 15 M	33% water	60–120 °C 7 d	1.67–8.88 Si/Al 0.96–2.82 Na/Al	N/A	Albite, gypsum, quartz, sanidine
[183]	2012	Copper	NaOH 10, 15	8–18%	60–120 °C 7 d	0.86–1.94 Na/Al	33.7	Albite, gypsum, quartz, sanidine
[153]	2012	Copper	NaOH/copper 0, 2, 4, 6%	15%	7–90 d, RT	N/A	~3	N/A
[132]	2019	Garnet, MK	SiO2/Na2O = 3.1 NaOH, SS	0.43	−20–80 °C −3 days	Garnet has less 2% Si, Al release	46	Grossular, andradite, dolomite, calcite, quartz, almandine, boehmite
[152]	2019	Gold, Al2O3	SH+gold @ 550 °C for 1 h +SS	N/A	3 days Temp based on RSM 25–89 °C	14.6 Si/Al	N/A	89.25% SiO2, 6.1% Al2O3, 1.24% K2O, 0.84% Fe2O3, 0.29% mgo, 0.09% SO3
[175]	2019	Gold	NaOH, KOH 2–10 M Good for paper	0.1–0.5	N/A	Leaching tests	N/A	N/A
[184]	2019	Gold	10 M KOH, KS, KA KS:KH 0–2	0.26	5 days @ 80, 100 °C	N/A	18	Silicon dioxide (SiO2), magnesium oxide (mgo), aluminum oxide (Al2O3), potassium oxide (K2O), and ferric oxide (Fe2O3),
[151]	2018	Gold, MK	NaOH 8, 9 M SiO2/Na2O = 3	N/A	28 d @RT	1.8–2.6 Si/Al Na/Al = 1	N/A	N/A
[148]	2018	Gold, MK, slag	NaOH 8 M, SS/SH = 1.25 SiO2/Na2O = 3.0	N/A	24 h @ RT 7, 28 d	Leaching test	N/A	N/A
[150]	2018	Gold	Leaching test	-	-	-	-	Quartz, chlorite, magnetite, jarosite, pyrophyllite, albite, clinochlore, sepiolite
[149]	2016	Gold, slag	NaOH 5, 10, 15	0.17–0.25	28 d @RT	N/A	22	Albite, gypsum, quartz, dolomite, pyrite, sodium aluminum silicate
[113]	2019	Iron, wool glass	NaOH 8 M, 10 M, and 12 M Mechanical activation	0.27	7 d @100 °C	4.59 Si/Al	112.8	Chamosite, Chantalite, Quartz, Geothite, Hematite
[144]	2018	Iron, fly ash	SS, SH 10 M, SS/SH = 2.5	0.4–0.8	14, 28 @ RT	N/A	8.27	N/A
[146]	2018	Iron	Silicate cement, NaOH,	0.7–1.0	12 h @RT	N/A	5.18	N/A
[145]	2016	Iron, brick picture	SiO2/Na2O = 3.58	30%	3 d @ 80 °C Combination	N/A	50.35	Quartz, goethite, aluminian, birnessite, and sodian
[104]	2011	Iron, Slag	SS, SH 10 M, SS/SH = 0.5 SiO2/Na2O = 3.6	0.35	7 d @ 30 °C	N/A	63.79	Quartz
[147]	2016	Iron, fly ash	NaOH 10 M, SiO2/Na2O 3.2, SS/SH mass ratio = 9.14	0.5	28 d @ RT	N/A	50	Anatase, antigorite, albite, amphibole, calcite, chlorite, dolomite, gypsum, quartz hematite, mullite, muscovite, pyrite

Ref.	Year	Precursors	Activators/Mix Design	A/P	Curing	Si/Al, Na, K/Al	UCS MPa	Mineralogy/Chemical Composition
[156]	2019	Lithium, phosphate, mk	SS, SH	4	24 h @ RT	Leaching test	~16	Calcite, phlogopite, muscovite, quartz, kaolinite, albite, microcline
[143]	2019	Marble, fly ash	SS, SH 2,4 M, SS/SH = 1	0.22–0.3	24 h @ 70 °C +7 days	N/A	6.52	Calcite, dolomite, quartz
[119]	2018	Marble, gypsum, fly ash, clay	SS, SH 8 M, SS/SH = 5	N/A	28 d @ RT	N/A	52	N/A
[185]	2017	Marble, slag	SiO_2/Na_2O = 0.96–1.40 NaOH, SS	0.4	28 d @ RT	N/A	42–60	N/A
[172]	2016	Marble	NaOH 1, 5, 10 M	~0.5	24 h @ 20, 45, 75 °C +2–90 d	Si/Al > 3	Wet curing	Quartz and zeolite
[122]	2019	Phosphate, MK	(NaOH + phosphate) calcined @550 and 800 °C + SS	0.4	−24 h RT −4 h @ 60 °C −28 days RT	2.4 Si/Al @550 °C 3.61 Si/Al @800 °C	40	34.09% fluoroapatite, 12.44% quartz, 11.15% calcite, 9.45% dolomite, 9.46% illite, 21%, palegorskite, 1.4% hematite
[186]	2020	Phyllite	SS, SH	0.29	−RT, 60 °C −7 and 28 days	0.45 for Si/Al	2–25	Quartz, muscovite, chamosite, albite
[112]	2019	Fly ash, quarry dust	SH 3, 6, 12 M SS/SH = 2	0.72	1, 3, 5 h @ 80 °C	N/A	19.2	Calcite mineral as well as dolomite, carbon and other minerals
[187]	2018	Red mud, mk, RHA	NaOH 5 M, SS/SH = 4	0.97	24 h @ 70 °C 60 d	3.85, 4.30, 4.45 and 5.30 Si/Al	30	Hematite, goethite and sodalite
[173]	2018	Silt, Fly ash, slag	SH, KH, 8 M, SS, KS	1	3–28 d	Leaching test	8	N/A
[166]	2017	Clay, calcined	NaOH 14 M, SiO_2/Na_2O = 3.2	0.63–1.88	24 h @ 20, 60 °C 21 d	Na/Al = 0.85 Si/Al 3.64–5.03	22.9	Quartz, calcite, kaolinite, illite, smectite, and albite
[135]	2017	Silt	SH	10% water	Air and wet cure	N/A	~12	Quartz, sodalite, albite, calcite, microcline
[96]	2016	Loess, fly ash	NaOH, KOH,	0.2–0.7 water	RT	Si/Al = 2–3	113.8	Muscovite, nimite, quartz, albite, calcite
[188]	2016	Quartz, clay, MK	KS, KH	0.3–0.34	1, 7, 28 d @ RT	N/A	~20	Quartz
[189]	2015	Clay	SS, SH, KOH	0.5	3–28 d @40, 80 °C	Si/Al = 2	7.58	Montmorillonite, alkali feldspar, and quartz
[165]	2015	Silt, calcined	Sodium and potassium aluminate 8–17 M Combination	N/A	15 min–28 d @ 60 °C	Al/NA = 0.647 Al/K = 0.53	6.7	Kaolinite, smectite, and illite (62% total), quartz (18%), calcite (17%) and feldspars (3%)

Ref.	Year	Precursors	Activators/Mix Design	A/P	Curing	Si/Al, Na, K/Al	UCS MPa	Mineralogy/Chemical Composition
[162]	2015	Clay, slag calcined	SH 5, 7, 10 M SS	0.4	3 d @ 60 °C 28 d	Na/Al = 1 Leaching test	1.7–38.90	Quartz (18%), calcite (17%), feldspars (3%), clay phase (62%)
[97]	2013	Silt, fly ash, slag	NaOH	0.28–1.20	3, 7, 28 d @RT	N/A	N/A	Gismondine, quartz, illite, montmod Uonite
[164]	2013	Silt calcined	NaOH 5 M	N/A	3 d @ 60 °C	Na/Al = 1	N/A	Quartz, calcite, kaolinite, illite/smectite
[109]	2019	Sphalerite, MK	1 mol Na2SiO3 and 12 mol H2O +Pb(NO3)2	0.49	−6 h @ 60 °C −RT for 7 days	N/A	2–15.5	45.72% dolo- mite, 35.26% calcite, 5.22% kaolinite, and 3.69% quartz
[108]	2019	Stone dust, fly ash	Stone dust: NaOH 1:1.6 @ 500 °C	N/A	−24 h @ 30 and 80 °C −RT or water curing for 96 h	N/A	N/A	SiO2 and caco3
[105]	2020	90% tungsten, 10% slag	SH 8 M, SS, SiO2/Na2O = 3.23, KOH 8, 10 M, waste glass	1/3, 1/4	-Primary 60 °C for 24 h −7, 14, 28, 56 and 90 days	~0.45 for Si/Al 0.104–0.214 for Na/Si	~17–33.05	Muscovite and quartz
[106]	2019	Tungsten, glass waste	Foaming agents: Al powder, SDBS, mno2 Dosage of Na2O (3.1%, 3.3%, and 3.5%) 10 M SH+SS	0.22	−40 °C, 60 °C, 80 °C, and 100 °C −7 days	N/A	3.8	Only chemical composition
[98]	2019	Tungsten, glad, MK	SiO2/Na2O = 3.2 NaOH 10 M, SS/SH = 3	0.4	24 h @ 60 °C 28 d	N/A	2.28–16.10	N/A
[128]	2017	Tungsten, glass	SiO2/Na2O = 1.75 NaOH 10 M	0.3	24 h @ 80 °C	3 = Si/Al	61	N/A
[124]	2017	Tungsten	NaOH 10 M, SS/SH = 4	1/3.6	Various combination	N/A	41	Muscovite, silica, sodium aluminosilicate, albite, pyrite
[140]	2016	Tungsten, grout	Na4SiO4 and NaOH 12 M	N/A	7, 14, 28 d, RT	N/A	14.3	N/A
[169]	2012	Tungsten	SS, SH 10 M	0.25	48 h @ RT +water cure 7–28 d	Si/Al = 3–4	~18	Quartz, muscovite
[138]	2010	Tungsten	NaOH 12 M SS/SH = 2.5	1.8%	24 h @ RT	Leaching test	8.4–39.6	Muscovite, quartz
[137]	2010	Tungsten	SH 12 M, SS, sodium carbonate	0.5	7, 14, 28 @RT	N/A	~45	N/A
[110]	2019	Vanadium, MK	NaOH	0.28–0.44	3, 7, 28 d @20–80 °C	N/A	31.5 mpa	Quartz, potassium mica
[107]	2019	Vanadium, MK, calcined	(NaOH + precursor) + water	0.35	7 d @RT	Leaching test	29.0	N/A

Ref.	Year	Precursors	Activators/Mix Design	A/P	Curing	Si/Al, Na, K/Al	UCS MPa	Mineralogy/Chemical Composition
[142]	2017	Vanadium, MK	SS	0.36	7, 14 @ RT	Si/Na/Al = 3:2:1	~25	Quartz, feldspar, plaster, hematite
[100]	2011	Vanadium, MK	NaOH @ 450 °C	N/A	12 h @ 20 °C 7 d	Na/Al = 0.8 1.5–2.35 Si/Al	55.7	quartz, feldspar, diopside
[190]	2011	vanadium	NaOH @ 750 °C 2 h SA	N/A	RT 3 d	6 Si/Al 0.8 Na/Al	36.2	N/A
[191]	2019	Zinc, MK	SS	0.49	6 h @60 °C +7 d	Leaching test	30	Quartz, calcite, andradite

A/P: activator to precursor ratio; UCS: unconfined compressive strength; SS/SH: sodium silicate to sodium hydroxide ratio; SS: sodium silicate; SH: sodium hydroxide; KS: potassium silicate;

KH: potassium hydroxide; RT: room temperature; MK: metakaolin; M: molar; N/A: not applicable.

Chapter 5: Thermally Treated Waste Silt as Filler in Geopolymer Cement

5.1 Introduction

Nowadays, sustainability is a basic principle considered by politicians and many organizations in society. As for the construction sector, there is a growing interest in manufacturing sustainable buildings and infrastructures with high percentages of recycled materials. However, quarries of gravels are still operative and natural aggregates production requires landfill management of the wastes/by-products. Annually, the construction sector demands about 3000 million tons of non-renewable natural aggregates. In 2018 for instance, mining and quarrying waste exceeded 623 million tons [1,20].

During the aggregate manufacturing process, water is used to wash the surface of the aggregates clean of dirt and mud. The water is then pumped out to sedimentation lakes or mine tailings nearby. For instance, during limestone production silt and clay particles are the main substances found in the sedimentation lakes. Clay minerals have the smallest particle size compared with silt and sand. In General, clay particles are formed from two main crystal layers of silica (tetrahedral) and alumina (octahedral) and their configuration, bonding type and metallic ions in the crystal lattice characterizes and separates different clay particles from one another [46]. The materials stored and kept in the sedimentation lakes could become an environmental issue.

Different methods and approaches have been developed over the past few years to reduce the undesirable impact of quarry waste on the environment. For instance, quarry waste has been used in cement mortars [50,58,192] and asphalt pavements [193–195].

A different approach includes recycling mineral fillers and quarry dust in geopolymer cement production [21,49,196–198].

Geopolymer cement is an alternative binder to ordinary Portland cement, which was first introduced by Davidovits in the 1970s during his efforts to produce nonflammable and noncombustible plastics. Geopolymer cements are materials rich in aluminum silicates which are transformed to tridimensional tecto-aluminosilicates structure in an alkaline solution. The geosynthesis is based on the ability of the aluminum ion (6-fold or 4-fold coordination) to induce crystallographical and chemical changes in the silica backbone [14,89]. A geopolymer cement could be made by adding alkali solutions to materials rich in aluminosilicates (such as metakaolin and fly ash).

Various studies have investigated the possibility of using clay and silt substances for geopolymer cement production. For instance, clay and fly ash were used as precursors to produce sustainable geopolymer bricks [199]. For this purpose, 11 different mixtures were produced by substituting different percentages of fly ash (0-100%) with clay. The results indicated that bricks created with 30-60% fly ash had promising physical properties and mechanical strength. In a different approach, Lampris et al, collected waste silt from different washing plants in the UK, which was mixed with metakaolin and fly ash to produce geopolymers [133]. Room temperature curing of the sample made entirely with silt reached 18.75 MPa after 7 days, whereas samples made with silt and metakaolin showed a higher compressive strength of 30.5 MPa. The addition of metakaolin and fly ash improved the geopolymer reaction/process which led to higher compressive strength. The authors suggested that the strength of silt-based geopolymers was enough to be used as aggregates in unbound applications.

During geopolymer cement production, small grain-sized aggregates which have a certain quantity of reactivity are added to reduce brittleness and minimize pore size and shrinkage values of the final mixture. These materials, which are referred to as fillers, partially react with the geopolymer matrix producing stronger networks [14]. For

instance, limestone, marble and basalt powder wastes were used to produce geopolymer composites [200]. The described study claimed that the usage of up to 50% limestone or marble waste powder increased the sample strength. Overall, all mentioned waste powders positively affected the overall strength, abrasion and water absorption of the geopolymer samples. Various inert and/or partially reactive waste materials have been used as fillers. The effect of different fillers such as quartz fume, illitic clay and recycled chamotte material on thermo-mechanical properties of geopolymer was studied [201]. The highest compressive strength for samples made with clay was obtained when 10% of clay was used as filler. However, the best performance in terms of lower porosity and higher strength was observed when 20% of quartz or chamotte was used in the mixture. In a similar study, calcined kaolinitic claystone and potassium silicate hardener was used to produce geopolymer samples [202]. Quartz, corundum, chamotte, and cordierite were used as fillers. The authors claimed that the viscosity of such mixes was low enough to allow the incorporation of up to 65% of filler. The geopolymer samples had a stable structure at an elevated temperature of 1000 °C and the shrinkage of geopolymer samples significantly reduced at high temperatures when the filler was used. The best fillers were corundum or chamotte and performed better compared with the other type of fillers [202].

In some studies, the silt and clay materials underwent thermal pretreatments. Due to the mineralogy and nature of clay, pretreatments could increase the reactivity of the precursors by altering their mineralogical properties. For example, a case study was conducted in a reservoir located in southern Italy aiming at tackling the loss of water storage capacity in the lakes, where alkaline activation of silt residues was suggested as a solution. The results indicated that the clay and silt could be calcined and reused in applications such as a binder, precast elements and bricks through alkaline activation [136]. The calcination of quarry dust reduces the crystalline structure and improves the reactivity of mineral fillers. Calcination requires the quarry dust to be heated at 600-

800 °C for an average duration of 2 hours [162]. However, the calcination temperatures could vary based on the mineralogy, type, or physical properties of quarry waste. For instance, the surface area and particle size were used as parameters to determine the optimum calcination temperature of low-grade clay [203]. The largest specific surface area of 18.43 m^2/g and the smallest median particle size of 16.4 µm were achieved at 550 °C. Therefore, the calcination temperature of 550 °C was selected as the most efficient temperature for the thermal treatment of the low-grade clay.

Quarry waste management has become an important aspect during the past decades and various methods have been proposed for reducing its impacts on the environment. In this regard, geopolymer cement has become an interesting and alternative method for aggregate by-product management. In most cases, waste minerals have been used as precursors in geopolymers production, while the possibility of using the by-products as filler has received less attention. Depending on the mineralogy of the mineral fillers, some may be less reactive and have low Si and/or Al content, which may not be suitable for being used as precursors. However, these materials may have promising performance if used as fillers in geopolymer mixtures. Thus, the main aim of the current study was to investigate the feasibility of including silt (a by-product of limestone aggregate production) in geopolymer cement production as a filler.

Furthermore, considering their final possible application as constructions materials, leaching tests were performed. The construction and/or pavement products are indeed constantly in contact with stormwater produced by rainfall events. These products experience varying stormwater conditions during their lifespan including acidic, or basic pH and different temperatures, depending on the time of the year [204]. This exposure may lead to the release of various organic and inorganic compounds into the stormwater, including heavy metals, nutrients and, for example, polycyclic aromatic hydrocarbons (PAHs) [205,206]. Previous studies have shown that the scale of contaminants released into stormwater from construction materials is comparable to

pesticide contamination in agricultural systems [204,207]. Therefore, the potential of new construction and paving products to release organic and inorganic compounds into the water bodies should be evaluated before their application in roads and buildings. Thus, in this study the potential of the geopolymer for releasing of harmful compounds was investigated through leaching tests, according to the European Commission (EC) Construction Products Regulation (CPR).

5.2 Materials and Methods

Two separate phases were planned for the current study. For the first phase, the aim was to determine the optimum calcination conditions of the waste silt obtained from S.A.P.A.B.A.'s sedimentation lakes in Italy. The second phase focused on determining the optimum amount of silt (%) that could be used in geopolymer cement mixture.

For the first phase, a DOE (design of experiment) was produced, and raw silt was calcined accordingly. A DOE is a branch of applied statistics that is used to plan, conduct, and analyze the effect of different input variables on the desired outcome(s) of a test or process. The selected input variables for the first phase were the calcination temperature and the calcination time, where the outcome was selected as the unconfined compressive strength (UCS). The DOE analysis indicated the best calcination time and temperature that produced the highest strength amongst all of the samples. The obtained data were then compared with mineralogical and environmental tests to determine the optimum calcination conditions of the waste silt.

The second phase, independent of the first section, focused on determining the optimum amount of silt that could be used in geopolymer cement mixtures. However, the optimum silt calcination conditions were taken from the first phase. Consequently, an additional DOE was designed, where the silt and activator type were selected as variables, each having 3 levels/types. The UCS was selected as the outcome variable.

Thus, the effect of the activator type and the silt percentage on the final UCS was studied. The overall workflow for the methodology is depicted in Figure 5.1.
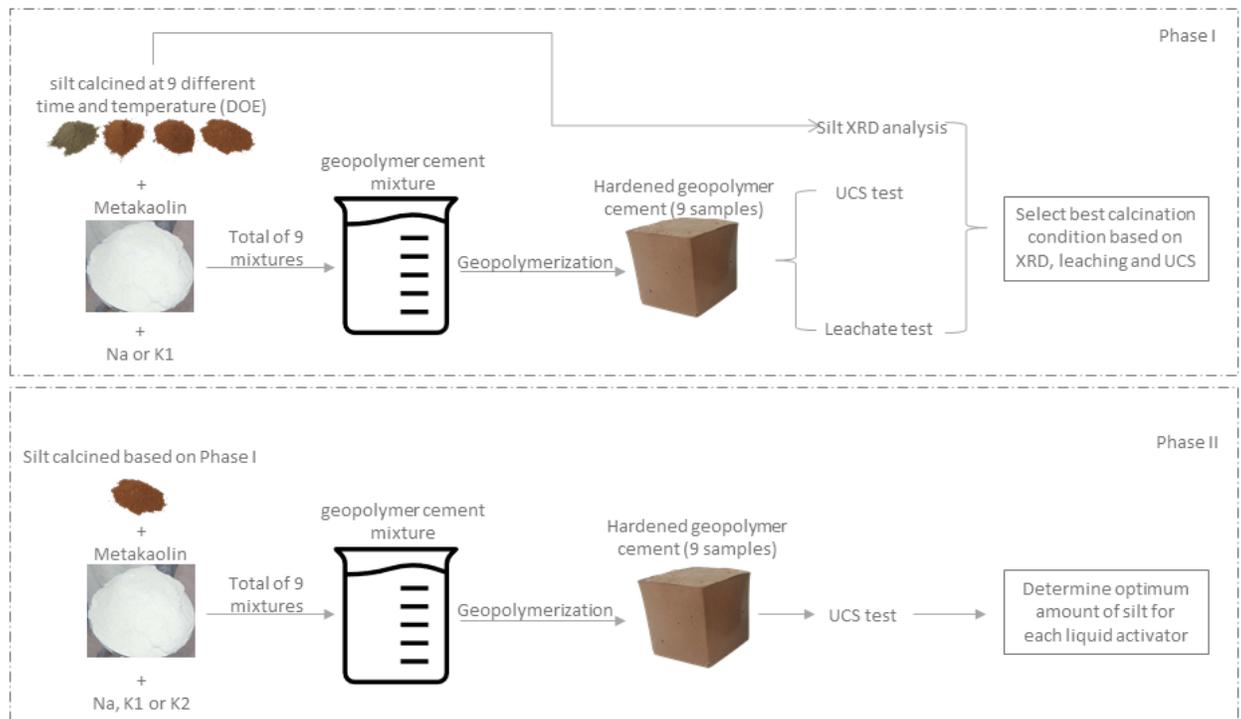
Figure 5.1. Methodology flow chart.

5.2.1 Silt Characterization and Thermal Treatment (Phase I)

As described in section 1.3, the silt was excavated from S.A.P.A.B.A.'s sedimentation lakes (Bologna, Italy). The materials used in geopolymer cement/concrete should be rich in both aluminum and silicates. The aluminosilicates can react with the liquid hardeners and can produce a geopolymer binder. Thus, the precursors and fillers should have both an appropriate mineralogy and chemical composition. Consequently, the chemical composition and mineralogy of the silt was determined. The data is fully demonstrated in section 1.3.

The initial data indicated a presence of 43.5% and 12.5% SiO_2 and Al_2O_3, respectively. However, the mineralogical data indicated that the silt had a high crystallinity, which

was composed of minerals including quartz, calcite, phyllosilicates with characteristic interplanar distances associable with chlorite, kaolinite/serpentine, illite/mica, feldspar such as albite and K-feldspar, and traces of dolomite.

To increase the reactivity of the silt, thermal treatment (calcination) was conducted using a static furnace (Pixsys ATR621, Venice, Italy) with a heating rate of 10 °C/min. To proceed with the calcination, a design of experiments (DOE) was established using JMP® software (Version 14.0. SAS Institute Inc., Cary, NC, USA, 1989–2019). The response surface method has gained popularity over time and has turned into a common mathematical and statistical tool for optimizing processes and evaluating the relationships between various input factors and responses. Moreover, this method produces reliable results and can decrease the number of tests required, reducing the needed time and expenses. Thus, a response surface method (RSM) was applied, where time and temperature were selected as the two independent factors, and the response was the unconfined compressive strength (UCS). A stepwise approach the using minimum BIC (direction forward, no rules) was used to build the final second-degree model. Consequently, a total of nine runs were produced, each with different times and temperatures for the calcination process (Table 5.1). The temperatures ranged between 200 and 850 °C, and the time was selected to be between 1 to 12 h. The runs were randomized to reduce type II errors as much as possible. The calcined silt obtained from each run was used to produce geopolymer cement samples. Each produced mixture was then tested for UCS. The calcination process is shown in Figure 5.2.

Table 5.1. DOE for silt calcination under different times and temperatures.

Run Order	Temp (°C)	Time (h)
1	200.0	6.5
2	295.2	10.4
3	754.8	10.4
4	295.2	2.6
5	850.0	6.5
6	525.0	6.5
7	525.0	12.0

| 8 | 754.8 | 2.6 |
| 9 | 525.0 | 1.0 |

Figure 5.2. Silt calcination process. Different calcination temperatures change the physical appearance of the silt. From left to right, the images show the uncalcined silt and the silt calcined at 550, 750, and 850 °C.

5.2.2 Geopolymer Binder Preparation and Testing Procedures (Phase I)

5.2.2.1 Sample Preparation

Sodium-based and commercially available potassium-based liquid (supplier's name, city, country) hardeners were used to produce the geopolymer cement mixtures. A sodium-based solution (labeled "Na") was prepared by mixing five parts sodium silicate (MR = 1.99) with one-part NaOH solution (10 molars) (NaOH 98% purity, thermofisher). The potassium-based solution (labeled "K1") was a commercial product with an MR of 1.7. As for the main precursor, a highly reactive metakaolin (labeled "MK") was used. Regardless of the type of liquid hardener, cubic samples were prepared by mechanically mixing metakaolin with the liquid solution (sodium or potassium) for 10 min. The calcined silt was added, and the mixing continued for an additional 5 min. The mixture was then poured into cubic Teflon molds ($4 \times 4 \times 4$ cm), covered and sealed with a plastic sheet to prevent water evaporation, and stored at room temperature for 24 h. After the curing process, the cubic samples were de-molded and were stored at room temperature for 30 days before any testing. This process was repeated, and the mixtures were separately made with different calcined silt. The detailed mixture design is shown in Table 5.2. The amount of the materials was selected

as such to satisfy the equation Na/Al = 1. This could reduce the leachate of the free sodium or potassium cations in the samples.

Table 5.2. Detailed mixture design for geopolymer cement production.

Liquid Type-Amount (g)	HardenerMK/Liquid Hardener	MK (%) *	Silt (%) *
Na-192.0	0.69	65.5	34.5
K1-192.0	0.53	50.5	49.5

* Total solid weight (MK + silt).

5.2.2.2 Unconfined Compressive Strength

After 30 days of curing, the unconfined compressive strength of the cubic samples was evaluated through a hydraulic press (Galdabini, Italy). A constant loading speed was applied, and all the procedures were based on the EN 1015-11: 2019 standard. For each run, three replicates were tested. The average UCS was used for further calculations.

5.2.2.3 Leaching Test

The horizontal dynamic surface leaching test (DSLT) was conducted in this study according to the CEN/TS 16637-2 standard proposed by the EC-CPR. The samples for the leaching tests ($4 \times 4 \times 4$ cm) were prepared with the same procedure described in Section 5.2.2.1 for geopolymers, with K1 and Na as liquid hardeners and calcination temperatures of 200, 295, 550, 750, and 850 °C. The samples were placed in glass tanks with sealed caps to prevent the liquid from evaporating. The space between the specimens and tank walls was more than 20 mm in all directions. Samples were placed on spacers at the bottom of the containers in order to have all of the sample sides in contact with the leachant. Deionized (DI) water was used as the leachant in this study. A sample surface to water volume of 80 L/m was chosen according to the CEN/TS 16637-2 standard. Leaching tests were conducted in 3 replicates prior to the statistical analysis of the results. The room and leachant temperature were controlled and maintained between 20–25 °C. The leachant in the containers was sampled and renewed at time intervals of 0.25, 1, 2.25, 4, 9, 16, 36, and 64 days with the duration

of each step being 0.25, 0.75, 1.25, 1.75, 5, 7, 20, and 28 days, respectively. Control experiments were conducted with DI water in containers in the absence of geopolymer specimens.

Samples from leaching and control tests were collected to evaluate the concentrations of Al, As, B, Ba, Ca, Cd, Co, Cr, Cu, Fe, K, Mg, Mn, Mo, Na, Ni, Pb, Sb, Se, Si, Tl, V, and Zn. The pH and electric conductivity of the liquid samples were also measured for samples from all of the time intervals. Concentrations of the compounds were measured using a Perkin-Elmer Optima 5300 DV ICP-OES instrument. The following equation (Equation (1)) was used to calculate the normalized concentrations of the leached compounds:

$$r_i = \frac{c_i\, V}{A} \tag{1}$$

where i is the sampling step, c_i is the concentration of the compound in the leachant (mg/L), V is the volume of the leachant (L), and A is the surface area of the specimens (m^2).

The cumulative concentrations of the leached compounds (Equation (2)) were calculated as follows:

$$C_n = \sum_{i=0}^{n} r_i \tag{2}$$

where C_n (mg/m^2) is the cumulative concentration at the step n of leaching test, and i is the sampling step.

5.2.3 Geopolymer Binder Preparation and Testing Procedures (Phase II)

A second DOE (Table 5.3) was designed, aiming to compare the effect of different types of liquid activators and the amount of silt on the final geopolymer cement strength. For this purpose, two of the previous liquid hardeners (Na and K1) plus a third

commercial potassium-based liquid (K2) were used (MR = 3.2). The amounts of silt selected were 150, 200, and 250 g. The amounts of MK for Na, K1, and K2 selected were 133, 101.9, and 54.66 g, respectively. For all mixtures, the liquid amount was selected as 192 g. The MK/liquid ratio was selected is such manner to fulfil Na (or K)/Al = 1.

Table 5.3. The effect of silt amount and activator type on UCS (DOE).

Run Order	Activator	Silt (g)	Silt (%) *
1	Na	150	53
2	K1	250	78
3	Na	250	65.3
4	K2	200	71
5	K2	250	81.6
6	K1	150	59.5
7	K2	150	65.3
8	K1	200	60.2
9	Na	200	60.1

* Total solid weight (MK + silt).

A full factorial design having a total of 9 (3 × 3) randomized runs was produced. The model was produced using the standard least squares with emphasis on effect leverage. The samples were prepared as they were in the previous phase, and the cubes were tested for compressive strength after 30 days of room temperature curing (EN 1015-11: 2019). Phase II of the study was independent of the first phase. However, the silt calcination conditions were taken from the first phase. Therefore, for all of the samples produced in the second phase, the silt was calcined at 750 °C for 2 h (further details are provided in the Discussion section). The detailed mixture design is presented in Table 5.4.

Table 5.4. Mix design proportions for liquid hardener and MK.

Liquid Hardener Type-Amount (g)	MK/liquid Hardener
Na-192.0	0.69
K1-based-192.0	0.53
K2-based-192.0	0.29

5.3 Results

5.3.1 Calcined Silt Mineralogical Characterization (Phase I)

A total of three samplings of the silt were performed to investigate the variations of the mineralogical composition in the sedimentation lakes. All of the samples were found to be composed of quartz, calcite, phyllosilicates with characteristic interplanar distances associable with chlorite, kaolinite/serpentine and illite/mica, and albite-like feldspar, as determined by means of XRD qualitative analysis. K-feldspar and traces of dolomite were also found, but they were not found in all of the samples.

The XRD semi-quantitative analysis revealed the presence of quartz and calcite as major constituents, with variability within about 30–40 wt% and 25–30 wt%, respectively. Significant amounts of illite/mica, chlorite, kaolinite/serpentine, and albite-like feldspar were also detected, with variability within about 12–20 wt%, 2–7 wt%, 5–11 wt%, and 4–12 wt%, respectively. Where present, K-feldspar were found up to about 9 wt%, whereas dolomite was found in small amounts up to about 2 wt%.

After the mineralogical characterization of the raw material, thermal treatments (calcination) were conducted at different times and temperatures, as detailed in Table 5.1, to increase the reactivity of the silt. Figure 5.3 reports the X-ray diffractograms of the control and calcinated silt.
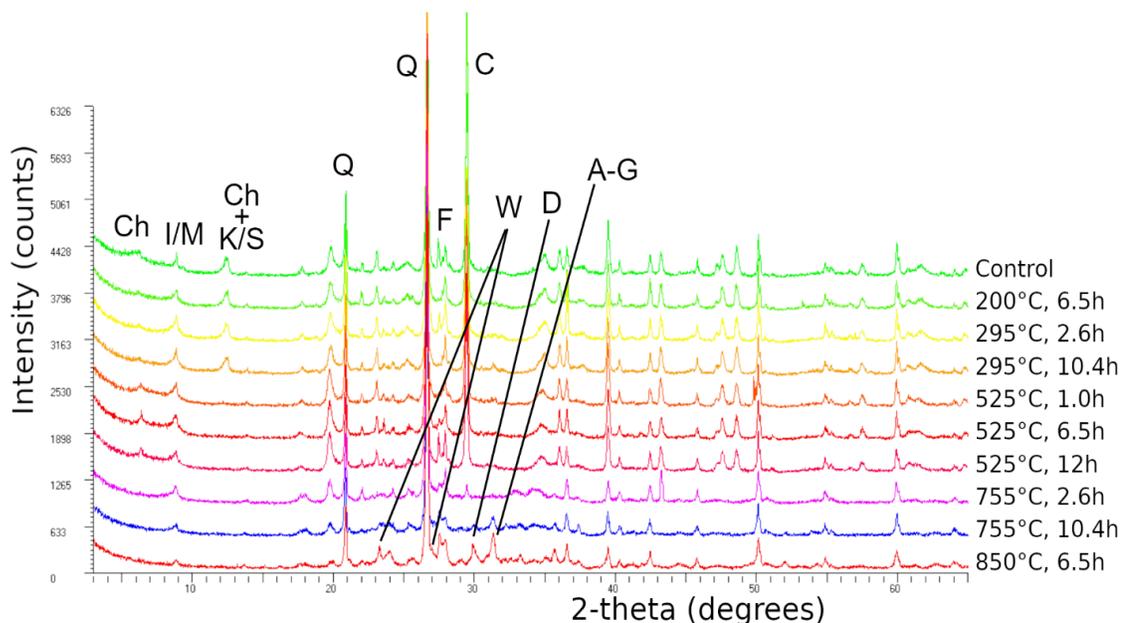
Figure 5.3. XRD profiles of the control and calcinated silt obtained with Cu Kα radiation. C = Calcite, Q = Quartz, W = Wollastonite, D = Diopside, A-G = Åkermanite–Gehlenite solid solution, I/M = Illite–Mica, Ch = Chlorite, K/S = Kaolinite/Serpentine, F = Feldspars.

No variation in the mineralogical composition of the calcinated silt was revealed by XRD analysis at temperatures up to 295 °C, independent of the calcination time. The thermal treatments at 525 °C, independent of the treatment time, caused an increase in the X-ray intensity of the diffraction peak at about 14 Å, which was also associated with a slight shift to a higher angle, the complete collapse of the peak at about 7 Å, and no significant variation of the other peaks. The calcination at higher temperatures (i.e., 750 °C and 850 °C) caused the complete collapse of the diffraction peak at about 14 Å and a decrease in the intensity of the peak at about 10 Å (runs 10 h at 750 °C and 6.5 h at 850 °C). Still, the almost total collapse of the calcite peaks (which collapsed at 750 °C for 10 h and at 850 °C for 6.5 h) and the formation of new mineral phases were observed. In particular, the treatment at 750 °C for 2.6 h produced a wollastonite-type (CaSiO$_3$) new phase, whereas the other two treatments also produced a diopside-like

(CaMgSiO$_2$O$_6$) phase and a mineral in the Åkermanite (Ca$_2$MgSi$_2$O$_7$)–gehlenite (Ca$_2$Al(SiAl)O$_7$) solid solution.

5.3.2 Binder Properties

5.3.2.1 Unconfined Compressive Strength-DOE Analysis (Phase I)

The average UCS obtained for the samples prepared with Na or K1-based liquid hardeners are presented in Table 5.5. Overall, an increase in the calcination temperatures led to an increase in the final compressive strength of the geopolymer cement samples. This trend was true for the samples made with both Na- and K-based liquid hardeners. However, the effect of calcination time on the final UCS differed for low and high temperatures. In this regard, an increase in calcination time at lower temperatures (< 525 °C) seemed to increase the final strength of the samples. However, at higher temperatures, an increase in the calcination time led to a decrease in the compressive strength. For instance, by increasing the time from 1 to 6.5 h, the compressive strength of the Na-based samples made with silt calcined at 525 °C increased. However, a further increase in calcination time led to a decrease in the final strength, with values from 49.40 to 43.57 MPa.

Table 5.5. Compressive strength obtained for different calcination conditions (DOE).

Run Order	Temperature (°C)	Time (h)	Na-UCS (MPa)	K1-UCS (MPa)
1	200.0	6.5	39.43	35.49
2	295.2	10.4	42.15	27.00
3	754.8	10.4	57.58	48.82
4	295.2	2.6	32.50	35.85
5	850.0	6.5	59.52	45.85
6	525.0	6.5	49.40	36.24
7	525.0	12.0	43.57	34.98
8	754.8	2.6	60.81	35.96
9	525.0	1.0	48.52	39.59

The obtained data were then inputted into JMP® software, and a response surface method analysis was applied. The input variables were selected as calcination time and temperature, and the resulting UCS for both Na- and K-based geopolymers were selected as the two responses. The summary of the fit and parameter estimates for the Na-based geopolymers are tabulated in Table 5.6 and Table 5.7, respectively. The R-squared value of 93.08% indicated a high confidence fit of the model (Table 5.6). The data presented in indicated a high impact of the temperature factor on UCS, with a t-ratio of 7.04 and high significance levels (<0.0021). However, time did not show a significant effect on the compressive strength.

Table 5.6. Summary of fit (Na-based liquid).

Statistical Term	Value
RSquare	0.930802
RSquare Adj	0.861603
Root Mean Square Error	3.621467
Mean of Response	48.16444
Observations (or Sum Wgts)	9

Table 5.7. Parameter estimates (Na-based liquid).

Term	Estimate	Std Error	t Ratio	Prob > |t|
Intercept	49.636366	1.891252	26.25	<0.0001
Temp (°C) (200,850)	12.754706	1.810732	7.04	0.0021
Time (h) (1,12)	−0.10259	1.81073	−0.06	0.9575
Temp (°C) × Time (h)	−6.439971	3.62145	−1.78	0.1500
Time (h) × Time (h)	−3.311813	3.275738	−1.01	0.3692

The interaction between calcination time and temperature for Na-based geopolymer cements is shown in Figure 5.4. The interaction also indicates that at higher temperatures, an increase in calcination duration could decrease the compressive strength of the samples. Moreover, the rate at which temperature impacts the UCS is higher when a lower calcination duration (1 h) is used compared to a higher calcination time.
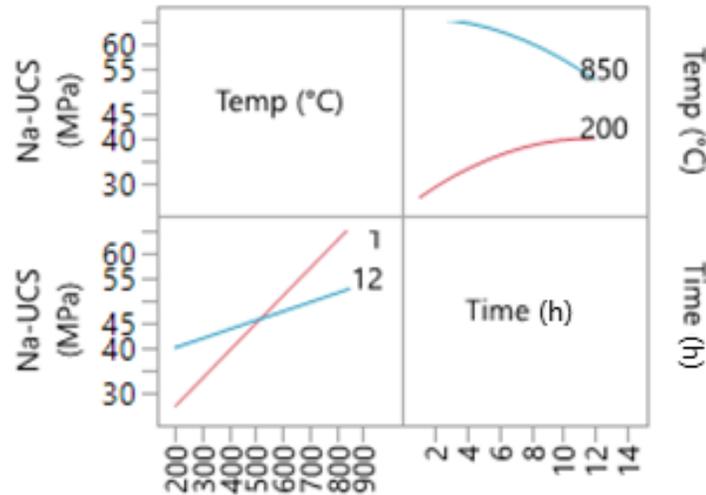
Figure 5.4. Interaction profile for time and temperature (Na-based liquid).

The prediction profiler is shown in Figure 5.5. This tool allows for the optimization of the factors and outcomes based on different desirability factors. Thus, to achieve the highest compressive strength, the parameters were changed accordingly. Consequently, by minimizing the calcination duration to 2 h, the maximum compressive strength of 65.52 MPa was predicted. Figure 5.6 shows the contour plot for sodium-based geopolymer samples. As indicated, the highest compressive strength is achievable when calcination temperatures are higher than 650 °C.
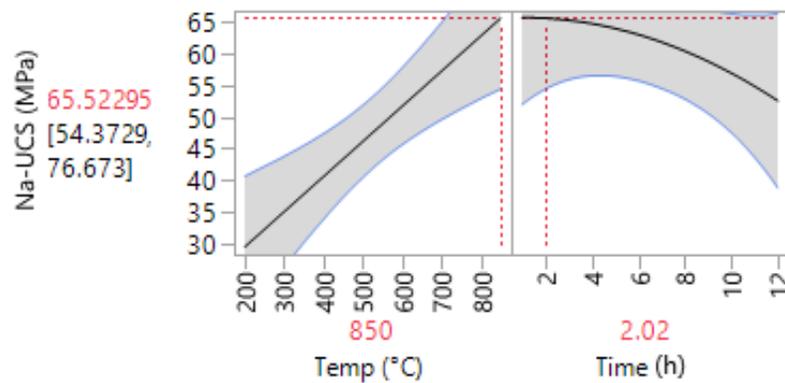
Figure 5.5. Prediction profiler for Na-based geopolymer cement.
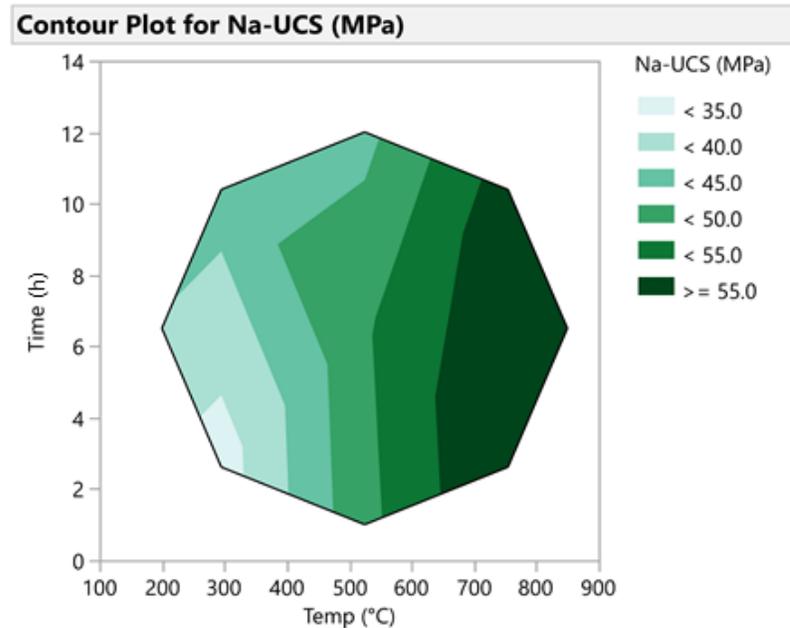
Figure 5.6. Contour plot for Na-based geopolymer cement.

The summaries of the fit and parameter estimates for the samples produced with potassium liquid hardeners are presented in Table 5.8 and

Table 5.9, respectively. Similarly, the model had an R-squared value of 0.9116, indicating a high precision fit of the model. Again, the temperature is what has the highest impact on the final strength. However, for the potassium-based models, the interaction between time and temperature is significant (< 0.05), with a positive interaction value of 4.03. Thus, as illustrated in Figure 5.7, an increase in both factors will result in the highest UCS possible.

Table 5.8. Summary of fit for K1-based samples.

Statistical Term	Value
RSquare	0.911692
RSquare Adj	0.823385
Root Mean Square Error	2.694961
Mean of Response	37.75333
Observations (or Sum Wgts)	9

Table 5.9. Parameter estimates for K1-based samples.

Term	Estimate	Std Error	t Ratio	Prob > ǀtǀ
Intercept	36.247273	1.407398	25.75	<0.0001
Temp (°C) (200,850)	6.4667096	1.34748	4.80	0.0087
Time (h) (1,12)	−0.443622	1.347478	−0.33	0.7585
Temp (°C) × Temp (°C)	3.3886312	2.437683	1.39	0.2369
Temp (°C) × Time (h)	10.854951	2.694949	4.03	0.0158
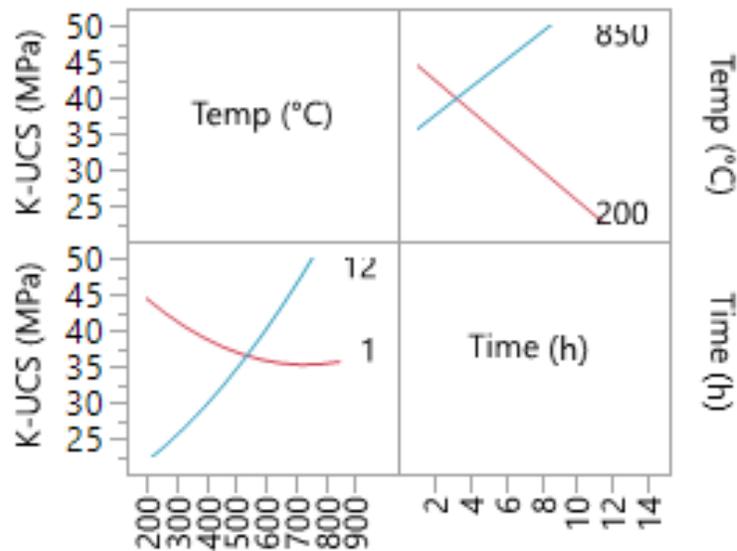
Figure 5.7. Interaction profile for time and temperature for K1-based samples.

The prediction profiler for potassium-based geopolymer cements indicated that the highest UCS can only be achieved if the high temperature (850 °C) and long calcination duration of 12 h are used (Figure 5.8). Calcination completed in shorter durations will result in lower UCS values. This is also indicated by the contour plot (Figure 5.9), which indicates the requirement of both high temperature and duration for achieving high compressive strength values.
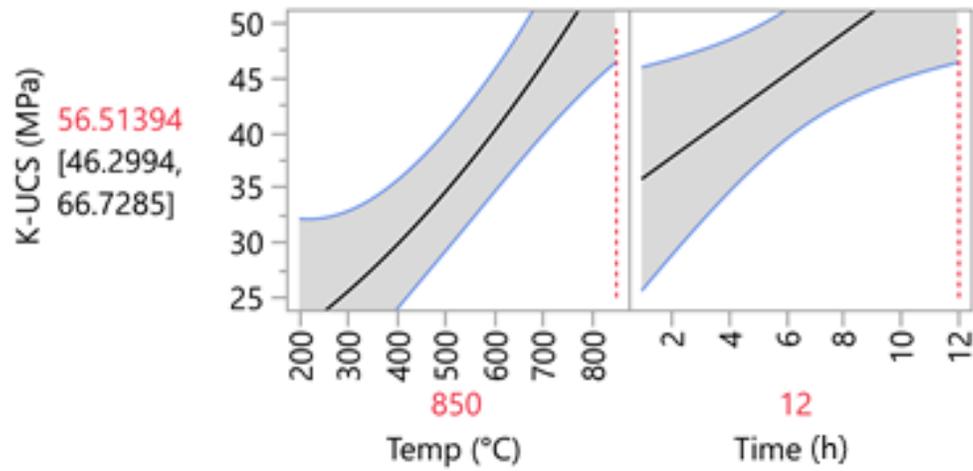
Figure 5.8. Prediction profiler for K1-based geopolymer cement.
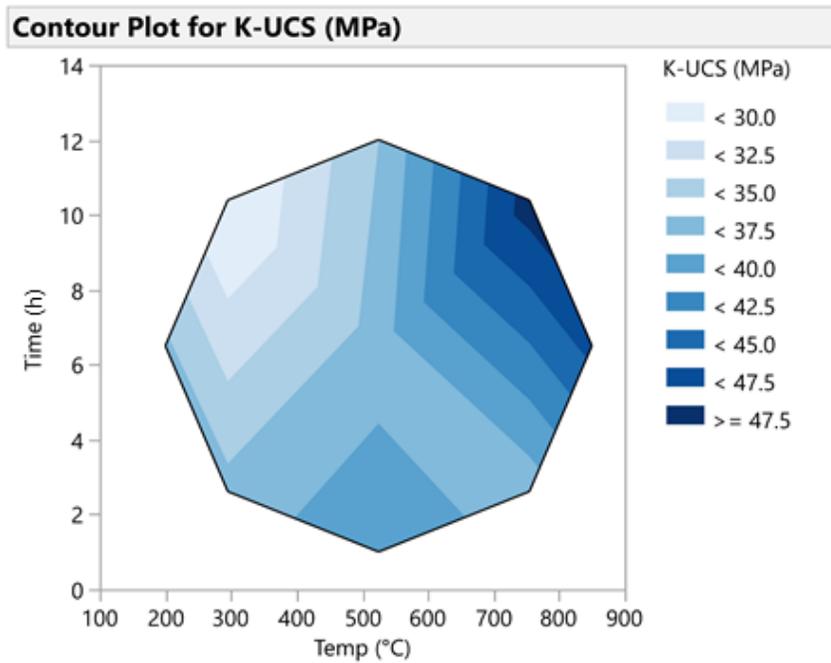
Figure 5.9. Contour Plot for K1-based geopolymer cement.

5.3.2.2 Horizontal Dynamic Surface Leaching Test (Phase I)

The changes in the pH values during the DSLT test for the K- and Na-based geopolymers are presented in Figure 5.10. The K-based geopolymers (K1) showed

higher pH values than the Na-based specimens at all calcination temperatures. K-based geopolymers calcinated at 200, 295, 550, 750, and 850 °C showed a pH ranging between 11.6–11.9, 10.9–11.4, 10.0–11.7, 9.9–10.0, and 9.5–9.8, respectively. The pH values for the Na-based geopolymers ranged from 11.2–11.7, 10.5–10.7, 9.9–10.4, 9.6–9.9, and 9.2–9.5 at calcination temperatures of 200, 295, 550, 750, and 850 °C, respectively.
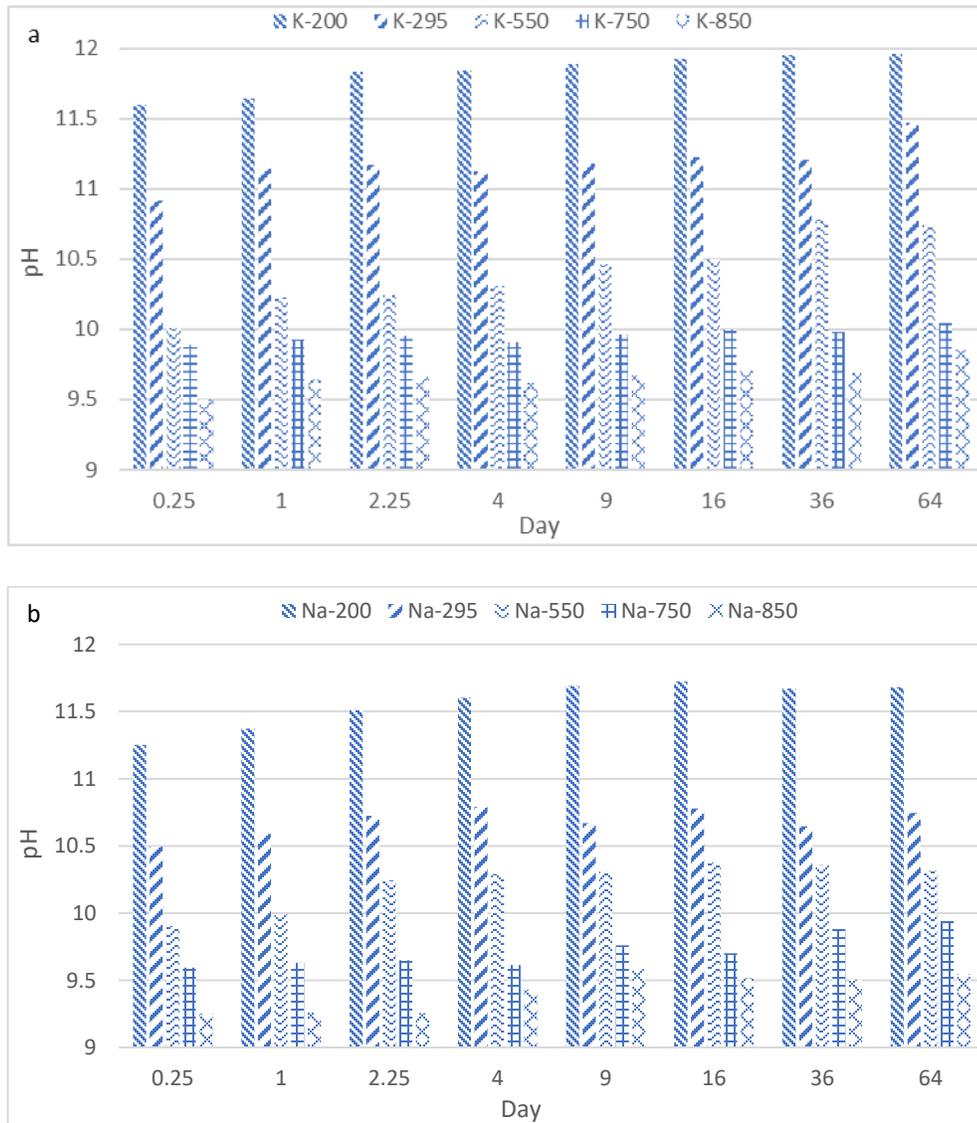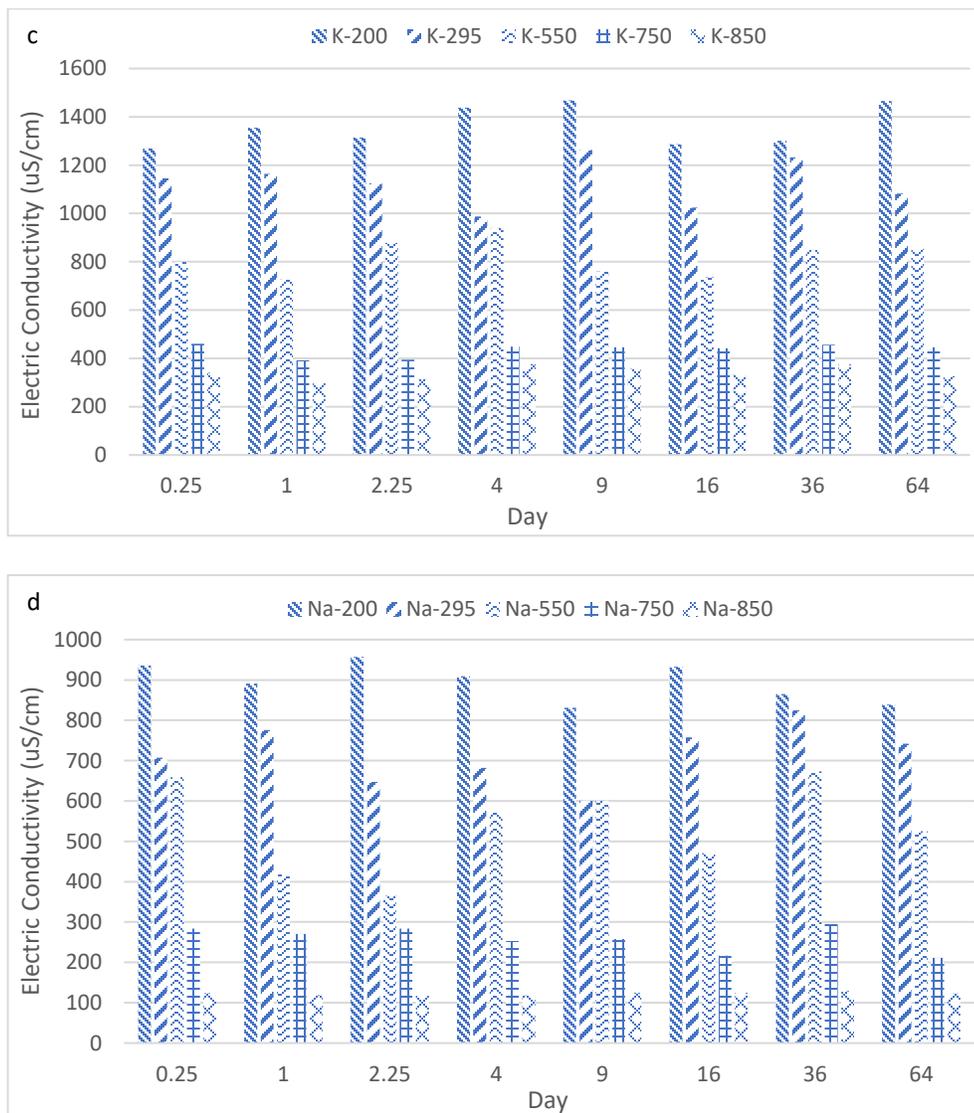
Figure 5.10. pH values (a,b) and electric conductivity (c,d) of leachants during the DSLT tests. K refers to the K1 liquid used in Phase I.

The evolution of the electric conductivity of K- and Na-based geopolymers was evaluated using the DSLT test and was reported for different time intervals from 0.25 to 64 days (Figure 5.10). According to the results, the mean value of electric conductivity for leachant in contact with K-based geopolymers was between 1269–1466, 988–1263, 736–940, 392–461, and 300–376 uS/cm depending on the DSLT time

interval. The Na-based specimens showed an electric conductivity of 839–957, 601–825, 365–673, 211–295, and 119–129 uS/cm for calcination temperatures of 200, 295, 550, 750, and 850 °C, respectively.

The cumulative concentration of released heavy metals and trace elements per unit of K- and Na-based geopolymer specimen surface are presented in Table 5.10. According to the results, no concentrations of Se, Tl, and V were observed in K- or Na-based geopolymer leachants during the DSLT test. Moreover, for the K-based geopolymers calcinated at 850 °C, the concentrations of Cd, Ni, Pb, and Sb were below the instrument detection limit for all of the DSLT time intervals. No concentrations of Cd, Co, Mn, Pb, or Sb were leached to the DI water from the Na-based geopolymers calcinated at 750 and 850 °C during the DSLT test. Additionally, the leachants from the Na-based geopolymers calcinated at 850 °C contained concentrations of Cu and Ni that were below the detection limit. The cumulative release of Al, Ca, K, Na, and Si in the leachants during the DSLT tests ranged between 53–1257, 12–147, 1300–36,858, 9–175, and 1648–19,586 mg/m2 for the K-based geopolymers, respectively. Cumulative concentrations of Al, Ca, K, Na, and Si of 81–1068, 7–115, 7–95, 2390–29,774, and 1148–16,648 mg/m2 o were detected in the leachants from the Na-based geopolymers in the DSLT test, respectively.

Table 5.10. The cumulative concentrations of the released heavy metals and trace elements from the surfaces of the geopolymer specimens (mg/m2).

Eleme nt	K-Based Geopolymer Specimens					Na-Based Geopolymer Specimens				
	K-200 *	K-295	K-550	K-750	K-850	Na-200	Na-295	Na-550	Na-750	Na-850
Al	1257.55	578.473	231.38	127.26	53.45	1068.91	587.90	317.46	139.68	81.017
As	5.62	2.75	1.15	0.56	0.28	4.66	2.19	0.92	0.44	0.26
B	73.45	38.19	19.09	7.63	3.81	53.61	23.05	9.91	5.65	3.05
Ba	13.84	5.53	2.21	0.93	0.39	11.21	4.59	2.52	1.39	0.62
Ca	147.56	78.20	46.92	23.46	12.90	115.09	63.30	37.34	16.43	7.06
Cd	0.66	0.28	0.13	0.06	ND	0.56	0.28	0.16	ND **	ND
Co	0.81	0.39	0.16	0.09	0.04	0.55	0.27	0.14	ND	ND
Cr	3.93	1.65	0.94	0.45	0.25	3.06	1.44	0.72	0.38	0.15
Cu	0.92	0.37	0.21	0.12	0.07	0.77	0.43	0.24	0.12	ND
Fe	103.57	56.96	27.34	12.30	4.92	83.89	50.33	24.66	10.35	6.01
K	36,858.1	15,480.41	6501.77	2600.71	1300.35	95.14	51.37	30.31	13.03	7.69
Mg	7.69	4.22	1.86	0.93	0.38	5.07	2.89	1.47	0.73	0.42
Mn	1.12	0.56	0.25	0.11	0.06	0.84	0.45	0.22	ND	ND
Mo	17.45	7.67	3.07	1.56	0.73	11.69	6.19	3.47	1.49	0.68
Na	175.34	82.41	43.67	19.21	9.03	29,774.44	15,184.96	8351.73	4509.93	2390.26
Ni	0.77	0.43	0.26	0.10	ND	0.56	0.31	0.18	0.08	ND
Pb	0.08	0.04	0.01	ND	ND	0.06	0.03	0.01	ND	ND
Sb	0.11	0.06	0.02	0.015	ND	0.09	0.05	0.02	ND	ND
Se	ND	ND	ND	ND	ND	ND	ND	ND	ND	ND
Si	19,586.1	9988.93	5493.91	3296.34	1648.17	16,648.21	8324.10	3662.60	2051.06	1148.59
Tl	ND	ND	ND	ND	ND	ND	ND	ND	ND	ND
V	ND	ND	ND	ND	ND	ND	ND	ND	ND	ND
Zn	67.19	33.59	14.10	5.92	2.42	49.04	21.09	11.60	6.72	2.96

* K-200: K-based geopolymer calcinated at 200 °C; ** ND: Not detected. K-based geopolymers refers to samples made with K1 liquid in Phase I.

5.3.3 Effect of Silt and Activator Type on UCS (Phase II)

The compressive strength correlated to the percentage of silt and liquid hardener type is shown in Table 5.11. The liquid types of Na, K1, and K2 refer to the sodium-based and two potassium-based liquid hardeners. The highest UCS of 57.46 MPa was reported for the samples made with K1 liquid, whereas the lowest value was reported for the K2 sample with 29.05 MPa. The silt amounts used for K1 and K2 were reported as 59.5 and 72.7% (total solid weight), respectively. The data were further analyzed in JMP® software, providing more information regarding the effect of the silt and liquid

type on the final mechanical strength of the samples. The interaction plots (Figure 5.11), further show the correlation between the studied factors and the output response. With an increase in the silt amount, the final compressive strength of the samples made with Na and K1 liquids decreased. However, for the samples made with K1 liquids, the compressive strength decrease is not as high as the ones for the Na liquids, where a loss of about 20 MPa was observed when the amount of silt was increased from 53 to 65.3% (total solid weight). The only samples that showed an increase in strength with an increase in silt content were the samples made with K2 liquid hardener. The produced model had an $R2 = 0.994$, which was shown to be significant ($p < 0.0013$).

Table 5.11. UCS for samples produced with different amount of silt and liquid type.

Liquid Type	Silt (g)	Silt (%) *	UCS (MPa)
Na	150	53	56.00
K1	250	78	50.10
Na	250	65.3	30.07
K2	200	71	34.07
K2	250	81.6	41.68
K1	150	59.5	57.46
K2	150	65.3	29.05
K1	200	60.2	52.08
Na	200	60.1	44.78

* Total solid weight (MK + silt).
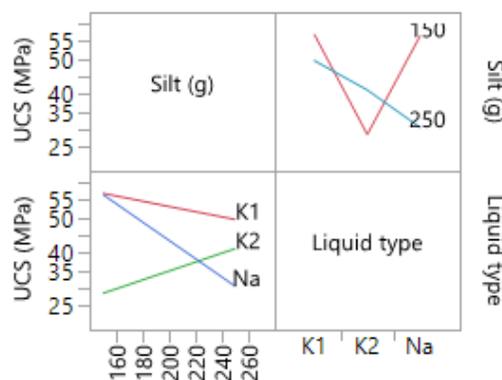
Figure 5.11. Interaction plots of samples produced with different silt amounts and liquid types.

5.4 Discussion

The results from the mineralogical analysis of the raw silt evidenced small variability in the silt composition, mainly in terms of the amount of the mineral phases rather than the type of phases. Only dolomite and K-feldspar were occasionally observed: the first was detected in just a few weighted percentages, and the second was detected up to about 9%; however, it was not affected by the calcination treatments and thus, in principle, did not participate in the change of reactivity of the silt. The variability is an important parameter for the mass production of samples. This could alter the final strength of the produced samples due to variation in the phase of the waste silt. However, the results did not show, nor did they affect the current test results since no variation in the phase was observed.

As expected, the XRD profile was not affected by the treatments for temperatures up to 295 °C. The lowest values for compressive strength, regardless of liquid type, were achieved at calcination temperatures below 295 °C. Based on the leaching results, low calcination temperatures lead to the undesirable leaching of alkali cations ($Na+$ or $K+$) and for all cases, sodium-based samples showed lower leaching values than potassium-based mixtures. The low UCS values and high leaching could be associated with the inert behavior of the silt calcined at low temperatures.

The variation of the XRD profile for calcination at 525 °C was consistent with the dehydroxylation of the interlayer hydroxide of the chlorite and the dehydroxylation of kaolinite/serpentine, regardless of the calcination time. This increased the reactivity of the silt and consequently increased the compressive strength for both the sodium and potassium-based mixtures (Table 5.5).

The treatments at about 750 °C for 2.6 hours caused the dehydroxylation also of the talc-like layer of chlorite and its complete amorphization as revealed by XRD, the almost total loss of calcite and the formation of a wollastonite-type ($CaSiO_3$) new

phase. All these types of transformations are well reported and described by Földvari (2011) [208]. The last two treatments, 750 °C for 10 hours and 850 °C for 6.5 hours, also determined the complete loss of calcite, a progressive dehydroxylation of illite/mica, and the formation of a diopside-like ($CaMgSiO_2O_6$) phase and a mineral in the Åkermanite ($Ca_2MgSi_2O_7$)–gehlenite ($Ca_2Al(SiAl)O_7$) solid solution in percentages up to about 10% [208].

The effectiveness of promoting aluminosilicate dissolution is higher in Na-based alkali solutions compared to K-based ones. Moreover, the viscosity of Na is much higher than K, making it harder to mix sodium-based geopolymer mixtures. However, based on the literature, K-based geopolymers should have higher compressive strength than Na-based samples, indicating that the rate of dissolution does not control the geopolymerization [14].

The results presented in Table 5.5 indicate that for all of the calcination conditions, the UCS obtained for Na-based mixtures are higher than the ones of the K-based samples. This could be related to the amount of silt used in the mixture. Only 100 g of silt (49.5% total solid weight) was added to the K1 samples during phase I, producing a maximum strength of 48.82 MPa using silt calcined at 750 °C for about 10 h. The silt acts as a partially reactive filler in the geopolymer mixture. For samples produced with K1, the filler amount was not sufficient, leading to the samples prone to cracking due to their brittleness. Generally, samples produced with metakaolin only will be very brittle unless a proper amount of filler is added to the mixture [209]. This could also be backed up with the results obtained during phase II of the study, where the effect of silt amount was investigated on the final strength of the samples. Table 5.11 indicates that the highest amount of UCS was obtained for the K1 samples produced with 150 g (59.5% total solid weight) of silt. Thus, increasing the amount of silt by 10%, an increase of approximately 10 MPa was observed for the K1 samples. However, by further increasing the amount of silt to 71%, the final strength slightly decreased to 50.10 MPa.

This could be related to the fact that for a higher silt amount, water (less than 2% of total solid part) was added to the mixture, decreasing the mixture viscosity. Water could decrease the maximum strength of the samples by decreasing the molarity of the alkali solutions [14]. Moreover, an excess amount of filler (silt) could remain unreacted in a mixture and could behave as an inert material. This could produce micropores inside the samples, which can decrease the final strength of the mixtures [105]. The results for phase II were in line with the literature since the UCS for K1 was higher than the ones for Na, regardless of silt amount. Both the Na and K1 samples experienced an increase in the strength when the silt amount was increased from 150 to 250 g, whereas the strength of the K2 samples increased with an increase in the silt content. K2 had the lowest amount of viscosity amongst all of the liquid hardeners, allowing more silt to be used within the mixture. Thus, by adding a higher amount of silt (>250 g), the final compressive strength could exceed 41.68 MPa, as reported in Table 5.11.

The results of the DSLT tests revealed that the pH of the leachants from the K-based and Na-based geopolymers increased with the reduction of the geopolymer calcination temperature at each test time interval (Figure 5.10). The lowest and highest observed pH were associated with Na-based geopolymers calcinated at 850 °C (9.2) and 200 °C (11.7), respectively. The same pattern was observed with the K-based geopolymers. The increasing of the pH values was due to the leaching of the alkaline elements into the leachant [210,211]. With increasing calcination temperatures for both the K- and Na-based geopolymers, the number of alkaline elements participating in the geopolymerization process and creating bonds in the potassium and sodium alumina–silicate gels increased [212]. This phenomenon resulted in lower rates of alkaline element release into the leachant and consequently lower pH values. This observation was in line with the mechanical results, where the geopolymers calcinated at higher temperatures showed higher geopolymerization rates and UCS values (Table 5.5).

The electric conductivity values of the leachants from the DSLT tests for the K- and Na-based geopolymers increased with decreasing calcination temperatures (Figure 5.10). This result was due to the higher release rate of Na and K ions into the leachant, which resulted in higher values of electric conductivity for the geopolymers calcinated at lower temperatures [213]. The maximum and minimum electric conductivity for the K-based geopolymers were 1468 (200 °C) and 300 (850 °C) uS/cm, respectively.

The results of the DSLT tests revealed that the cumulative concentrations of released heavy metals and trace elements into the leachant solution during the DSLT tests were influenced by the geopolymer calcination temperature and pH of the leachant. According to Table 5.10 the concentration of all the released elements reduced by increasing the calcination temperature. The cumulative released concentrations of the elements, including Cd, Ni, Pb, and Sb, from the K-based geopolymer surface and of Cd, Co, Mg, Ni, Pb and Sb for the Na-based geopolymers, reduced constantly with the increase in the calcination temperature, to a point where no ions of concern were detected (750 and 850 °C). The same pattern was observed for other elements, with a reduction up to 96% for the cumulative released concentrations from the surface unit of the geopolymers. This observation may be explained by two factors. First, as described earlier, a more complete degree of geopolymerization occurred at higher calcination temperatures for both the Na- and K-based geopolymers. As a result, trace elements had stronger bonds with the structure of the geopolymer, which led to lower rates of release into the leachant [214]. Second, as described earlier, the pH of the leachant in contact with the geopolymers calcinated at lower temperatures were higher than that of the geopolymers calcinated at lower temperatures. The high pH may have increased the mobility of the metals, [215,216] and the trace elements, which resulted in higher rates of release into the leachant during the DSLT tests.

Overall, the DSLT leaching test results revealed that the cumulative release of heavy metals and trace elements, including As, B, Ba, Ca, Cd, Co, Cr, Cu, Fe, K, Mg, Mn,

Mo, Na, Ni, Pb, Sb, Se, Si, Tl, V, and Zn, from the Na-based and K-based geopolymers under investigation in the present study were in the same range as other reported studies on geopolymer mortars and cement-based materials [217]. Moreover, the cumulative release of elements per unit surface of the geopolymers were lower than thresholds of the EU Water Framework Directive (The Water Framework Directive 2000/60/EC).

From a mechanical point of view, every sample, regardless of calcination condition and liquid type, showed compressive strength above 30 MPa. This could be comparable to the strengths obtained for ordinary concrete mixtures used in the construction sector. However, calcination temperatures below 750 °C showed excess leaching of alkali cations. Moreover, new mineral phases were only observable for calcination temperatures of 750 and 850 °C. Thus, the optimum calcination temperature was selected as 750 °C for all liquid types satisfying mineralogical, mechanical, and environmental criteria. The optimum amount of silt was selected as 53 and 59.5% (total solid part) for the Na and K1 samples, respectively. However, more than 81.6% silt could be added to the samples produced with K2 liquid, which had the lowest viscosity. Recycling as much silt as possible could be environmentally friendly and could provide a circular economy for S.A.P.A.B.A.

To sum up, calcination of silt appears to be a promising option for increasing the final strength of the sample, allowing the reuse of the aggregate production by-product, silt.

5.5 Conclusions

The current study investigated the feasibility of using thermally treated waste silt obtained from S.A.P.A.B.A. as filler in geopolymer cement production. The data obtained from XRD indicated a presence of 43.5% and 12.5% of SiO_2 and Al_2O_3, respectively. However, the mineralogical data indicated a high crystallinity rate of the silt, which was composed of minerals including quartz, calcite, phyllosilicates with characteristic interplanar distances associable with chlorite, kaolinite/serpentine,

illite/mica, feldspar such as albite and K-feldspar, and traces of dolomite. Therefore, various thermal treatment conditions were applied, and their effect on the final strength of the samples were studied. Leaching tests were conducted to further study the behavior of the calcined silt.

Based on the presented results, the following conclusions can be drawn:

- Overall, higher calcination temperatures led to higher compressive strength values.

- Low calcination temperatures (<250 °C) did not change the mineral compositions of the calcined silt.

- Phase change occurred at higher calcination temperatures, leading to the dehydroxylation of the chlorite at 550 °C and the complete loss of calcite (T > 750 °C).

- DSLT leaching test results showed that increasing the calcination temperature of the K- and Na-based geopolymers resulted in the lower cumulative leaching of heavy metals and trace elements.

- The concentrations of the released elements from the geopolymer specimens were in the same range as cement-based materials and were lower than those of the EU Water Framework Directive thresholds.

- An excess amount of filler could decrease the compressive strength of the final mixture.

- The optimum amount of silt was selected as 53 and 59.5% of the total solid part for the Na and K1 liquids, respectively.

- The K2 liquid had the lowest viscosity compared to the other liquids, allowing the addition of more than 81.6% of silt into geopolymer cement samples.

- The optimum calcination temperature was selected as 750 °C for all liquid types, satisfying mechanical, mineralogical, and environmental criteria.

Chapter 6: Mechanical, thermal and microstructure properties of silt-based geopolymer paving blocks

6.1 Introduction

Sustainability has turned into a fundamental element in scientific research. The 12th objective of the sustainable development goals, "responsible consumption and production", proposed by the United Nations focuses on consumption and production patterns that consider and ensure sustainability. Engineers have tackled this challenge from various perspectives and have provided sustainable solutions. For instance, waste management is just one of the several approaches toward a sustainable future. However, recycling becomes more challenging when the material in question is difficult to treat and handle. Silt and clayey materials are good examples of such materials.

Silt and clay materials could be obtained in the form of sediments from the silting of harbors, rivers and reservoirs. The construction sector has made efforts to recycle the high volume of silt and clay in several applications such as paving blocks. For instance, 12.5% of natural sand was substituted with dredged marine sediments in a successful attempt of producing recycled paving blocks. Substitution of a higher amount of waste material was reported to produce very low Tensile Splitting Strength (T) results and demanded higher water dosages during mixing [218]. The contaminated sedimentations from a dredged harbor were innovatively transformed into paving blocks through the application of CO_2 curing [219]. The curing allowed for the densification of the samples leading to the improved compressive strength of the samples by 2.8 times.

The aggregate production sector also produces high volumes of waste mineral fillers, which could benefit from innovative and sustainable waste management techniques. Waste silt is a by-product of the aggregate washing process during limestone production. The materials are stored in sedimentation lakes adjacent to aggregate quarries. In general, limestone is collected from quarries or riverbeds. However, the by-product/waste silt could have variations in terms of mineralogy, chemistry and reactivity and could behave differently when used in any application. Thus, a full understanding of the raw material is essential before its application [166].

Various approaches have been undertaken for recycling waste mineral fillers and by-products which have been fully reviewed by [220–223]. Among the many available methods, recycling waste by-products into geopolymer binder and concrete has also proven to be sustainable [21]. The term geopolymer is used by scientists to describe the products of the reaction of a solid rich in aluminosilicate with an aqueous alkali hydroxide/ silicate solutions [14]. For instance, a fine powder was partially replaced with fly ash at different levels to produce geopolymer mortars [224]. Various mechanical and durability tests were conducted on the geopolymer mortars and it was indicated that the substitution of 30% fly ash proved to enhance the mechanical properties of the final product. In a separate study, recycled aggregates were included in a fly ash geopolymer mixture [225]. The authors proposed that the addition of such aggregates to geopolymer mixture reduced its physical and mechanical properties. However, the mechanical properties of the fly ash geopolymer improved when ground granulated blast furnace slag (GGBFS) was added to the mixture. Various waste materials could be recycled into geopolymer mixtures and it is not limited to fine powders. For instance, recycled bricks [226], unseparated construction and demolition waste [227], recycled waste tires [228], waste cathode ray tube glass [229] and basalt fibers [230] are only some of the many approaches used by researchers to tackle waste management.

Among the mentioned methods, various attempts have been made for producing geopolymer based paving blocks containing waste materials and fillers. For instance, obtained clayey sediments and water potabilization sludge were used to produce an optimized geopolymer cement taking into account different calcination conditions, mix design parameters and curing conditions [166]. The geopolymer cement was then used to produce eco-friendly precast elements including paving blocks. Chemical analysis and mechanical performance of the geopolymer paving blocks proved the feasibility of using the sedimented clayey materials to produce precast building material.

In addition to paving applications, geopolymer cement has been used to produce masonry building blocks. For instance, red mud and granulated blast furnace slag were mixed to form building blocks [231]. The sand was partially substituted with the slag increasing the compressive strength of the final material. The addition of 30 % red mud was proposed to be the optimum content providing adequate strength and stiffness. The authors also indicated that the mixtures containing cement mortar and geopolymer showed better performance than mixtures produced only with geopolymers.

Fire and heat resistance of building elements could be an exceptional characteristic, which could extend the structure's service life during fires. Geopolymers were first introduced by Joseph Davidovits in the early 1970s, where his primary aim was to produce nonflammable and noncombustible plastics [14]. Some geopolymer binder and cement mixtures are capable of strength gain when exposed to extreme heat, which could be beneficial for building fire/heat resistant structures. The strength gain of different geopolymer mixtures has been evaluated. The results indicated that mixtures having fly ash as precursors could benefit from strength gain when exposed to extreme temperatures [232,233]. An extensive review of bricks made of waste material could be found in [234].

Metakaolin was partially substituted with powdered clay bricks in an attempt to produce green geopolymer bricks [235]. Moreover, waste plastic and crushed clay

bricks were used as the aggregates. The mixtures showed a moisture absorption between 3.66 to 5.32%. The authors concluded that the paving bricks could be used in a wide range of applications including in harsh environments.

The recycling of waste mineral fillers into geopolymer paving blocks has been shown to be successful. However, the application of waste silt into geopolymer materials is scarce. The current study aims to investigate the feasibility of recycling waste silt obtained from a local aggregate/asphalt production company (Bologna, Italy) in geopolymer paving blocks.

6.2 Materials

The aggregates including silt, sand (0-4 mm) and gravel (4-8 mm) were provided by S.A.P.A.B.A. The detailed properties of the raw material are presented in section 1.3. Moreover, the silt was thermally treated at 750 °C for 2 hours [47]. The calcined silt was used as a filler for geopolymer brick production. The raw and calcined silt are shown in Figure 6.1.

Figure 6.1. Silt sedimentation lakes at S.A.P.A.B.A., Italy.

6.3 Experimental program

6.3.1 Geopolymer cement

The geopolymer cement was produced by mixing metakaolin with an alkaline solution composed of potassium silicate (PS) (MR=3.0) and 99.8% pure NaOH (SH) pellets (Thermo Fisher). The mixture had a mk/silt of 0.3 and a liquid/solid of 0.6. To ensure adequate fluidity of the mixture, the $H_2O/(Na,K)_2O$ was set to 23.57.

After sample preparation, the materials were poured into 4x4 cm cubic molds, covered with plastic lids to prevent water evaporation and stored at room temperature for 1 day. The samples were demolded the following day and were further cured at room temperature for 28 days. The fully cured samples were tested for compressive strength using a hydraulic press. A total of 3 cubic samples were tested for the unconfined compressive strength (UCS) at ambient temperature. To evaluate the heat resistance of the geopolymer cement at high temperature, three additional cubic samples were produced and cured similarly. The samples were then exposed to extreme heat (1000 °) in a static furnace for 2 hours and tested for UCS.

Thermal analysis (TA) is related to a set of methods, which investigate the properties of materials exposed to high temperatures. For this study, a Simultaneous Thermogravimetry and Differential Thermal Analysis (TGA/DTA) was conducted for temperatures between 0 to 1000 °C. The decomposition and mass loss were studied by the Thermogravimetric Analysis (TGA), while the nature of the reactions (endo/exothermic) and possible phase changes were determined by the Differential Thermal Analysis (DTA). The UCS and TGA/DTA on the geopolymer cement samples could identify potential strength or flaws of geopolymer bricks at high temperatures. This is beneficial since the final paving blocks could be used for pedestrian pathways of galleries, where an understanding of material's behavior at high temperatures (i.e., fire) is essential.

 The microstructure of the geopolymer cement was studied using Scanning Electron Microscopy (SEM) imaging.

6.3.2 Geopolymer brick

The geopolymer cement was mixed with limestone aggregates to produce the experimental geopolymer paving blocks. Figure 6.2 shows the aggregate gradation curve used for the current study [43]. Moreover, the geopolymer cement to aggregate ratio was set to 0.40, providing suitable workability of the mixture during molding. The mixtures were poured in special plastic molds (20x10x6 cm) and vibrated to release any trapped air bubbles. The molds were covered and cured at room temperatures for five days. The samples were then oven cured for 48 hours at 60 °C. A final room temperature curing for 28 days were applied. The final product is shown in Figure 6.3. A total of 9 geopolymer blocks were produced and the samples were classified based on EN 1338 standard, which specifically characterizes concrete paving blocks. Consequently, the following tests were conducted on the experimental samples:

- Shape and dimensions

- Weathering resistance in terms of water absorption

- Tensile splitting strength (T)

- Abrasion resistance

- Slip/skid resistance
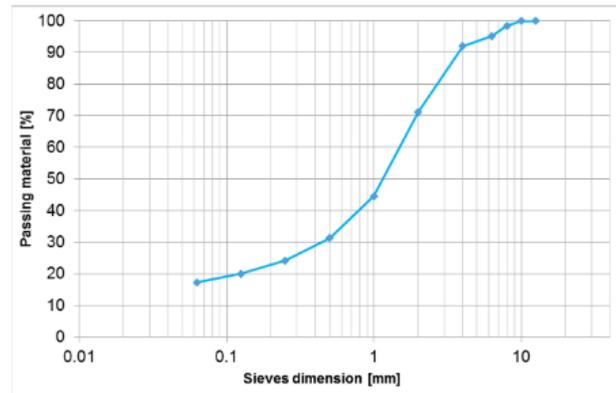
Figure 6.2. Aggregate gradation curve used to produce experimental paving blocks

Figure 6.3. Geopolymer bricks containing waste silt

6.4 Results and Discussion

6.4.1 Geopolymer cement

Two sets of identical geopolymer cement mixtures were produced and cured for 28 days at room temperature. In addition to room temperature curing, one set was placed in a static furnace and was further cured at 1000 °C for 2 hours, whereas the other set underwent no additional curing. Figure 6.4 illustrates the specimens, where the sample cured at 1000 °C is denoted as "A". Clear signs of macro cracks and pores was observable for sample A showing the aftereffects of extreme heat exposure. The surface

of the heated sample was rougher, and brittle compared to the one of the control samples.
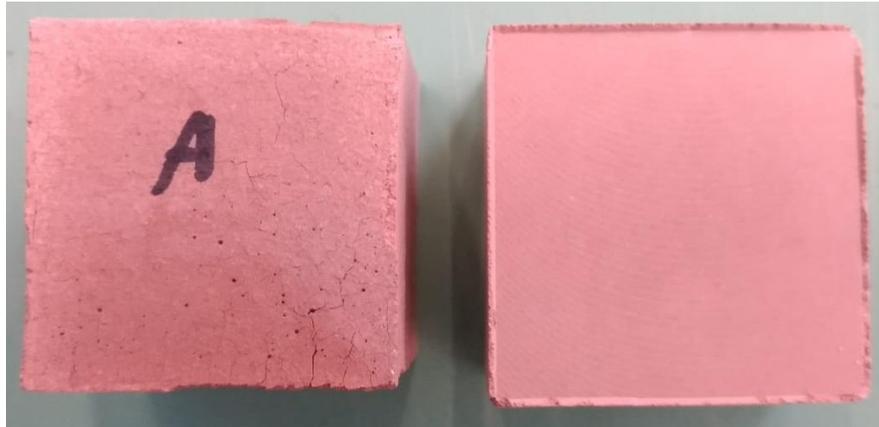
Figure 6.4. Geopolymer cement specimens. The designated sample (A) underwent thermal exposure of 1000 °C for 2 hours.

6.4.1.1 Geopolymer cement Unconfined Compressive Strength

The UCS results of the geopolymer cement cubes returned an average value of 40.41 MPa for the control sample cured at room temperature (25 °C). However, curing the sample for 2 hours at 1000 °C resulted in an approximate loss of 36 % (14.6 MPa) in terms of compressive strength. The exposure of geopolymer samples to elevated temperatures could lead to loss or gain of compressive strength. The former could be due to thermal incompatibility of the material, whereas the latter generally occurs for a further geopolymerization or sintering of unreacted precursors [232]. The drop of the silt-based geopolymer cement strength after extreme heating could be related to mineralogy of the waste silt, which has shown to be partially reactive [47,48]. Thus, unlike fly ash-based geopolymer cements, the unreacted silt particles could not benefit from the strength gain during exposure to elevated heating [233]. Nevertheless, the strength loss of the geopolymer cement at 1000 °C was within the limits (<60%) suggested by Davidovits [14].

6.4.1.2 Thermal Analysis (TA) of geopolymer cement

The thermal properties of the geopolymer cement were further evaluated through thermogravimetric analysis. The changes in mass, DTG and DTA are shown in Figure 6.5. The total mass loss (%) for the geopolymer cement recorded at 1000 °C was 18.3%, which is higher than the proposed values (<5% @1000 °C) for a thermally stable geopolymer. However, the 36% loss of compressive strength was about half of the assumed value of <60% (at 1000 °C) indicating acceptable strength values [14]. The loss of about 2% of total mass is observable between 20-100 °C which is associated with loss of physically bonded water. The dehydration process produces pores and cracks on the surface of the geopolymer and is also responsible for its shrinkage. The endothermic peak of the TDA and DTG curve also indicate the loss of chemically bonded water (zeolite water), which occurs at temperatures ranging from 100-300 °C depending on the heating setup and rate of the experiment. Temperatures above 300 °C will result in the dihydroxylation of different OH groups available within the geopolymer mixture [14]. The sharp endothermic peak indicated by the DTA graph (650-750 °C) indicates a phase change, which could be related to collapse of calcite and formation of new mineral phases. As discussed in our previous work [47], these phases could be a wollastonite-type ($CaSiO_3$) new phase, a diopside-like ($CaMgSiO_2O_6$) phase and/or a mineral in the Åkermanite ($Ca_2MgSi_2O_7$)–gehlenite ($Ca_2Al(SiAl)O_7$) solid solution.
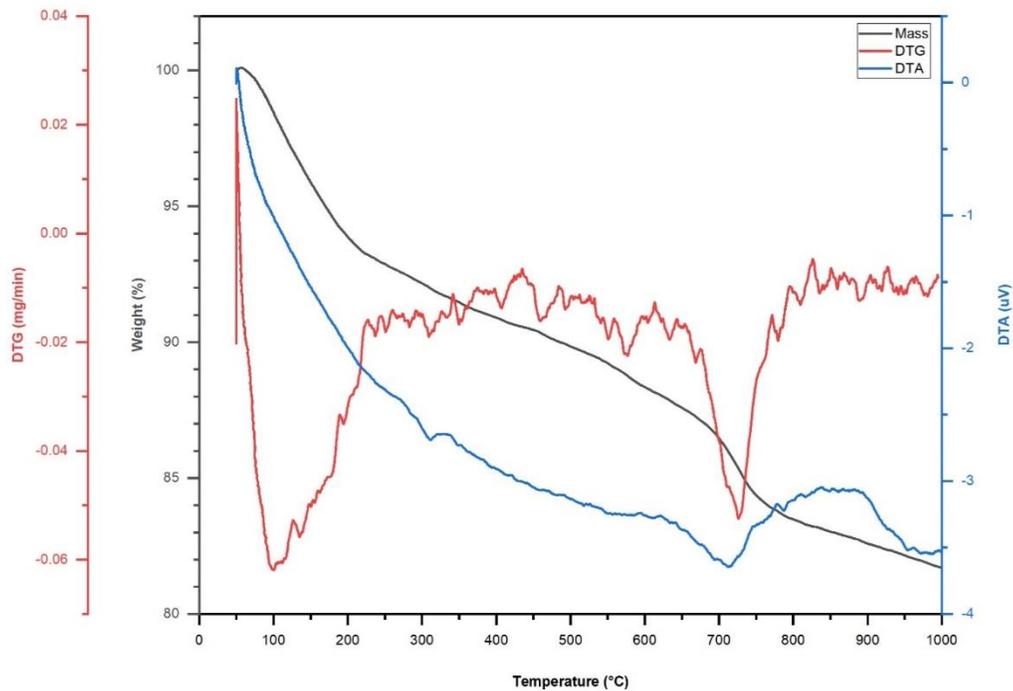
Figure 6.5. TGA/DTA graphs for geopolymer cement samples

6.4.1.3 Geopolymer cement Microstructure

The morphology of silt-based geopolymer cement is demonstrated in Figure 6.6 through SAM images. The formed geopolymer gels are the product of the reaction of MK and waste silt with potassium silicate and sodium hydroxide. The microstructures show micropores and microcracks measuring up to 5 µm in length. The curing conditions could play a major role on the micropore and microcrack formation within the geopolymer cement mixture. The loss of moisture should be avoided since it could produce microcracks within the mixture. It is for this reason that curing at controlled humidity is suggested [236,237]. Despite the microcracks, the mixtures composition seems to be homogenous, suggesting a well-formed geopolymerized network. Unidentified particles are observable in Figure 6.6c and Figure 6.6d, which could be unreacted MK and/or silt particles. The layered structure of the MK-based geopolymer

135

cement is clearly observable in Figure 6.6d, which is agreeable with other findings [238,239]. Improved sample curing conditions through moisture control and vibrations could reduce the produced pores, increasing the overall compressive strength of the geopolymer cement.
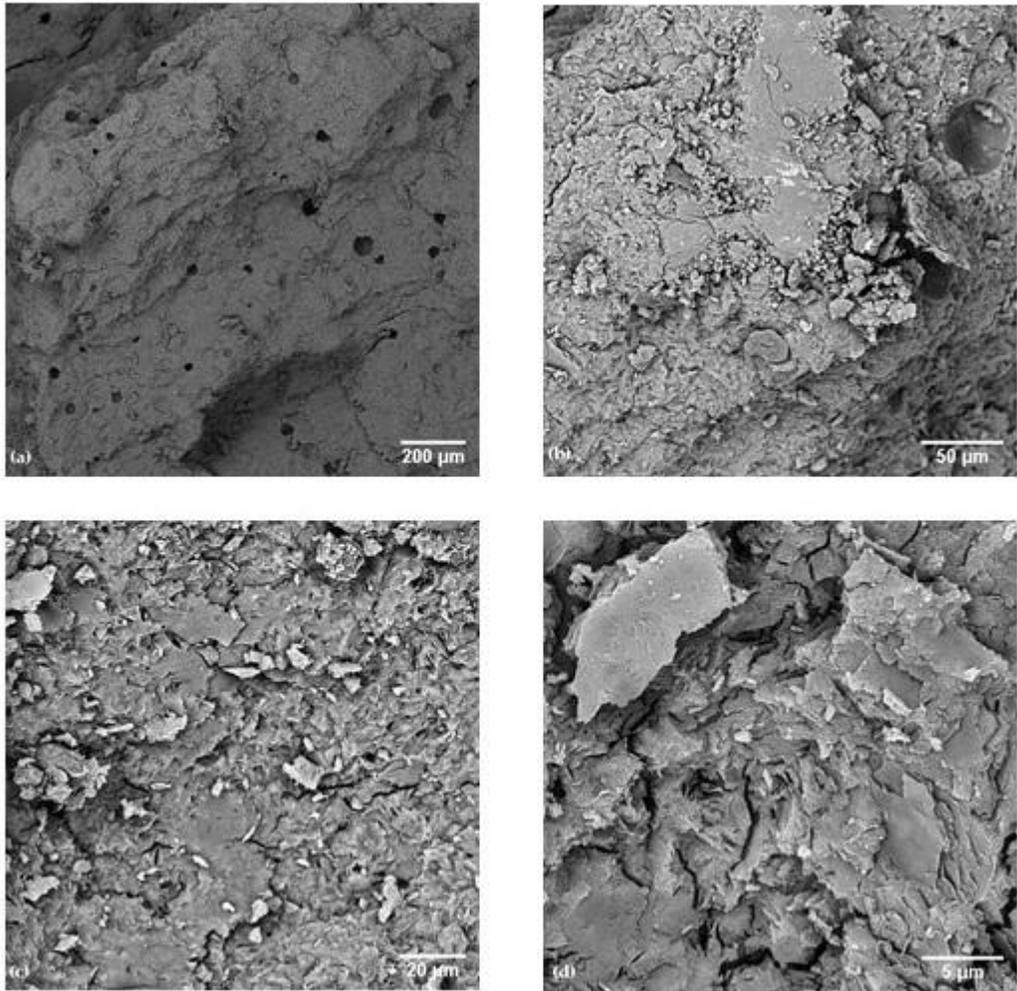
Figure 6.6. SEM images at four different magnifications for geopolymer cement

6.4.2 Geopolymer brick

The geopolymer concrete bricks were produced by mixing the geopolymer cement with predetermined proportions of sand and gravel. The bricks were tested according to the EN 1338 standard. In the following sections, the results related to the tests specified in the standard are presented.

6.4.2.1 Measurements

The geometric measurements of the paving blocks were taken based on the EN 1338 standard. A total of nine blocks were produced, where the measurements of 5 blocks were recorded to the nearest millimeter. Table 6.1 shows the measured dimensions, deviation, and permissible deviations of 5 geopolymer bricks. The results meet the required specifications of the EN 1338 standard suggesting that the geopolymer cement does not affect the workability and casting properties of the mixture to produce bricks.

Table 6.1. Geopolymer paving block average measurements and deviations.

Measurement	Length (mm)	Width (mm)	Height (mm)
Geopolymer blocks	200	100	50
Deviation	±0.36	±1.76	±0.66
Permissible deviation	±2	±2	±3

6.4.2.2 Water Absorption

The water absorption approach was selected to determine the weathering resistance of the paving blocks. Table 6.2 shows the average values obtained for the water absorption.

Table 6.2. Average water absorption data and limits.

Paving Block	Water Absorption (%)
Geopolymer block	6.12
EN 1338	<6% (class 1-Mark B)
Stnd. Dev.	0.08

The water absorption is one of the most important tests required for materials used in pedestrian walk paths. The saturation level of paving blocks is directly related to the porosity of the material, providing indirect information regarding the air voids content of the material. The observed microcracks (Figure 6.6) could also be related to the slightly high moisture content of the bricks. However, the moisture absorption may not be entirely related to the porosity of the samples. Sing et. al. (2020) suggested that portion of water could have reacted with the excess of Na_2O or K_2O from the alkaline solutions resulting in an increase in water absorption [231]. Nevertheless, the reported moisture content was within the suggested values. the silt was calcined at 750 °C for 2 hours prior to use in the geopolymer bricks. A study conducted by Ghani et. al. (2021) suggested that calcination of precursors could dramatically reduce the water absorption of geopolymer samples [240].

6.4.2.3 Tensile Splitting Strength

Table 6.3 presents the tensile splitting strength (T) results for the experimental paving blocks. The average value of T and failure load (F) of the blocks were measured as 2.51 MPa and 235.6 (N/mm), respectively. The standard states that T should not be lower than 2.5 MPa in any sample and the overall strength should be higher than 3.6 MPa. Ordinary concrete bricks could reach the suggested strength values after 28 days of curing. The tensile splitting strength values reported for paving blocks vary according to the proportion and type of waste material used [166]. The curing conditions also vary from one study to another, making it hard to find a scientific trend through comparative studies. However, the obtained T values for the geopolymer paving blocks were higher than those reported for the concrete blocks [241]. Nevertheless, both specimens have shown potential and could be further optimized and improved prior to industrial implementation.

Applying pressure during molding of the samples will most likely increase the final strength of the samples. Moreover, the adopted casting method could be responsible

for the formation of air voids, suggested by the relatively low mechanical properties. The adoption of vibration at high frequencies and pressure during the molding procedure could decrease the porosity of the material, improving both properties.

Table 6.3. Average tensile splitting strength of geopolymer paving blocks after 28 days.

Paving Block	T(MPa)	F (N/mm)
Geopolymer block	2.51	235.6
EN 1338 limit	>3.6	>250
Stnd. Dev.	0.16	1.04

6.4.2.4 Abrasion Resistance

The abrasion resistance of the geopolymer paving bricks were determined using the wide wheel abrasion test (Figure 6.7). The obtained results are summarized in Table 6.5. The average of three experimental bricks had an abrasion of 21.97 mm, classifying the bricks as Class 3-Mark H based on the 1338 standard. Geopolymer bricks were able to outperform previous studied concrete bricks [241] in terms of abrasion resistance and were categorized in a higher performance class based on the EN 1338 standard. The curing conditions, mix design, and final surface of the paving blocks can directly affect the abrasion value [43]. Thus, improved resistance in terms of abrasion could be achieved through better curing of the bricks or by the inclusion of various materials such as waste rubber [71,72].

Figure 6.7. Wide wheel abrasion test on geopolymer paving blocks.

Table 6.4. Abrasion resistance for the geopolymer paving blocks.

Paving Block	Groove Dimension (mm)	Classification (EN 1338)
1	22.11	-
2	21.95	-
3	21.84	-
Average	21.97	Class 3-Mark H
Stnd. Dev.	0.11	

6.4.2.5 Skid Resistance

Regardless of the design and application, the safety of the users is of most importance. The unpolished slip-resistance value (USRV), as indicated in Annex I of the EN 1338 standard is one of the most important functional characteristics for paving blocks. The USRV indicates the suitability of paving blocks' finishing surface for pedestrians.

The USRV of three identical paving blocks is shown in Table 6. The geopolymer paving blocks did not show a very high skid and slip resistance values. The average value was only 45, which was 37.5% lower than those obtained for our previous study [241]. However, no limitations or suggestions are given by the EN 1338 standard. The USRV values could be enhanced easily by using a mold with rougher surface and texture. The used mold had a flat and shiny surface lacking any texture, which led to brick surfaces with low skid resistance values.

Table 6.5. Skid resistance of geopolymer paving blocks.

Paving Block	USRV
1	45
2	47
3	46
Average	45
Stnd. Dev.	1

6.5 Conclusion

Geopolymer cement paste was produced, and its mechanical, thermal and morphological properties was evaluated. An average of approximately 40 MPa was obtained for the 28 days compressive strength of the geopolymer cement. This strength dropped by 36% after exposing the cubic samples to 1000 °C for 2 hours. The thermal stability, phase change and mass loss of the geopolymer cement was further investigated through a simultaneous thermal analysis (TGA/DTA). The mass loss of the paste demonstrated the evaporation of physical and zeolite water for temperature ranging between 100-250 °C. Moreover, a possible phase change at 750 °C was shown by the DTA graphs, which could be related to the collapse of the calcite structure within the geopolymer mixture. The SEM images indicated micropores within the mixture, which could be related to the mixing and casting process.

The geopolymer cement was then mixed by coarse and fine aggregates to produce geopolymer concrete paving blocks and were tested according to the EN 1338 standard. Overall, recycling waste silt into geopolymer bricks demonstrated acceptable performance in terms of moisture absorption and abrasion resistance (EN 1338 standard). The produced prototype of paving blocks showed acceptable performance and could be successfully used in the industrial sector. However, further optimizations in the production and casting procedure are needed to overcome the limited mechanical properties.

PART III: ASPHALT PAVEMENTS

PART III aimed at understanding the effect of adding waste filler on different properties of asphalt pavements. Untreated and thermally treated waste silt were added as filler to HMA pavement in Chapter 7. The study was extended to recycling waste silt into a semi-flexible pavement. A new geopolymer-based grouting material was introduced.

The studies presented in this section have been published as follows:

1. Waste silt as a filler in hot mix asphalt: a case study (Submitted)

2. Double-step recycling of thermally treated waste silt in semi-flexible pavements-preliminary study (Submitted)

Chapter 7: Waste silt as a filler in hot mix asphalt: a Laboratory characterization

7.1 Introduction

The asphalt pavement sector is facing new challenges requiring the improvement of pavements performance to meet with the needs of the users and to provide greener solution for a sustainable future. Successful attempts have been made to improve both the performance of asphalt pavements and their environmental impact through the inclusion of waste and recycled materials.

The literature is rich in positive experimental applications of waste materials added into asphalt concretes, enhancing the existing properties of the pavements and providing extra capabilities and functionalities [242–246]. For instance, partial substitution of mineral aggregates with crumb rubber tire could reduce asphalt layers stiffness providing a safer environment for pedestrians [9]. Other approaches require the total or partial substitution of Hot Mix Asphalt (HMA) fillers with waste mineral fillers [247–251].

Fillers occupy between 5 to 12% of asphalt mixture and are very fine materials which mostly pass sieve sizes 0.063 (EN 13043) or 0.075 (ASTM D242) mm depending on the standard used. In contrast to its little amount in a bituminous mixture, its contribution on the physical and chemical properties of material is significant. For instance, fillers complete and satisfy gradation curves and can alter the strength and volumetric properties of mixtures [252]. Fillers could also reduce the optimum binder content through increasing asphalt binder volume. Moreover, the resistance of pavements against low temperature fatigue cracking and rutting is increased [253,254]. The fillers could also influence the thermal sensitivity, aging and thermal performance

of the asphalt mixtures [251,255]. Excessive usage of common filler could produce several environmental risks such as depletion of natural resources. For this reason, finding affordable and sustainable alternatives to replace common fillers in asphalt pavements seems necessary.

Aggregate plants and quarries are providing daily supplies of aggregates to be used in civil engineering applications. Keeping up with the annual supply demands of about 3000 million tons of non-renewable natural aggregates [256], requires non-stop extraction and production of raw materials. During this process, various waste powders are produced that are of hidden value and could be used as a potential substitute for the conventional fillers for construction materials. The type of by-product depends on the stone or material being processed and the extraction and production procedures at the plants.

The influence of several waste filler types on different properties of asphalt pavements have been reviewed by various authors [246,257,258]. In line with the same trend, the effect of clay materials as filler replacements have been studied on pavement properties. For example, natural filler was substituted with 15% of bentonite clay [259]. The partial substitution led to an increased indirect tensile strength and flow values of the HMA mixtures.

Similarly, bentonite clay was used as a filler in hot mix asphalt samples [260]. However, the clay was used in both normal and thermally treated conditions. The clay was calcined at different temperatures ranging from 400-800 °C, where the best treatment was selected based on Atterberg limits aiming for minimized plasticity and swelling of the bentonite clay. Overall, the 100% substitution of the natural filler with the thermally treated bentonite clay showed an increase in several mechanical properties of HMA.

The results from the two different studies shows that thermal treatment of the waste filler could result in better performance of HMA mixtures. A similar trend was observed when the use of normal kaolin and thermally treated kaolin clay as filler in HMA mixture was investigated [261]. Samples produced with 100% thermally treated clay showed to have better performance in terms of Marshall stability and Indirect Tensile Strength (ITS) compared to those of normal kaolin.

Unlike previous studies, the use of normal and thermally treated waste silt obtained from local aggregate/asphalt production plant located in Bologna (Italy) was investigated in the present research. The natural limestone filler was completely replaced with the waste fillers. It is worth noting that silt particles can absorb high amount of water compared to the limestone filler. Thus, the thermal treatment of the silt was carried out in order to eliminate any physically and chemically bonded water within its structure allowing it to be more suitable as HMA filler. No literature was found on the application of waste silt as filler replacement into HMAs, making it a novel and innovative approach towards sustainable pavements.

7.2 Materials

Silt was extracted from the sedimentation lakes, oven dried, sieved and crushed to a very fine powder (Section 1.3). The silt obtained at this stage is referred to as untreated or normal silt.

In addition to the normal state, the waste silt was thermally treated using a static furnace. For this purpose, the silt was calcined at 750 °C for a duration of 2 hours [47]. Calcination is the process of heating of materials to high temperatures in the absence or limited supply of air. The basic purpose of calcination is to remove the impurities and increase the reactivity of compounds. The calcined silt is also referred to as thermally treated silt. The untreated and thermally treated silt and a conventional

limestone filler were used as the filler to produce HMA mixtures. The untreated and treated silt is shown in Figure 7.1.

Figure 7.1. Untreated (left) and thermally treated (right) silt.

An X-ray powder diffraction (XRD) (Rigaku, Tokyo, Japan) was used to analyze the compounds of the silt indicating the presence of quartz (32%), calcite (28%), illite/micas (21%), chlorite (5%) with traces of dolomite and feldspars (Figure 7.2).
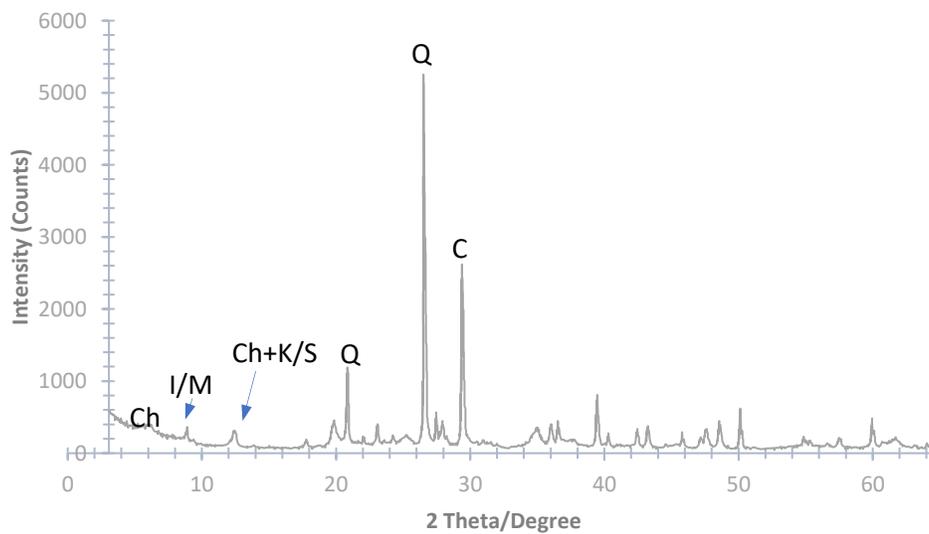
Figure 7.2. XRD analysis of waste silt. The sharp peaks indicate a crystalline structure for the silt.

The aggregates including sand (0-4 mm) and gravel (4-8 mm) were provided by S.A.P.A.B.A. A 50/70 normal bitumen binder was used. The rheological properties of binder are given in Table 7.1.

Table 7.1. Rheological Properties of Binder

Test	Unit	Value	Standard
Penetration @ 25 ˚C	Dmm	50 – 70	EN 1426
Sofetening Point	˚C	50	EN 1427
Dynamic Viscosity @ 60 ˚C	Pa.s	≥145	EN 12596
Fraass	˚C	-8	EN 12593

7.3 Methodology

Two different experimental phases were defined for the current study. With the first part covering the rheological properties of the mastics, the second part was dedicated to the mechanical performance of HMA samples.

The rheological studies were carried out on the mastics, which was composed of 44% bitumen and 56% filler. The aforementioned values were calculated based on the mix design of the HMA, considering the 5.5% of bitumen and 7% of filler on the total mass of the mixture [77]. Three mastics were prepared following that dosage: the control mastic (M-C), the mastic with normal silt (M-SN) and the one with calcined silt (M-SC).

An Anton Paar MCR302 Dynamic Shear Rheometer using 8 mm parallel plate settings (2 mm gap) was used to study the rheological behavior of the produced mastics. An Amplitude Sweep (AS) test was performed to determine the linear viscoelastic (LVE) range of the mastics (EN 1477). The samples were tested at a constant frequency of 1.59 Hz at 10 °C.

A Frequency Sweep (FS) test was then applied considering the lowest linear viscoelastic limit obtained by means of AS test on the three mastics. The FS test allows to evaluate the mastics' behavior and strength under various loading conditions. The

samples were tested at different temperature of 10, 20, 30, 40, 50 and 60 °C for frequencies ranging between 0.01 and 10 Hz. For each mixture, the complex shear modulus (G^*) and phase angle (δ) were calculated.

The permanent deformation of each mastic was determined using Multiple Stress Creep Recovery (MSCR) test (ASTM D7405). MSCR tests were performed at 60 °C on mastic samples loaded at a constant creep stress for 1 second followed by a zero-stress recovery of 9 seconds. The samples underwent shear creep loading and recovery at two stress levels, namely 0.1 kPa and 3.2 kPa. Two cycles each having 20 runs at 0.1 kPa and 10 runs at 3.2 kPa were performed on the mastics. The non-recoverable creep compliance (J_{nr}) and the percent recovery after the latest ten runs at 0.1 and the ten runs at 3.2 kPa were assessed. The J_{nr} values were determined as the ratio between the average non-recoverable strain for 10 creep and recovery cycles, and the applied stress for those cycles. On the other hand, the percent recovery was evaluated considering the recoverable strain, as the ratio between the average recoverable strain after 10 cycles and the applied stress.

As for the second part of the experimental program, an HMA formed by 38% of sand (0-4 mm) and 62% of gravel (4-8 mm) was produced. The control samples had a binder content of 5.5% (on total weight of the mixture) and the limestone filler amount was set to 7%. For the two experimental HMAs, the normal and calcined silt were used in total substitution of the limestone filler. To evaluate the effect of filler type on the mechanical properties, HMA samples were prepared according to the Marshall method. The aggregates gradation was kept constant for all mixture types.

The optimum binder content (OBC) of the mixtures containing untreated silt (labelled HMA-SN) and thermally treated silt (labelled HMA-SC) were determined (EN 12697-30). A total of 9 mixtures for each set was produced and the OBC was determined based on the highest Marshall stability (EN 12697-34).

The mechanical characterization of the samples was conducted on specimens produced with the optimum binder content. The air voids content of the Marshall samples was calculated based on the EN 12697-8 standard. To study the resistance of the mixtures against moisture a total of six samples (for each set) were produced using the Marshall method. Three samples were tested with dry conditions (25 °C) and the remaining three were tested after being submerged in water at 40 °C for 72 hours. The Indirect Tensile Strength (ITS) (EN 12697-23) test was then conducted on the 6 samples. The susceptibility of the mixtures to moisture was evaluated by comparing the ITS of wet and dry samples based on EN 12697-12. Moreover, all samples were tested in terms of Indirect Tensile Stiffness Modulus (ITSM, EN 12697-26 Annex C) at three different temperatures of 10, 20 and 30 °C to evaluate the possible change in the thermal sensitivity of the mixtures given by the addition of the waste fillers.

7.4 Results and Discussion

7.4.1 . Bituminous mastic analysis

7.4.1.1 . Frequency sweep analysis

The complex shear modulus and phase angle master curves of the three mastics are presented in Figure 7.3. The linear visco-elastic analysis indicated similar behavior for M-C and M-SC samples in terms of the complex shear modulus. Thus, samples produced with calcined silt provided similar stiffness as the control samples produced with limestone filler. The same trend was followed at all frequency ranges. However, lower stiffness was observed for M-SN samples, which were produced with normal silt.

The elastic response of the three mastics showed to be similar throughout the range of frequencies and/or temperatures. With an increase in temperature and loading (lower frequency values), all three mastics showed fully viscous behavior (i.e., the phase angle is approx. 90°). At the opposite conditions, the three mastics behaved more like an

elastic material. Overall, the addition of the experimental fillers did not alter the rheological properties of the tested mastics and its trend. On the other hand, the addition of normal silt leads to a general reduction of the complex shear modulus if compared to the control mastic. According to the XRD analysis of section 5.3.1, the calcination of silt led to a complete collapse of calcite ($CaCO_3$) peaks. The calcination of calcite at high temperatures, decomposes the material into CaO and carbon dioxide (gas form) [262]. Thus, calcined silt has more CaO compared to untreated silt, which could explain the better behavior of the M-SC mastic compared to M-C.
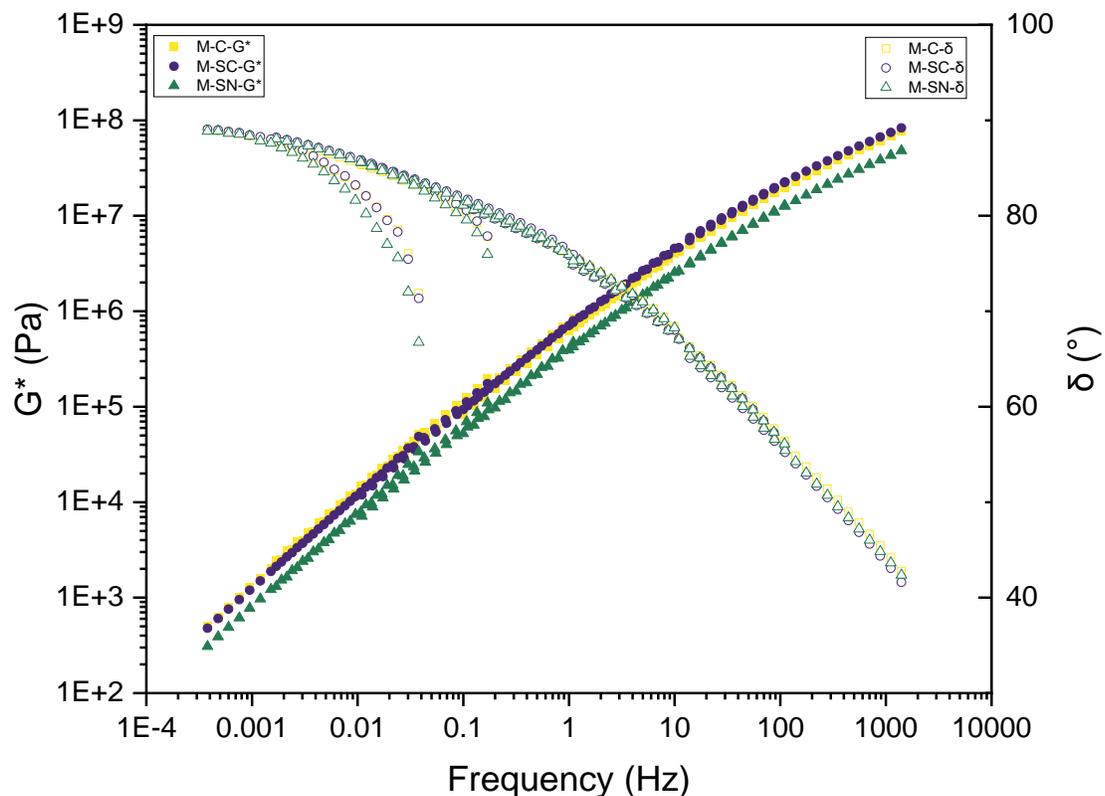
Figure 7.3. Complex modulus and phase angle master curves for all mastic samples

7.4.1.2 . Multiple stress creep recovery

The accumulated strain obtained from the MSCR test at 60 °C is shown in Figure 7.4. The addition of untreated silt to the mixture resulted in an important increase in the accumulated strain, when compared to M-C and M-SC. However, the samples produced with thermally treated silt as filler (M-SC) had the lowest values for accumulated strain and performed slightly better than the control sample (M-C). The rate of change in strain values starts to increase when the 3.2 kPa loading was applied after the 20th cycle and significantly increases after the 200th second.

The resistance of binders to permeant deformation (rutting) could be studied through the J_{nr} parameter. Higher susceptibility towards permanent deformation is related to higher J_{nr} values. The reported J_{nr} value for M-SN was the lowest compared to the remaining samples. The inclusion of untreated silt increased the J_{nr} parameter by 1.54 times. However, thermally treated silt showed an improved performance in terms of rutting and reduced the non-recoverable creep compliance by 9.54% compared to the M-C mastic.

The average values of the percent recovery and J_{nr} of the three mastics are reported in Table 7.2. The average values of the percent recovery of all samples, regardless of filler type and stress level, were close to zero, while the J_{nr} was greater than zero for all mastics. This is an indication of viscous behavior of the mastics at high temperature. The percent recovery and the J_{nr} values confirmed the rheological data collected during the FS test. Moreover, the mastic produced with the thermally treated silt behaved similarly to the mastic with standard limestone filler.
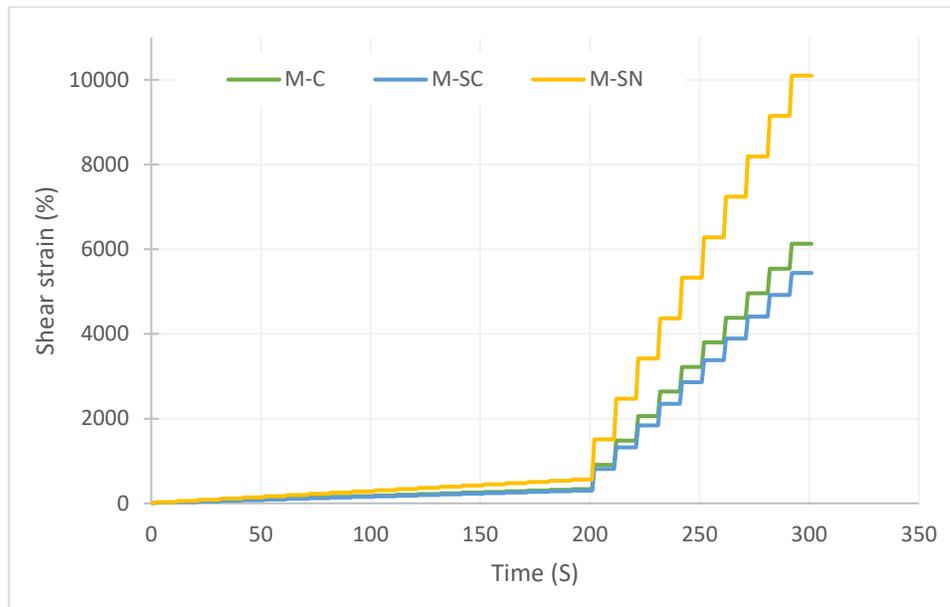
Figure 7.4. MSCR test at 60 °C for all mastic samples

Table 7.2. Average recoverable strain and non-recoverable compliance at 3.2 kPa.

Sample	Percent recovery (%)	J_{nr} (%)
M-C	0	6.015
M-SC	0	5.438
M-SN	0	9.267

7.4.2 Hot Mix Asphalt Results

7.4.2.1 Optimum binder content and air voids

The control mix design (HMA-C) obtained from previous analysis had an OBC of 5.5% on the mass of aggregates. However, the samples produced with untreated (HMA-SN) or calcined silt (HMA-SC) could require a different amount of binder, considering the possible different absorption properties of the powders. Thus, the optimum binder content of the experimental HMAs was calculated.

For each mixture, three different binder content of 5.0, 5.5 and 6.0% were selected resulting in 9 Marshall samples for each HMA. The samples were produced according to the EN 12697-34 standard applying 75 blows to each side during sample compaction. Samples were immersed in water for 30 minutes at 60 °C and were tested for the Marshall stability test. The average data for the Marshall stability and air voids content (Va, EN 12697-8) are summarized in Table 7.3 and presented in Figure 7.5.

Table 7.3. Marshall stability and air voids content for HMA mixtures

Sample	Binder (%)	Stability (KN)	Va (%) *	Avg. Va (%)
HMA-C	5.5	17.20	3.27	3.27
HMA-SN1	5	11.53	4.03	
HMA-SN2	5.5	13.25	3.89	3.91
HMA-SN3	6	11.67	3.81	
HMA-SC1	5	12.99	3.76	
HMA-SC2	5.5	16.68	3.91	3.87
HMA-SC3	6	15.27	3.93	
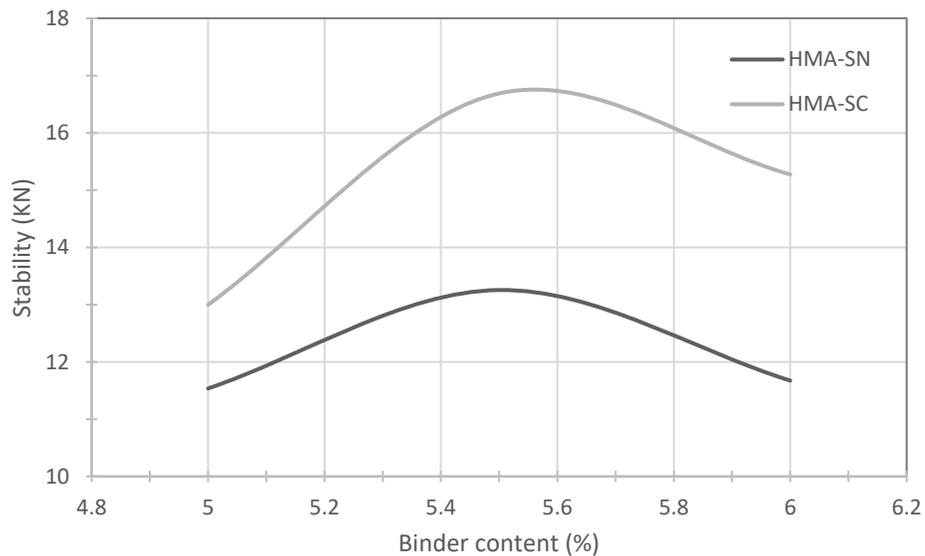
Figure 7.5. Marshall stability for HMA samples.

The maximum Marshall stability of 17.20 kN was reported for the control sample (HMA-C). The mixtures produced with thermally treated silt followed closely showing a maximum stability equal to 16.68 kN. The lowest Marshall stability value was obtained when untreated silt was used as filler in the mixtures. The performance of calcined silt was better in terms of stability when compared to the untreated silt. A similar trend was observed when thermally treated and untreated bentonite clays were used as filler in HMA mixtures [260]. However, the returned value for the optimum binder content was 5.5% for both mixtures. Thus, the substitution of the limestone filler with untreated or calcined silt did not affect the optimum binder content value. Moreover, the reported stability values were higher than the 11 kN suggest by the Italian technical specifications for this type of bituminous mixture.

The air voids content calculated for samples produced with optimum binder content is also shown in Table 7.3. The highest compaction rate was related to the control sample. The addition of waste silt to asphalt mixtures increased the air voids content regardless of the type of silt used. However, all values were within the range of 3 - 4.5% suggested by the Italian technical specifications taken as a reference.

7.4.2.2 Indirect Tensile Strength

The mechanical properties of the mixtures were further investigated by the means of the Indirect Tensile Strength (ITS) in compliance with the EN 12697-23 standard. For each set of mixture, 3 sets of samples were prepared with the Marshall compactor (75 blows each side). Prior to testing, each specimen was conditioned at 25 °C for 4 hours. The average ITS for each mixture is shown in Figure 7.6.

The results of the one-way ANOVA indicated no significant difference ($p = 0.4598$) between the control, HMA-SN and HMA-SC mixtures. Thus, the inclusion of untreated or thermally treated to asphalt mixtures does not affect the mechanical properties of the bituminous mixture. Overall, all the three mixtures showed values higher than 0.7 MPa

suggested by the Italian technical specifications as threshold value for this type of mixture.
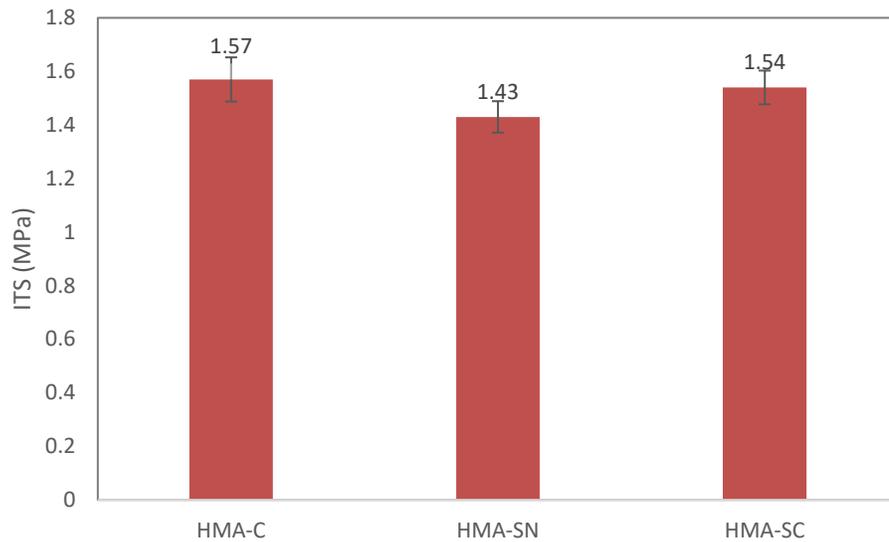
Figure 7.6. Average Indirect Tensile Strength of HMA mixtures at 25 °C.

7.4.2.3 . Indirect Tensile Strength Ratio

The Indirect Tensile Strength Ratio (ITSR) measures the loss of strength due to the damage caused by moisture. For this purpose, a total of 3 samples was prepared for each set according to the Marshall method. The samples were kept in a water bath at 40 °C for a duration of 72 hours (EN 12697-12). The ITSR is the ratio of the indirect tensile strength of wet (water conditioned) specimens to that of dry specimens, expressed in percent (Figure 7.7).
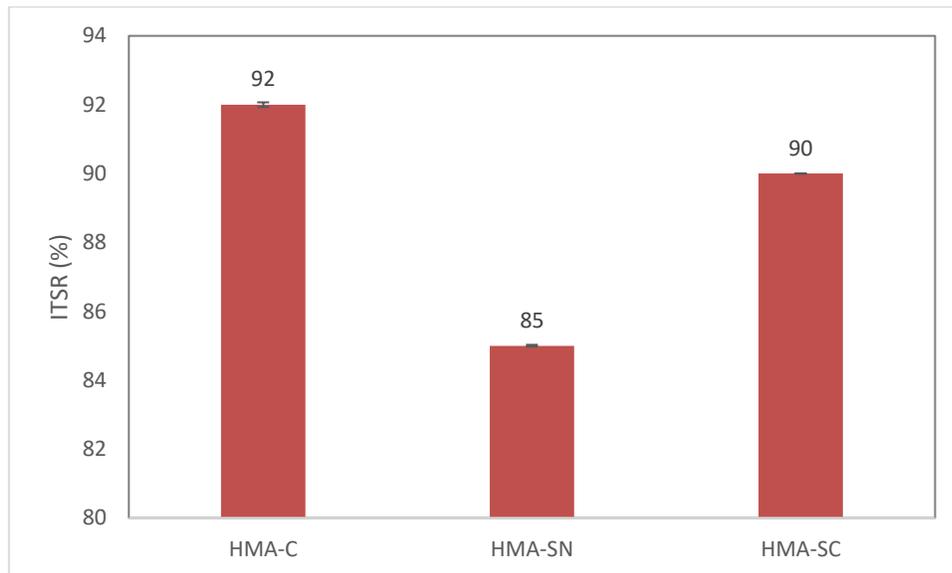
Figure 7.7. Indirect tensile strength ratio for HMA mixtures.

The lowest indirect tensile strength ratio of 85% was recorded for the HMA-SN mixture. The inclusion of untreated silt led to an increase in water sensitivity of the mixtures. This could be related to the natural behavior of silt and clay particles, which have higher water absorption rates than of limestone filler. However, thermal treatment of waste silt at 750 °C had shown to be effective in reducing the moisture susceptibility of the mixtures and increased by 5.0%. The best performance in terms of ITSR was reported for the control sample not containing any waste samples. The Italian specifications suggests that the ITSR values should be greater than 75%.

7.4.2.4 Indirect Tensile Stiffness Modulus

The ITSM values for the asphalt mixtures are shown in Figure 7.8. Each sample was tested at three different temperatures of 10, 20 and 30 °C. Overall, the control samples showed the highest modulus for all the tested temperatures. The lowest values were obtained for samples produced with normal silt. One-way ANOVA was conducted to further investigate the effect of mixture type on the final ITSM value. No significant difference ($p = 0.1321$) was observed for the ITSM values of different samples

measured at 10 °C. Thus, regardless of filler used, all HMAs performed similarly at low temperature. On the other hand, a significant difference (p= 0.00005) was observed for samples tested at 20 °C. The addition of silt reduces the stiffness of the mixture, with a minor effect if the calcined silt is used. Finally, mixtures made with calcined silt and normal filler showed similar performance in terms of ITSM at 30 °C. All in all, although the substitution of limestone filler with waste silt showed a detrimental effect in terms of stiffness, the ITSM values for the experimental mixtures were considerably high considering that a neat bitumen was used for the mixture.
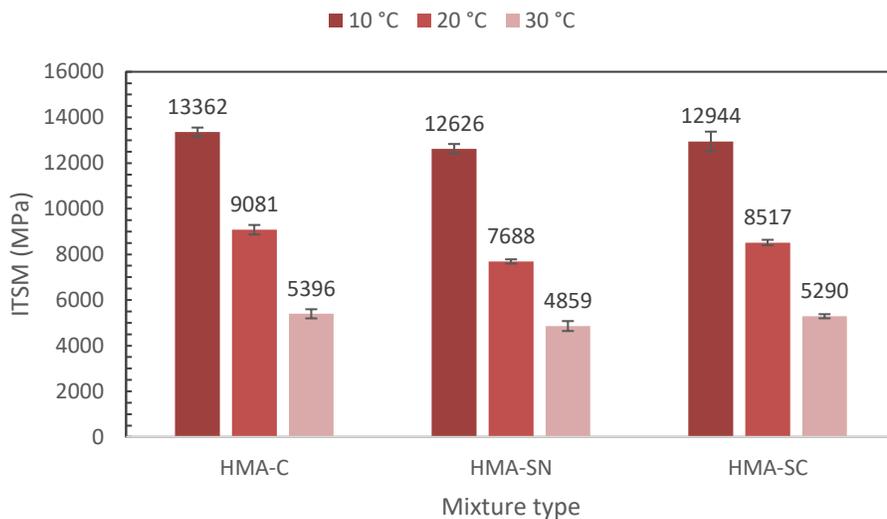
Figure 7.8. ITSM for HMA mixtures

7.5 Conclusion

Untreated and thermally treated waste silt from local aggregate production plant were used as a replacement for convenient limestone filler for the production of HMAs. The evaluation of the effects given by the adoption of the waste fillers was studied in a two-stage laboratory analysis, studying the binder-filler interaction and the HMA physical and mechanical properties.

The following conclusion could be drawn from the results here presented:

- The addition of thermally treated silt had no significant effect on the rheological properties of the mastic in terms of complex modulus and phase angle. On the other hand, the untreated silt demonstrated a detrimental effect for these rheological properties.

- In terms of rutting performance, thermally treated silt had the highest resistance against permanent deformation. This was observable in lower accumulated strain and lower non-recoverable compliance values. Untreated silt showed the lowest resistance against rutting.

- The replacement of limestone filler with waste silt did not alter the optimum binder content of the mixture as well as the porosity of the produced samples. Thus, the presence of waste silt does not negatively affect the workability and compactability properties of the bituminous mixture.

- The inclusion of untreated silt as filler resulted in a reduction in the ITS values. On the contrary, thermally treated silt demonstrated similar performance to the control sample. The same trend was recorded for the water susceptibility of the mixtures.

- The ITSM results were in line with the static mechanical characterization: a slight reduction in stiffness was recorded for the HMA-SC mixture, while a clear drop in ITSM values occurred when untreated silt was adopted. However, the thermal sensitivity of the mixture was not influenced by the substitution of limestone filler with waste powders.

Based on the presented preliminary results, the use of waste silt as filler could be a potential solution towards a sustainable and eco-friendly HMAs. Silt calcination proved to be beneficial since it reduces the influence of the waste material on the rheological and mechanical properties of the bituminous mixture. A partial substitution of limestone filler instead of the current total replacement could possibly provide better mechanical performance. Further studies are needed to back up this assumption.

Chapter 8: Thermally treated waste silt as geopolymer grouting material and filler for semi-flexible pavements

8.1 Introduction

The non-stop growth in infrastructures construction and their developments could drastically affect the worldwide supply of natural aggregates. The aggregate production plants annually produce about 3000 million tons of non-renewable natural aggregates [1]. With that, different types of waste materials and by-products are produced which could potentially be of a high value. However, due to a lack of recycling strategies, waste by-products have been stockpiled and landfilled giving rise to potential environmental and safety issues. To sustainably prevent the future shortage of natural aggregates and resolve the issues related to waste landfilling, various researchers have promoted the recycling of by-products into asphalt pavements.

Semi-flexible pavements (SFP) inherit the flexibility of common asphalt pavement and simultaneously benefit from the rigidity of cement concrete pavements. The SFP has a porous skeleton with high air voids content of 25 to 30%. The voids are filled a with special cementitious grouting material. Improved rutting resistance, durability, skid resistance and driving comfort are merely some of the benefits of semi-flexible pavements which have been pointed out by several studies [263]. However, similar to any other cementitious materials, the SFPs have a higher carbon dioxide footprint when compared to traditional bituminous pavements. Sustainable solutions such as the use of geopolymer-based binders as the grouting solution in SFP could reduce the carbon dioxide footprint of the final product.

Geopolymer network is formed when highly reactive precursors such as metakaolin (MK) are mixed with alkaline-based liquid hardeners such as potassium/sodium silicates. The precursors must be rich in aluminum and silicates to produce a strong enough 3D polymer network [238].

To maximize the environmental sustainability of the final product, several experimental applications have been tested trying to couple the use of geopolymers from recycled precursors and waste or second-hand materials as constituents for low impact construction materials.

Reclaimed asphalt pavement (RAP) and geopolymer-based grouts were used to produce semi-flexible asphalt pavements that would not require heating or mechanical compaction energy [264]. Different geopolymer-based grouts combinations consisting of fly ash, ground granulated blast furnace slag, silica fume, and metakaolin were produced and were used to grout porous asphalts made with RAP with varying air void content. The results suggested that grouts with high flowability and strength combined with low RAP content demonstrated the best results.

A mixture of slag, fly ash, sodium silicate and sodium hydroxide was milled for 2 hours and were mixed with water to produce mechanochemical activated geopolymer gout [265]. Different fly ash to slag ratios and molarities of sodium hydroxide solutions were produced and the data were compared with conventional geopolymer cement grouts. The data revealed that the mechanical properties such as the compressive strength and ultrasonic pulse velocity of the mechanochemically grout samples were higher than those of the control mixture.

A waste mud from Panasqueira (Portugal) Tungsten mine was used to produce different geopolymer-based grouts [266]. In addition, various cement-based grouting materials were produced. The mechanical properties of the final semi-flexible pavements indicated a better performance for cement-grouted asphalt pavements. The authors

stated that the curing conditions of the geopolymer grouts need to be further studied. Nonetheless, geopolymer grouted materials containing waste tungsten mud demonstrated valuable potential for being used as a grouting material. Several experimental applications of geopolymer for SFPs verified that the mix design phase of the grouting material is fundamental for the performance of the final material. The application of statistical modeling such as response surface methodology (RSM) could be beneficial [267]. The study successfully optimized the grouting formula based on various response outputs including fluidity, dry-shrinkage ratio and compressive strength after 7 days of curing and compressive strength after 28 days.

The feasibility of using geopolymer-based grouts in SFPs has been investigated by various researchers. However, the data on geopolymer grouts containing waste mineral fillers is very rare. This paper aims at double-recycling waste silt obtained from a local aggregates production plant in Bologna, Italy. The waste silt was thermally treated and then used as a filler in the open-graded asphalt skeleton of the SFP. As of many available options, replacing the filler in asphalt pavement with waste mineral powders has gained attention [268–270].

In an asphalt pavement, the filler is referred to the fine particle that passes the 0.063 mm sieve and generally makes up about 5 to 10 percent of the total asphalt pavement. The dispersion of filler in asphalt binder produces the asphalt mastic which is responsible for bonding the aggregates together providing a strong load-bearing structure [271,272]. Fillers could also decrease the optimum binder content, increase pavement performance at lower temperatures, influence the thermal sensitivity and so the performance of the mixtures [251,253–255]. Furthermore, the calcined silt was also used as filler to produce the geopolymer-based grouting material. No literature was found on the double use of waste silt as filler for the asphalt concrete skeleton and for the geopolymer grouting material for SFPs, making the current study a novel and innovative approach toward sustainable pavements.

8.2 Materials

8.2.1 untreated and thermally treated silt

The waste silt used for the current study was obtained from S.A.P.A.B.A. Material passing sieve 0.063 mm were used as the filler for producing porous asphalt mixtures. According to the data presented in section 1.3, the silt had adequate amount of SiO_2 and Al_2O_3 making it a potential option to be used as filler in geopolymer grout production. However, primary results indicated low reactivity of the raw silt [47]. For this purpose, the silt was calcined using a static furnace. A constant temperature of 750 °C was applied to the raw silt for 2 hours. As a result, the reactivity of the silt was increased and was more suitable to be used as the filler in geopolymer cement grout production. The calcined silt is also referred to as thermally treated silt. Similar to section 7.2, the thermally treated silt and a conventional limestone filler were used as the filler to produce porous asphalt mixtures.

8.2.2 Grouting material

Two different types of grouts were used. A cement-based grout was obtained from local company in Bologna, Italy. This grouting material was used as the control sample. The second type of grout was produced from a geopolymer-based cement. For this purpose, an alkali solution consisting of potassium silicate (MR = 3.0) and sodium hydroxide (98% purity, 8M, Thermofisher) and water was produced. The alkali solution was prepared 24 hours prior to mixing with precursors and waste filler. The liquid part was mixed with an industrial metakaolin and mixing was continued for 5 minutes. This allowed the metakaolin to mix with the liquid and produce a homogeneous mixture. The last stage continued by adding the thermally treated silt to the mixture as the filler. The mixing was continued for an additional 5 minutes.

8.2.3 Aggregates, bitumen and cellulose fiber

The aggregates including sand (0-4 mm) and gravel (4-8 mm) were provided by S.A.P.A.B.A. The sand had bulk density (g/cm3) (UNI 1097-6), sand equivalent (uni 933-8) and harmful fines (gMB/KG) (UNI 933-9) of 2.658, 90 and 0.5, respectively. The bulk density of gravel was 2.667 (g/cm3). Conventional basalt cellulose fiber was used to produce porous asphalt samples. In addition to thermally treated silt, common limestone filler was used as the filler of the control samples. A PmB 25/55 modified bitumen was used as binder for the asphalt concretes. The rheological properties of the bitumen are given in Table 8.1.

Table 8.1. Rheological Properties of PmB 25/55 bitumen.

Test	Unit	Value	Standard
Penetration @ 25 ˚C	Dmm	25-55	EN 1426
Sofetening Point	˚C	70	EN 1427
Dynamic Viscosity @ 160 ˚C	Pa.s	0.4 - 0.7	EN 12596
Flash point	˚C	250	EN ISO 2595

The same type of aggregates, basalt fiber and modified bitumen was used for both gap-graded asphalt mixtures. The only change for the experimental mixture was the total substitution of limestone filler with the calcined silt.

8.3 Experimental program

The experimental plan was divided into two sections. The first part investigated and verified the use of calcined silt as filler in porous asphalt, whereas the second section compared the mechanical properties of the different grouted asphalt concretes. In summary, two different types of mixtures were produced. The first batch used calcined silt as the filler and were grouted with a geopolymer binder. The second batch was used as the control and were produced with the company's limestone filler and cement-based grout.

8.3.1 Gap-graded asphalt mix design

A specific mix design for gap-graded asphalt was adopted based on the aggregates available. Some preliminary tests verified the optimum binder content for the experimental mixture with waste calcined silt, which was found unchanged if compared to the reference asphalt concrete with limestone filler. The details of the mix design are shown in Table 8.2. The aggregate gradation curve is shown in Figure 8.1.

Table 8.2. Porous asphalt mixture proportions

Test	Amount (%)
Optimum binder content	4.2
Aggregate	90.67
filler	4.78
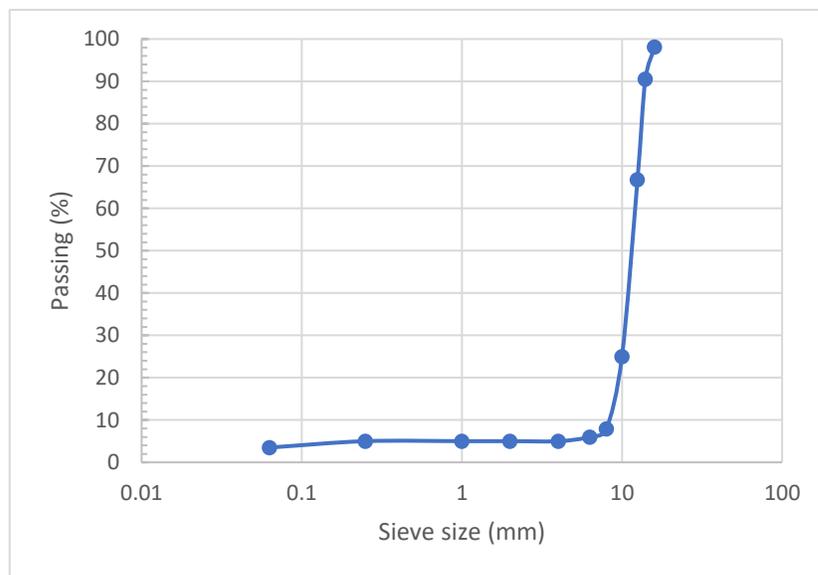
Figure 8.1. Porous asphalt gradation curve.

Two different mixtures were prepared based on the details mentioned in Table 8.2. The first set was produced with a common limestone filler (labelled as PA-C), whereas the second set was produced with calcined silt as the filler (labelled as PA-SC).

The porous asphalt samples were produced using a gyratory compactor (EN 12697-31). The internal angle of the compactor was set to 1.250 °C and a 600 KPa load was applied. Samples with a diameter of 100 mm were produced at 50 and 130 cycles applying a speed of 30 RPM.

The air voids content was calculated based on the EN 12697-8 standard. The air void content was suggested to be between 25 to 30% providing adequate interconnected pores, making the specimens suitable for grouting.

The mechanical properties of the mixtures were investigated with static and dynamic tests. For this purpose, a total of six samples (for each set) were produced using a gyratory compactor (50 cycles). The Indirect Tensile Strength (ITS) (EN 12697-23) test was then conducted on the samples. A constant loading of 50 mm/min was applied until sample failure. The determined maximum load was used to calculate the ITS. Three samples were tested under dry at 25 °C conditions and the remaining three were tested after being submerged in water (40 °C) for 72 hours. The susceptibility of the mixtures to moisture was evaluated by comparing the ITS of wet and dry samples based on EN 12697-12 (Indirect Tensile Strength Ratio, ITSR).

The Indirect Tensile Stiffness Modulus (ITSM) was obtained by applying controlled strain rate loads to the specimens in the indirect tensile configuration. The test followed the EN 12697–26 Annex C standard and was conducted at three different temperatures of 10, 20 and 30 °C in order to evaluate the thermal sensitivity of the asphalt concretes. The samples were conditioned for at least four hours before testing.

8.3.2 Grout formulation and structure

Two different types of grouting mixtures were used for the current study. A common cement-based grout was used as the control sample. The grout was produced by mixing 70% of specific cement with 30% of water. The liquid mixture was mixed for five minutes to produce a homogenized material.

The geopolymer-based grout was produced by mixing the precursor, alkaline hardener and the calcined waste silt according to the specified ratios presented in Table 8.3. For this purpose, metakaolin was mixed with potassium silicate and sodium hydroxide solution for 5 minutes. The calcined silt was then added as the filler and the mixing was continued for an additional 5 minutes. A liquid to solid ratio of 1.5 was adopted to ensure adequate fluidity of the geopolymer mixture, considering that the grouting material should penetrate the porous skeleton of the asphalt concrete, filling the voids.

Table 8.3. Geopolymer-based grout mix design

Material	Amount (% total weight)
Metakaolin	24
Calcined silt	16
KOH (solution)	48
NaOH (8M)	12

The grouting mixtures were characterized in terms of unconfined compressive strength (UCS). The data are presented in Table 8.4. The cement and geopolymer grouts were produced according to Table 3. The mixtures were then placed inside cubic molds (4*4*4 cm) and were cured for 28 days at room temperature. The samples were unmolded and were tested for UCS using a hydraulic press. The highest strength was obtained for the control samples. It is worth mentioning that the most widespread Italian technical specifications for grouted macadam, suggest 35 MPa as lower limit for the UCS after 28 days of curing.

Table 8.4. Average UCS results for geopolymer-based and cement-based grouting mixtures.

Grout	UCS (MPa)
Geopolymer-based grout	13.9 ± 0.4
Control grout	38.8 ± 1.5

8.3.3 grouting of porous asphalt specimens

The samples were put inside Marshall molds where the bottom section was sealed to prevent possible leaking of the grouting material. The prepared grouts were stirred thoroughly prior to use to ensure a homogenized mixture. The material was then poured on top of the porous asphalt specimens. This act was continued until the surface of the samples were covered by the grouting material (Figure 8.2). The samples were cured at room temperatures for 24 hours. All specimens were demolded and cured for 28 days. The grouted samples containing the control limestone filler were designated as GM-C, whereas geopolymer grouts containing calcined silt were labeled as GM-SC.

Figure 8.2. Grouted macadam samples.

The air voids content of the asphalt specimens was calculated before and after grouting. The data is summarized in Table 8.5. Both porous asphalt mixtures showed to have the required 25-30% air voids suggested by Italian specifications. The grouting of the samples dropped the air voids content to 7.11 and 8.94 for the GM-C and GM-SC samples, respectively.

Table 8.5. Air voids content for porous and grouted macadam asphalt samples.

Specimen	Air voids (%)
PA-C	26.22
PA-SC	25.18
GM-C	7.11
GM-SC	8.94

8.4 Results and Discussion

8.4.1 Porous asphalt mixture characterization

8.4.1.1 Indirect Tensile Strength (ITS)

The effect of different asphalt fillers on the mechanical properties of porous asphalt samples were investigated through the Indirect Tensile Strength (ITS) in compliance with the EN 12697-23 standard. All specimens were cured at 25 °C for 4 hours before testing. The ITS results are summarized in Figure 8.3.

The control porous asphalt samples produced with common limestone filler showed an ITS value of 0.605 MPa, whereas the samples produced with thermally treated silt followed up closely showing a 11.9% loss of strength compared to the control samples. The statistical analysis showed an insignificant difference in terms of ITS between the PA-C and PA-SC samples (p=0.568). The addition of waste silt does not significantly affect the cohesion properties of the porous asphalt. Furthermore, it is worth noting that the minimum required ITS for this type of mixture is generally 0.40 MPa according to the most common Italian technical specifications.
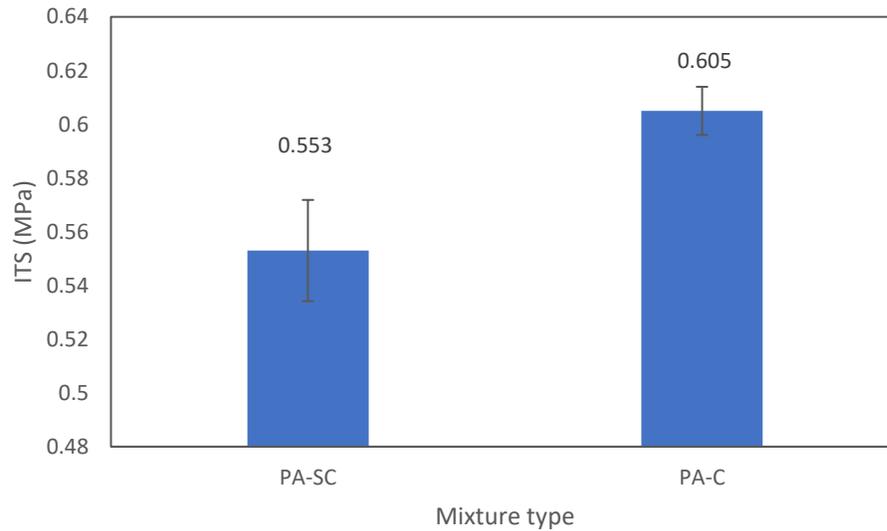
Figure 8.3. Average ITS for porous samples.

8.4.1.2 Indirect Tensile Strength Ratio results

The Indirect Tensile Strength Ratio (ITSR) was used to compare the resistance of the asphalt mixtures produced against moisture damage. For each specimen type, 3 replicas were tested after imbibition in a water bath at 40 °C for 72 hours before testing. The average ITSR values for the porous asphalt specimens are shown in Figure 8.4. The control sample produced with limestone filler had the highest resistance against moisture damage demonstrating an ITSR value of 94%. The inclusion of calcined silt led to a slight reduction in the moisture damage resistance presenting an ITSR value of 92%. The statistical analysis showed no significant difference between the two groups (p=0.218). As for the previous ITS analysis, the ITSR values were above the suggested lower limit for porous asphalt (ITSR > 75 %).
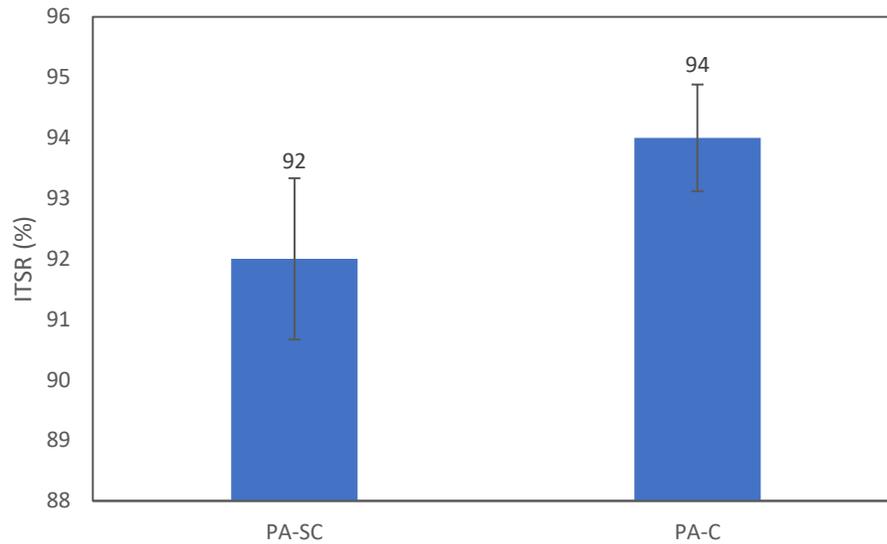
Figure 8.4. Average ITSR results for porous samples.

8.4.1.3 Indirect Tensile Stiffness Modulus (ITSM)

The summary of the average ITSM values is presented in Figure 8.5 for the porous specimens. The thermal sensitivity of the mixtures was studied by testing the samples at 10, 20 and 30 °C. When calcined silt was used as filler in porous asphalt, lower ITSM values were obtained at every testing temperature. Moreover, the ITSM of the control mixture was less susceptible to variations in temperature compared to the PA-SC mixtures. One-way ANOVA was conducted to determine the significance of the results for each testing temperature. The results showed that at both high and low testing temperatures, a significant difference was observed between the two groups. However, samples tested at 20 °C proved to be similar in terms of ITSM values.
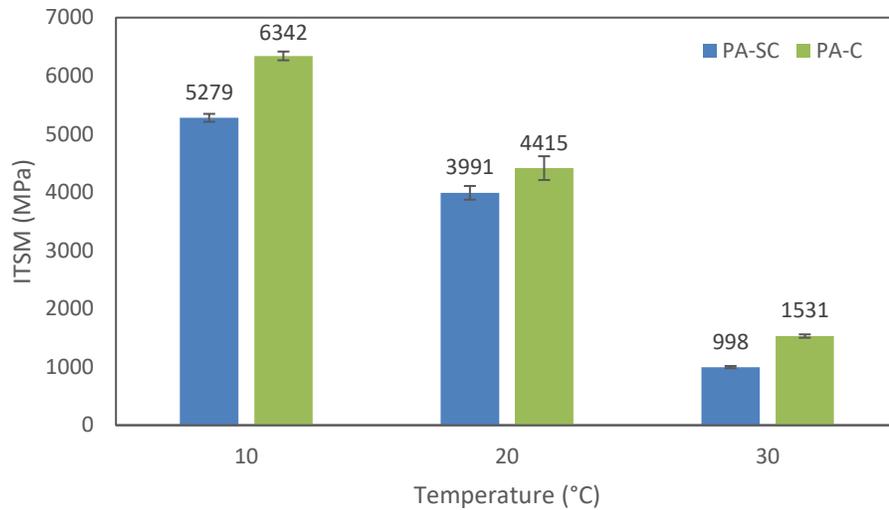
Figure 8.5. Average ITSM values for porous asphalt.

8.4.2 Grouted Macadam Asphalt Mixtures characterization

8.4.2.1 Indirect Tensile Strength results

The ITS data of the grouted samples are shown in Figure 8.6. The highest ITS value of 2.16 MPa was obtained for the control samples, whereas an ITS of 1.55 was measured for the geopolymer cement grouted macadam specimens. The lower values for the geopolymer grouted samples could be related to the low strength of the geopolymer mortar. The grout was designed in such a way to ensure enough fluidity of the sample. Thus, the liquid to solid ratio of the mixture was much higher than the 0.45-0.55 ratios suggested by various studies [14,238]. Higher liquid ratios could result in a drop in the compressive strength of the sample due to the brittleness of the produced geopolymer cement. The statistical analysis indicated a significant difference between the different types of grouted mixtures in terms of the ITS (p=0.0184).

171
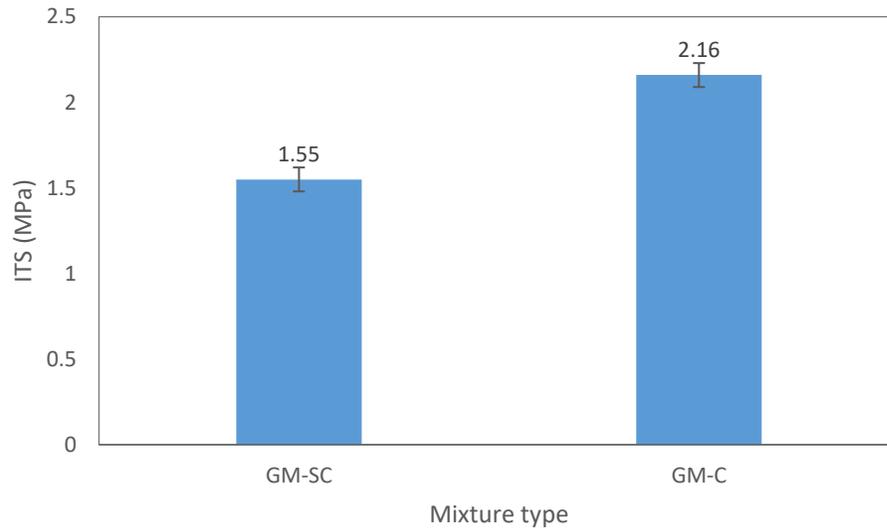
Figure 8.6. Average ITS of grouted mixtures

8.4.2.2 Indirect Tensile Strength Ratio results

The ITSR of grouted samples is shown in Figure 8.7. The control sample presented an ITSR of 93%, while the ITSR of the geopolymer grouted samples dropped by 13%. However, no significant difference was observed in terms of ITSR between the two groups (p=0.061). This loss of strength could be related to the fact that geopolymer cement have high water absorption rates [14]. Moreover, this could be coupled with the water absorption abilities of the silt, which could lead to partial swelling of the geopolymer-based grout.
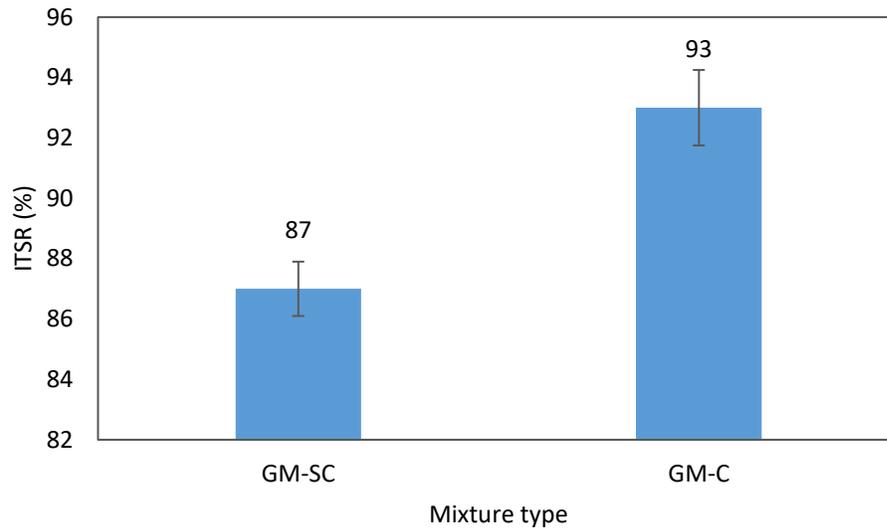
Figure 8.7. Average ITSR of grouted macadam samples.

8.4.2.3 Indirect Tensile Stiffness Modulus results

Figure 8.8 depicts the ITSM values obtained at three different testing temperatures of 10, 20 and 30 °C. The grouted samples showed an ITSM value of 8991 MPa at 10 °C, which decreased by 4.42% when compared to the control sample. The loss of stiffness was observed for every testing temperature: at 20 and 30 °C a decrease of 42.97 and 39.40% was reported, respectively.

The geopolymer cement had a low UCS value of 13.97 MPa which was approximately 64% lower than the control grout cement. The lower stiffness modulus of the experimental grouted asphalt concrete could be related to the lower mechanical properties of the geopolymer-based grouting material.
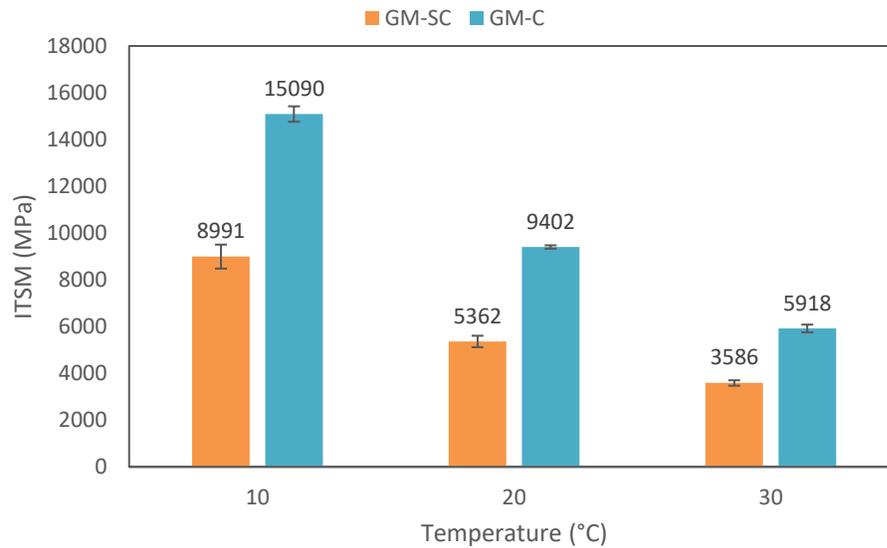
Figure 8.8. Average ITSM values for grouted macadam samples.

8.5 Conclusion

This paper promoted a double recycling technique, where a thermally treated waste silt was used as filler for the bituminous skeleton and for the geopolymer-based grouting material of grouted asphalt concrete. The proposed recycling technique could benefit the road industry by reducing production costs (aggregates extraction and cement production), increasing the sustainability of road pavements. The resulted semi-flexible pavement containing waste silt was compared with a conventional grouted mixture. The main conclusions are as follows:

- The air voids content of the porous samples was within the suggested range of 25-30%. Thus, the inclusion of thermally treated waste silt as filler does not alter the workability and compactability properties of the porous asphalt concrete.

- The ITS and ITSR values of both porous samples were similar. Slight decrease of the indirect tensile strength was observed when calcined silt was added. However, both values were considerably above the lower

cohesion limit suggested for porous asphalts. Similar trend was observed for the ITSR.

- The ITSM values of the control porous asphalt were higher than those of the geopolymer grouted samples.

- The ITS and ITSR of the grouted mixtures indicated better performance for the control mixture if compared to the experimental one. A drop of approximately 28% was observed when geopolymer was used as the grouting material. The ITSR of the geopolymer was 6.5% lower than that of the control specimen.

Due to the lower mechanical performances of the geopolymer-based grouting material, the experimental samples showed lower ITSM values.

Based on the preliminary results, the use of thermally treated waste silt as filler in porous asphalt demonstrated promising results. However, the use of waste calcined silt to produce geopolymer-based grouting materials led to a significant drop in the mechanical properties of the final grouted asphalt concrete. Future studies will focus on the optimization of the grouting mixture aiming to replicate the performance of the cement-based one.

Chapter 9: Conclusion

The current study aimed at providing novel solutions on recycling limestone aggregate production by-product, waste silt, into new paving solutions. The waste silt was obtained from S.A.P.A.B.A. which is an asphalt and aggregate production plant in Bologna, Italy. Recycling of the silt could provide a circular economy for the company and more importantly minimize the impact of the sedimentation lakes on the environment. Consequently, a total of three major objectives were determined that followed the overall aim of recycling waste silt in novel paving solutions. This was pursued in three different parts, where the silt was used in cement-bound, geopolymer cements and asphalt pavement. The outcome of the objectives was paving blocks and asphalt pavement wearing courses that demonstrated acceptable performance. The detailed conclusion of each part is discussed in the following paragraphs.

In PART I, the investigations focused on recycling waste silt into cement-bound materials. A DOE was applied and a total of 49 randomized cement mortar samples were produced. The aim of the implemented DOE was to optimize mixtures by maximizing the amount of silt used within the mixtures in such way that it would not affect the mechanical properties of the samples. The obtained results demonstrated the possibility of substituting up to 20% of natural sand with waste silt in cement mortar mixtures. The corresponding maximum compressive and flexural strength were reported as 22 MPa and 4.0 MPa, respectively. Moreover, the prediction function of the JMP software indicated that the inclusion of only 16% silt to cement mortar samples could increase the compressive and flexural strength by 36.4 and 62.5 %, respectively. The investigation continued by exploring the possibility of including silt in concrete paving block. For this purpose, a DOE was produced and a total of 12 different aggregate blends consisting of gravel, sand, and silt were produced and were tested for

tensile splitting strength (EN 1338). The optimized mix design having 15% gravel, 65% sand, and 20% of silt was chosen and the produced mixture was fully characterized based on EN 1338 standard. The results showed to be promising and the produced bricks could be used in paving blocks after further modifications.

PART II explored the possibility of producing silt-based geopolymer cement and concrete specimens that could be used in civil engineering applications. The application of mining waste and quarry dust in geopolymers were thoroughly summarized. The literature indicated thermal calcination of the waste material as an important step for producing geopolymer samples containing waste quarry dust. Thus, a RSM was applied, and the best calcination time and temperature of waste silt was determined. A calcination time of 2 hours at 750 °C was determined based on the mineralogical, mechanical and environmental properties of the calcined silt. Higher calcination temperatures produced higher compressive strength indicating an increase in the reactiveness of the calcined silt. Precursors should be highly reactive material with amorphous phases. However, high crystalline phases were still evident for the thermally treated waste silt indicating the feasibility of using the calcined material merely as a filler in geopolymer cement production. The same optimum calcination procedure was adopted and silt-based geopolymer cement for the production paving blocks were produced. The geopolymer cement showed an UCS of 40 MPa after 28 days of curing. Exposure of the geopolymer cement to high temperature (1000 °C for 2 hours), decreased the UCS by 36%. The thermal stability, phase change and mass loss of the geopolymer cement was further investigated through a simultaneous thermal analysis (TGA/DTA). Evaporation of physical and zeolite water for temperature ranging between 100-250 °C was observed, which is a typical behavior of geopolymer cements. The silt was then mixed with a predefined aggregate blend to produce the final paving blocks. The produced prototype of paving blocks showed acceptable performance and could be successfully used in the industrial sector. However, further

optimizations in the production and casting procedure are needed to overcome the limited mechanical properties.

The possibility of including waste silt in different asphalt pavement types including HMA, porous asphalt and grouted macadam was discussed in PART III. The first objective was to evaluate the possibility of using normal and untreated silt as filler in HMA. The obtained data were compared with a control sample containing normal limestone filler. The results indicated that the addition of waste fillers did not increase the optimum binder content of HMA samples. Moreover, it did not show any adverse effect on the air voids content of the samples. In terms of the ITS values, sample produced with calcined silt and the control samples showed similar performance. However, the inclusion of untreated silt as filler resulted in 9% drop in ITS values compared to the control sample. The moisture sensitivity of HMA-SN was highest compared to the remaining samples showing and ITSR value of 85%. This could be related to the water absorption ability of untreated silt that could result in stripping of binder from aggregates. In addition to the mechanical properties, a dynamic shear rheometer was used to evaluate the effect of different filler types on the produced bitumen mastic. The rheological data showed similar behavior for both control and HMA-SC samples in terms of G*, delta and MSCR test values. However, the addition of untreated silt as filler reduced the stiffness of the mastic and increased the viscous behavior of the binder. In terms of rutting performance, thermally treated silt had the highest resistance against permanent deformation. This was observable in lower accumulated strain % and lower non-recoverable compliance values. A separate study was conducted to explore the mechanical properties of semi-flexible pavements grouted with a geopolymer cement. The semi-flexible pavement consisted of a porous asphalt skeleton, which had thermally treated silt as the filler. The geopolymer grout was also produced using the calcined silt as the filler, promoting a double recycling approach for recycling waste silt. The results indicated higher mechanical performance

in terms of ITS, ITSR and ITSM for the control samples produced with cement-based grouts and limestone filler. However, none of the samples demonstrated values lower than those suggested by Italian specifications. An improved geopolymer grout could improve the performance of the semi-flexible pavement.

To sum up, different approaches for recycling waste silt were proposed and tested. In general, several factors could be taken into account during recycling of such material. For instance, the final strength and performance of the products containing waste silt should be similar to products containing no waste material. Durability could also be added as an important parameter to consider during recycling. It is highly recommended to perform Life Cycle Analysis (LCA) studies on each of the proposed techniques and methods to fully evaluate their sustainability. The waste silt is a by-product of S.A.P.A.B.A. making it free of charge. This would lower the final cost of the products produced with the silt. The environmental test conducted on the geopolymer samples indicated no hazardous leachant. Moreover, the advantages of geopolymers to ordinary Portland cement has been discussed by various studies, of which one could point to its lower carbon dioxide emission rates. Currently, the production of HMA and porous asphalt mixtures seems more practical compared to the other approaches. This is due to the operating asphalt plant at S.A.P.A.B.A. On the other hand, proper infrastructures are needed to produce geopolymers on site. Nevertheless, the silt could be sold as raw material to nearby companies which produce geopolymer-based products.

References

1. Eurostat *Generation of waste by waste category, hazardousness and NACE Rev. 2 activity (env_wasgen)*; 2020;

2. Ossa, A.; García, J.L.; Botero, E. Use of recycled construction and demolition waste (CDW) aggregates: A sustainable alternative for the pavement construction industry. *J. Clean. Prod.* **2016**, *135*, 379–386, doi:https://doi.org/10.1016/j.jclepro.2016.06.088.

3. A., M.A.; R., G.A.; M., E.-B.S.; A., S.S. Performance Evaluation of Construction and Demolition Waste Materials for Pavement Construction in Egypt. *J. Mater. Civ. Eng.* **2018**, *30*, 4017270, doi:10.1061/(ASCE)MT.1943-5533.0002127.

4. Kumar, R. Influence of recycled coarse aggregate derived from construction and demolition waste (CDW) on abrasion resistance of pavement concrete. *Constr. Build. Mater.* **2017**, *142*, 248–255, doi:https://doi.org/10.1016/j.conbuildmat.2017.03.077.

5. Xiao, J.; Ma, Z.; Sui, T.; Akbarnezhad, A.; Duan, Z. Mechanical properties of concrete mixed with recycled powder produced from construction and demolition waste. *J. Clean. Prod.* **2018**, *188*, 720–731, doi:https://doi.org/10.1016/j.jclepro.2018.03.277.

6. Bravo, M.; de Brito, J.; Pontes, J.; Evangelista, L. Mechanical performance of concrete made with aggregates from construction and demolition waste recycling plants. *J. Clean. Prod.* **2015**, *99*, 59–74, doi:https://doi.org/10.1016/j.jclepro.2015.03.012.

7. Panizza, M.; Natali, M.; Garbin, E.; Ducman, V.; Tamburini, S. Optimization and mechanical-physical characterization of geopolymers with Construction and Demolition Waste (CDW) aggregates for construction products. *Constr. Build.*

Mater. **2020**, *264*, 120158, doi:https://doi.org/10.1016/j.conbuildmat.2020.120158.

8. Panizza, M.; Natali, M.; Garbin, E.; Tamburini, S.; Secco, M. Assessment of geopolymers with Construction and Demolition Waste (CDW) aggregates as a building material. *Constr. Build. Mater.* **2018**, *181*, 119–133, doi:https://doi.org/10.1016/j.conbuildmat.2018.06.018.

9. Makoundou, C.; Sangiorgi, C.; Johansson, K.; Wallqvist, V. Development of functional rubber-based impact-absorbing pavements for cyclist and pedestrian injury reduction. *Sustain.* **2021**, *13*, doi:10.3390/su132011283.

10. Qian, L.-P.; Xu, L.-Y.; Alrefaei, Y.; Wang, T.; Ishida, T.; Dai, J.-G. Artificial alkali-activated aggregates developed from wastes and by-products: A state-of-the-art review. *Resour. Conserv. Recycl.* **2022**, *177*, 105971, doi:https://doi.org/10.1016/j.resconrec.2021.105971.

11. Mangi, S.A.; Raza, M.S.; Khahro, S.H.; Qureshi, A.S.; Kumar, R. Recycling of ceramic tiles waste and marble waste in sustainable production of concrete: a review. *Environ. Sci. Pollut. Res.* **2022**, 1–22.

12. Awoyera, P.O.; Adesina, A.; Gobinath, R. Role of recycling fine materials as filler for improving performance of concrete - a review. *Aust. J. Civ. Eng.* **2019**, *17*, 85–95, doi:10.1080/14488353.2019.1626692.

13. Cherif, B.A.; Ali, F.; Tarek, M.; Massouh, F. Mechanical Behavior of the Extraction Mud Dam for Use in the Manufacture of CEB. *Civ. Eng. J.* **2021**, *7*, 1774–1786, doi:10.28991/cej-2021-03091759.

14. Davidovits, J. *Geopolymer chemistry and application*; Fourth Edi.; Institut Geopolymere: Saint-Quentin, France, 2015; ISBN 9782951482098623.

15. Hassan, A.; Arif, M.; Shariq, M. Use of geopolymer concrete for a cleaner and sustainable environment – A review of mechanical properties and microstructure. *J. Clean. Prod.* **2019**, *223*, 704–728, doi:https://doi.org/10.1016/j.jclepro.2019.03.051.

16. Ren, B.; Zhao, Y.; Bai, H.; Kang, S.; Zhang, T.; Song, S. Eco-friendly geopolymer prepared from solid wastes: A critical review. *Chemosphere* **2021**, *267*, 128900, doi:https://doi.org/10.1016/j.chemosphere.2020.128900.

17. Kwek, S.Y.; Awang, H. Utilisation of recycled silt from water treatment and palm oil fuel ash as geopolymer artificial lightweight aggregate. *Sustain.* **2021**, *13*, doi:10.3390/su13116091.

18. Daniel, O.; J., K.M. Stabilizing Sandy Silt Soil with Fly-Ash Based RCA Geopolymer in Pavement Base Layers. *Tran-SET 2020* 2022, 76–86.

19. European commission Council Directive 1999/31/EC of 26 April 1999 on the landfill of waste. *Off. J. Eur. Communities* **1999**.

20. European Union *UEPG-European Aggregates Association. A sustainable industry for a sustainable Europe. Annual review*; 2020;

21. Solouki, A.; Viscomi, G.; Lamperti, R.; Tataranni, P. Quarry Waste as Precursors in Geopolymers for Civil Engineering Applications: A Decade in Review. *Materials (Basel).* **2020**, *13*, 3146, doi:10.3390/ma13143146.

22. Saghafi, B.; Nageim, H. Al; VisuliosMPhil, P.; Ghazireh, N. Use of waste limestone dust and steel slag in UK highways type 1 unbound mixtures. *Proc. Inst. Civ. Eng. - Constr. Mater.* **2012**, *166*, 99–107, doi:10.1680/coma.11.00029.

23. Sung Do, H.; Hee Mun, P.; Suk keun, R. A study on engineering characteristics of asphalt concrete using filler with recycled waste lime. *Waste Manag.* **2008**, *28*, 191–199, doi:10.1016/j.wasman.2006.11.011.

24. Puppala, A.J.; Saride, S.; Williammee, R. Sustainable Reuse of Limestone Quarry Fines and RAP in Pavement Base/Subbase Layers. *J. Mater. Civ. Eng.* **2011**, *24*, 418–429, doi:10.1061/(asce)mt.1943-5533.0000404.

25. Chang, F.C.; Lee, M.Y.; Lo, S.L.; Lin, J.D. Artificial aggregate made from waste stone sludge and waste silt. *J. Environ. Manage.* **2010**, *91*, 2289–2294, doi:10.1016/j.jenvman.2010.06.011.

26. Cavaleri, L.; Borg, R.P.; Mantia, F.P. La; Liguori, V. Quarry limestone dust as

fine aggregate for concrete. In Proceedings of the IOP Conference Series Materials Science and Engineering; 2018; pp. 1–11.

27.   Medina, G.; Sáez del Bosque, I.F.; Frías, M.; Sánchez de Rojas, M.I.; Medina, C. Durability of new recycled granite quarry dust-bearing cements. *Constr. Build. Mater.* **2018**, *187*, 414–425, doi:10.1016/j.conbuildmat.2018.07.134.

28.   Felekoglu, B. Utilisation of high volumes of limestone quarry wastes in concrete industry (self-compacting concrete case). *Resour. Conserv. Recycl.* **2007**, *51*, 770–791, doi:10.1016/j.resconrec.2006.12.004.

29.   Uysal, M.; Yilmaz, K. Effect of mineral admixtures on properties of self-compacting concrete. *Cem. Concr. Compos.* **2011**, *33*, 771–776, doi:10.1016/j.cemconcomp.2011.04.005.

30.   Benarchid, Y.; Taha, Y.; Argane, R.; Benzaazoua, M. Application of Quebec recycling guidelines to assess the use feasibility of waste rocks as construction aggregates. *Resour. Policy* **2018**, *59*, 68–76, doi:10.1016/j.resourpol.2018.01.004.

31.   Kitouni, S.; Houari, H. Lightweight concrete with Algerian limestone dust: Part I: Study on 30% replacement to normal aggregate at early age. *Cerâmica* **2014**, *59*, 600–608, doi:10.1590/s0366-69132013000400017.

32.   Shi, C.; Wu, Z.; Lv, K.; Wu, L. A review on mixture design methods for self-compacting concrete. *Constr. Build. Mater.* **2015**, *84*, 387–398, doi:10.1016/j.conbuildmat.2015.03.079.

33.   Yildizel, S.A.; Tayeh, B.A.; Calis, G. Experimental and modelling study of mixture design optimisation of glass fibre-reinforced concrete with combined utilisation of Taguchi and Extreme Vertices Design Techniques. *J. Mater. Res. Technol.* **2020**, *9*, 2093–2106, doi:https://doi.org/10.1016/j.jmrt.2020.02.083.

34.   Abouhussien, A.A.; Hassan, A.A.A. Optimizing the durability and service life of self-consolidating concrete containing metakaolin using statistical analysis. *Constr. Build. Mater.* **2015**, *76*, 297–306,

doi:https://doi.org/10.1016/j.conbuildmat.2014.12.010.

35. Chen, S.-H.; Chang, C.-S.; Wang, H.-Y.; Huang, W.-L. Mixture design of high performance recycled liquid crystal glasses concrete (HPGC). *Constr. Build. Mater.* **2011**, *25*, 3886–3892, doi:https://doi.org/10.1016/j.conbuildmat.2011.04.012.

36. Rezaifar, O.; Hasanzadeh, M.; Gholhaki, M. Concrete made with hybrid blends of crumb rubber and metakaolin: Optimization using Response Surface Method. *Constr. Build. Mater.* **2016**, *123*, 59–68, doi:https://doi.org/10.1016/j.conbuildmat.2016.06.047.

37. Ferdosian, I.; Camões, A. Eco-efficient ultra-high performance concrete development by means of response surface methodology. *Cem. Concr. Compos.* **2017**, *84*, 146–156, doi:https://doi.org/10.1016/j.cemconcomp.2017.08.019.

38. Cotto-Ramos, A.; Dávila, S.; Torres-García, W.; Cáceres-Fernández, A. Experimental design of concrete mixtures using recycled plastic, fly ash, and silica nanoparticles. *Constr. Build. Mater.* **2020**, *254*, 119207, doi:https://doi.org/10.1016/j.conbuildmat.2020.119207.

39. Bouziani, T. Assessment of fresh properties and compressive strength of self-compacting concrete made with different sand types by mixture design modelling approach. *Constr. Build. Mater.* **2013**, *49*, 308–314, doi:https://doi.org/10.1016/j.conbuildmat.2013.08.039.

40. de Matos, P.R.; Sakata, R.D.; Gleize, P.J.P.; de Brito, J.; Repette, W.L. Eco-friendly ultra-high performance cement pastes produced with quarry wastes as alternative fillers. *J. Clean. Prod.* **2020**, *269*, 122308, doi:10.1016/j.jclepro.2020.122308.

41. Schankoski, R.A.; de Matos, P.R.; Pilar, R.; Prudêncio, L.R.; Ferron, R.D. Rheological properties and surface finish quality of eco-friendly self-compacting concretes containing quarry waste powders. *J. Clean. Prod.* **2020**, *257*, doi:10.1016/j.jclepro.2020.120508.

42. Polydorou, T.; Constantinides, G.; Neocleous, K.; Kyriakides, N.; Koutsokeras, L.; Chrysostomou, C.; Hadjimitsis, D. Effects of pre-treatment using waste quarry dust on the adherence of recycled tyre rubber particles to cementitious paste in rubberised concrete. *Constr. Build. Mater.* **2020**, *254*, 119325, doi:10.1016/j.conbuildmat.2020.119325.

43. Tataranni, P. Recycled Waste Powders for Alkali-Activated Paving Blocks for Urban Pavements : A Full Laboratory Characterization. *Infrastructures* **2019**, *4*, doi:10.3390/infrastructures4040073.

44. Box, G.E.P.; Wilson, K.B. On the Experimental Attainment of Optimum Conditions. *J. R. Stat. Soc. Ser. B* **1951**, *13*, 1–45.

45. Smiti, A. A critical overview of outlier detection methods. *Comput. Sci. Rev.* **2020**, *38*, 100306, doi:10.1016/j.cosrev.2020.100306.

46. Nehdi, M.L. Clay in cement-based materials: Critical overview of state-of-the-art. *Constr. Build. Mater.* **2014**, *51*, 372–382, doi:10.1016/j.conbuildmat.2013.10.059.

47. Solouki, A.; Fathollahi, A.; Viscomi, G.; Tataranni, P.; Valdrè, G.; Coupe, S.J.; Sangiorgi, C. Thermally treated waste silt as filler in geopolymer cement. *Materials (Basel).* **2021**, *14*, 5102, doi:10.3390/ma14175102.

48. Moro, D.; Fabbri, R.; Romano, J.; Ulian, G.; Calafato, A.; Solouki, A.; Sangiorgi, C.; Valdrè, G. Thermal, X-ray Diffraction and Oedometric Analyses of Silt-Waste/NaOH-Activated Metakaolin Geopolymer Composite. *J. Compos. Sci.* **2021**, *5*, 269, doi:10.3390/jcs5100269.

49. Copetti Callai, S.; Tataranni, P.; Sangiorgi, C. Preliminary Evaluation of Geopolymer Mix Design Applying the Design of Experiments Method. *Infrastructures* **2021**, *6*, 35, doi:10.3390/infrastructures6030035.

50. Solouki, A.; Viscomi, G.; Tataranni, P.; Sangiorgi, C. Preliminary Evaluation of Cement Mortars Containing Waste Silt Optimized with the Design of Experiments Method. *Mater.* 2021, *14*.

51. Yeo, J.S.; Koting, S.; Onn, C.C.; Mo, K.H. An overview on the properties of eco-friendly concrete paving blocks incorporating selected waste materials as aggregate. *Environ. Sci. Pollut. Res.* **2021**, doi:10.1007/s11356-021-13836-3.

52. Torres de Rosso, L.; Victor Staub de Melo, J. Impact of incorporating recycled glass on the photocatalytic capacity of paving concrete blocks. *Constr. Build. Mater.* **2020**, *259*, 119778, doi:https://doi.org/10.1016/j.conbuildmat.2020.119778.

53. López Gayarre, F.; Suárez González, J.; Blanco Viñuela, R.; López-Colina Pérez, C.; Serrano López, M.A. Use of recycled mixed aggregates in floor blocks manufacturing. *J. Clean. Prod.* **2018**, *167*, 713–722, doi:10.1016/j.jclepro.2017.08.193.

54. Zhao, Z.; Courard, L.; Groslambert, S.; Jehin, T.; Léonard, A.; Xiao, J. Use of recycled concrete aggregates from precast block for the production of new building blocks: An industrial scale study. *Resour. Conserv. Recycl.* **2020**, *157*, 104786, doi:10.1016/j.resconrec.2020.104786.

55. Penteado, C.S.G.; Viviani De Carvalho, E.; Lintz, R.C.C. Reusing ceramic tile polishing waste in paving block manufacturing. *J. Clean. Prod.* **2016**, *112*, 514–520, doi:10.1016/j.jclepro.2015.06.142.

56. Djamaluddin, A.R.; Caronge, M.A.; Tjaronge, M.W.; Lando, A.T.; Irmawaty, R. Evaluation of sustainable concrete paving blocks incorporating processed waste tea ash. *Case Stud. Constr. Mater.* **2020**, *12*, e00325, doi:10.1016/j.cscm.2019.e00325.

57. Ganjian, E.; Jalull, G.; Sadeghi-Pouya, H. Using waste materials and by-products to produce concrete paving blocks. *Constr. Build. Mater.* **2015**, *77*, 270–275, doi:10.1016/j.conbuildmat.2014.12.048.

58. Hadj Sadok, R.; Belas, N.; Tahlaiti, M.; Mazouzi, R. Reusing calcined sediments from Chorfa II dam as partial replacement of cement for sustainable mortar production. *J. Build. Eng.* **2021**, *40*, 102273, doi:10.1016/j.jobe.2021.102273.

59. Mousavi, S.S.; Bhojaraju, C.; Ouellet-Plamondon, C. Clay as a Sustainable Binder for Concrete—A Review. *Constr. Mater.* **2021**, *1*, 134–168, doi:10.3390/constrmater1030010.

60. Yang, J.; Du, Q.; Bao, Y. Concrete with recycled concrete aggregate and crushed clay bricks. *Constr. Build. Mater.* **2011**, *25*, 1935–1945, doi:10.1016/j.conbuildmat.2010.11.063.

61. Wang, L.; Chen, L.; Tsang, D.C.W.; Li, J.S.; Baek, K.; Hou, D.; Ding, S.; Poon, C.S. Recycling dredged sediment into fill materials, partition blocks, and paving blocks: Technical and economic assessment. *J. Clean. Prod.* **2018**, *199*, 69–76, doi:10.1016/j.jclepro.2018.07.165.

62. Udawattha, C.; Galabada, H.; Halwatura, R. Mud concrete paving block for pedestrian pavements. *Case Stud. Constr. Mater.* **2017**, *7*, 249–262, doi:10.1016/j.cscm.2017.08.005.

63. Blayi, R.A.; Sherwani, A.F.H.; Ibrahim, H.H.; Abdullah, S.J. Stabilization of high-plasticity silt using waste brick powder. *SN Appl. Sci.* **2020**, *2*, 1989, doi:10.1007/s42452-020-03814-8.

64. Galetakis, M.; Raka, S. Utilization of limestone dust for artificial stone production: an experimental approach. *Miner. Eng.* **2004**, *17*, 355–357, doi:https://doi.org/10.1016/j.mineng.2003.10.031.

65. Alharbi, F.; Almoshaogeh, M.; Shafiquzzaman, M.; Haider, H.; Rafiquzzaman, M.; Alragi, A.; ElKholy, S.; Bayoumi, Els.A.; EL-Ghoul, Y. Development of Rice Bran Mixed Porous Clay Bricks for Permeable Pavements: A Sustainable LID Technique for Arid Regions. *Sustain.* 2021, *13*.

66. Salem Alsanusi; Loubna Bentaher Prediction of Compressive Strength of Concrete from Early Age Test Result Using Design of Experiments (RSM). *Int. J. Civil, Environ. Struct. Constr. Archit. Eng.* **2015**, *9*, 1522–1526.

67. Muthukumar, M.; Mohan, D. Optimization of mechanical properties of polymer concrete and mix design recommendation based on design of experiments. *J.*

Appl. Polym. Sci. **2004**, *94*, 1107–1116, doi:10.1002/app.21008.

68. Eriksson, L.; Johansson, E.; Wikström, C. Mixture design - Design generation, PLS analysis, and model usage. *Chemom. Intell. Lab. Syst.* **1998**, *43*, 1–24, doi:10.1016/S0169-7439(98)00126-9.

69. Gencel, O.; del Coz Díaz, J.J.; Sutcu, M.; Kocyigit, F.; Rabanal, F.P.Á.; Alonso-Martínez, M.; Barrera, G.M. Thermal Performance Optimization of Lightweight Concrete/EPS Layered Composite Building Blocks. *Int. J. Thermophys.* **2021**, *42*, 1–14, doi:10.1007/s10765-021-02804-1.

70. Zhu, F.; Li, Z.; Dong, W.; Ou, Y. Geotechnical properties and microstructure of lime-stabilized silt clay. *Bull. Eng. Geol. Environ.* **2019**, *78*, 2345–2354, doi:10.1007/s10064-018-1307-5.

71. Patil, A.R.; Sathe, S.B. Feasibility of sustainable construction materials for concrete paving blocks: A review on waste foundry sand and other materials. *Mater. Today Proc.* **2020**, *43*, 1552–1561, doi:10.1016/j.matpr.2020.09.402.

72. Da Silva, F.M.; Gachet Barbosa, L.A.; Lintz, R.C.C.; Jacintho, A.E.P.G.A. Investigation on the properties of concrete tactile paving blocks made with recycled tire rubber. *Constr. Build. Mater.* **2015**, *91*, 71–79, doi:10.1016/j.conbuildmat.2015.05.027.

73. Zaumanis, M.; Arraigada, M.; Wyss, S.A.; Zeyer, K.; Cavalli, M.C.; Poulikakos, L.D. Performance-based design of 100% recycled hot-mix asphalt and validation using traffic load simulator. *J. Clean. Prod.* **2019**, *237*, 117679, doi:10.1016/j.jclepro.2019.117679.

74. Lizárraga, J.M.; Ramírez, A.; Díaz, P.; Marcobal, J.R.; Gallego, J. Short-term performance appraisal of half-warm mix asphalt mixtures containing high (70%) and total RAP contents (100%): From laboratory mix design to its full-scale implementation. *Constr. Build. Mater.* **2018**, *170*, 433–445, doi:https://doi.org/10.1016/j.conbuildmat.2018.03.051.

75. Dinis-Almeida, M.; Castro-Gomes, J.; Sangiorgi, C.; Zoorob, S.E.; Afonso,

M.L. Performance of Warm Mix Recycled Asphalt containing up to 100% RAP. *Constr. Build. Mater.* **2016**, *112*, 1–6, doi:10.1016/j.conbuildmat.2016.02.108.

76. Behera, M.; Bhattacharyya, S.K.; Minocha, A.K.; Deoliya, R.; Maiti, S. Recycled aggregate from C&D waste & its use in concrete - A breakthrough towards sustainability in construction sector: A review. *Constr. Build. Mater.* **2014**, *68*, 501–516, doi:10.1016/j.conbuildmat.2014.07.003.

77. Cesare, S.; Piergiorgio, T.; Claudio, L.; Francesco, M. Application of Mining Waste Powder as filler in Hot Mix Asphalt. *MATEC Web Conf.* **2019**, *274*, 04002, doi:10.1051/matecconf/201927404002.

78. Giustozzi, F.; Mansour, K.; Patti, F.; Pannirselvam, M.; Fiori, F. Shear rheology and microstructure of mining material-bitumen composites as filler replacement in asphalt mastics. *Constr. Build. Mater.* **2018**, *171*, 726–735, doi:10.1016/j.conbuildmat.2018.03.190.

79. Qi, C.; Fourie, A. Cemented paste backfill for mineral tailings management: Review and future perspectives. *Miner. Eng.* **2019**, *144*, 106025, doi:10.1016/j.mineng.2019.106025.

80. Ryan, M.J.; Kney, A.D.; Carley, T.L. A study of selective precipitation techniques used to recover refined iron oxide pigments for the production of paint from a synthetic acid mine drainage solution. *Appl. Geochemistry* **2017**, *79*, 27–35, doi:10.1016/j.apgeochem.2017.01.019.

81. Rigopoulos, I.; Török, Á.; Kyratsi, T.; Delimitis, A.; Ioannou, I. Sustainable exploitation of mafic rock quarry waste for carbon sequestration following ball milling. *Resour. Policy* **2018**, *59*, 24–32, doi:10.1016/j.resourpol.2018.08.002.

82. Gameiro, F.; De Brito, J.; Correia da Silva, D. Durability performance of structural concrete containing fine aggregates from waste generated by marble quarrying industry. *Eng. Struct.* **2014**, *59*, 654–662, doi:10.1016/j.engstruct.2013.11.026.

83. Lottermoser, B.G. Recycling, reuse and rehabilitation of mine wastes. *Elements*

2011, *7*, 405–410, doi:10.2113/gselements.7.6.405.

84. Mao, Y.; Biasetto, L.; Colombo, P. Metakaolin-based geopolymer coatings on metals by airbrush spray deposition. *J. Coatings Technol. Res.* **2020**, doi:10.1007/s11998-019-00310-6.

85. Ranjbar, N.; Zhang, M. Fiber-reinforced geopolymer composites: A review. *Cem. Concr. Compos.* **2020**, *107*, 103498, doi:https://doi.org/10.1016/j.cemconcomp.2019.103498.

86. Łach, M.; Korniejenko, K.; Mikuła, J. Thermal Insulation and Thermally Resistant Materials Made of Geopolymer Foams. *Procedia Eng.* **2016**, *151*, 410–416, doi:https://doi.org/10.1016/j.proeng.2016.07.350.

87. Liew, Y.-M.; Heah, C.-Y.; Li, L.; Jaya, N.A.; Abdullah, M.M.A.B.; Tan, S.J.; Hussin, K. Formation of one-part-mixing geopolymers and geopolymer ceramics from geopolymer powder. *Constr. Build. Mater.* **2017**, *156*, 9–18, doi:https://doi.org/10.1016/j.conbuildmat.2017.08.110.

88. Van Jaarsveld, J.G.S.; Van Deventer, J.S.J.; Lorenzen, L. The potential use of geopolymeric materials to immobilize toxic metals: Part I. Theory and applications. *Miner. Eng.* **1997**, *10*, 659–669, doi:10.1016/s0892-6875(97)00046-0.

89. Davidovits, J. GEOPOLYMERS: Man-Made Rock Geosynthesis and the Resulting Development of Very Early High Strength Cement. *Mater. Eduucation* **1994**, *16*, 1–25.

90. Davidovits, J. Geopolymer Cement a review. *Geopolymer Inst. Libr. Tech. Pap.* **2013**, 1–11.

91. Silverstrim, T.; Rostami, H.; Larralde, J.C and Samadi-Maybodi, A. Flyash cementitious material and method of making a product 1997.

92. Li, N.; Shi, C.; Zhang, Z.; Wang, H.; Liu, Y. A review on mixture design methods for geopolymer concrete. *Compos. Part B Eng.* **2019**, *178*, 107490, doi:10.1016/j.compositesb.2019.107490.

93. Sangiorgi, C.; Lantieri, C.; Tataranni, P.; Castro-Gomes, J.; Gabriel, M. Reuse of mining waste into innovative alkali-activated-based materials for road pavement applications. In *Functional Pavement Design - Proceedings of the 4th Chinese-European Workshop on Functional Pavement Design, CEW 2016*; 2016; pp. 1735–1744 ISBN 978-1-138-02924-8.

94. Tataranni, P.; Sangiorgi, C. Synthetic Aggregates for the Production of Innovative Low Impact Porous Layers for Urban Pavements. *Infrastructures* **2019**, *4*, 48, doi:10.3390/infrastructures4030048.

95. Cerveira, A.; Correia, E.; Cristelo, N.; Miranda, T.; Castro, F.; Fernández-Jiménez, A. Statistical Analysis of the Influence of Several Factors on Compressive Strength of Alkali Activated Fly Ash. In Proceedings of the Procedia Structural Integrity; Elsevier B.V., 2017; Vol. 5, pp. 1116–1122.

96. Liu, Z.; Cai, C.S.; Liu, F.; Fan, F. Feasibility study of loess stabilization with fly ash-based geopolymer. *J. Mater. Civ. Eng.* **2016**, *28*, doi:10.1061/(ASCE)MT.1943-5533.0001490.

97. Chen, Y.X.; Sun, X.L.; Li, Z.H. Mechanical properties of fly ash-slag-dredged silt system stimulated by alkali. *Adv. Mater. Res.* **2013**, *807–809*, 1140–1146, doi:10.4028/www.scientific.net/AMR.807-809.1140.

98. Beghoura, I.; Castro-Gomes, J. Design of alkali-activated aluminium powder foamed materials for precursors with different particle sizes. *Constr. Build. Mater.* **2019**, *224*, 682–690, doi:10.1016/j.conbuildmat.2019.07.018.

99. Qiu, T.; Kuang, J.; Shi, F. Effect of alkali on the geopolymer strength. *Adv. Mater. Res.* 2011, *168–170*, 1827–1832.

100. Jiao, X.; Zhang, Y.; Chen, T.; Bao, S.; Liu, T.; Huang, J. Geopolymerisation of a silica-rich tailing. *Miner. Eng.* **2011**, *24*, 1710–1712, doi:10.1016/j.mineng.2011.09.008.

101. Manjarrez, L.; Nikvar-Hassani, A.; Shadnia, R.; Zhang, L. Experimental Study of Geopolymer Binder Synthesized with Copper Mine Tailings and Low-

Calcium Copper Slag. *J. Mater. Civ. Eng.* **2019**, *31*, doi:10.1061/(ASCE)MT.1943-5533.0002808.

102. Kotwica, L.; Chorembala, M.; Kapeluszna, E.; Stepien, P.; Deja, J.; Illikainen, M.; Golek, L. Influence of calcined mine tailings on the properties of alkali activated slag mortars. *Key Eng. Mater.* **2018**, *761 KEM*, 83–86, doi:10.4028/www.scientific.net/KEM.761.83.

103. Kumar, R.; Das, P.; Beulah, M.; Arjun, H.R.; Ignatius, G. Utilization of Iron Ore Tailings for the Production of Fly Ash - GGBS-Based Geopolymer Bricks. *J. Adv. Manuf. Syst.* **2017**, *16*, 275–290, doi:10.1142/S0219686717500172.

104. Niu, F.; Zhou, S.; Liu, S.; Zhang, J. Study of manufacture process and properties of tailings and slag based geopolymers. *Adv. Mater. Res.* 2011, *156–157*, 803–807.

105. Sedira, N.; Castro-Gomes, J. Effect of activators on hybrid alkaline binder based on tungsten mining waste and ground granulated blast furnace slag. *Constr. Build. Mater.* **2020**, *232*, doi:10.1016/j.conbuildmat.2019.117176.

106. Kastiukas, G.; Zhou, X.; Wan, K.T.; Gomes, J.C. Lightweight alkali-activated material from mining and glass waste by chemical and physical foaming. *J. Mater. Civ. Eng.* **2019**, *31*, doi:10.1061/(ASCE)MT.1943-5533.0002610.

107. Luo, Y.; Bao, S.; Zhang, Y. Preparation of one-part geopolymeric precursors using vanadium tailing by thermal activation. *J. Am. Ceram. Soc.* **2019**, doi:10.1111/jace.16835.

108. Sakamoto, K.; Wajima, T. Preparation of geopolymer cement from crushed stone by-product using alkali fusion. *Int. J. GEOMATE* **2019**, *17*, 17–22, doi:10.21660/2019.63.4536.

109. Wan, Q.; Rao, F.; Song, S.; Leon-Patino, C.A.; Ma, Y.; Yin, W. Consolidation of mine tailings through geopolymerization at ambient temperature. *J. Am. Ceram. Soc.* **2019**, *102*, 2451–2461, doi:10.1111/jace.16183.

110. Luo, Y.; Bao, S.; Zhang, Y.; Yuan, Y. Recycling vanadium-bearing shale

leaching residue for the production of one-part geopolymers. *Mater. Res. Express* **2019**, *6*, doi:10.1088/2053-1591/ab3755.

111. Paiva, H.; Yliniemi, J.; Illikainen, M.; Rocha, F.; Ferreira, V.M. Mine tailings geopolymers as a waste management solution for a more sustainable habitat. *Sustainability* **2019**, *11*, doi:10.3390/su11040995.

112. Kürklü, G.; Görhan, G. Investigation of usability of quarry dust waste in fly ash-based geopolymer adhesive mortar production. *Constr. Build. Mater.* **2019**, *217*, 498–506, doi:10.1016/j.conbuildmat.2019.05.104.

113. Defáveri, K. do C. e S.; dos Santos, L.F.; Franco de Carvalho, J.M.; Peixoto, R.A.F.; Brigolini, G.J. Iron ore tailing-based geopolymer containing glass wool residue: A study of mechanical and microstructural properties. *Constr. Build. Mater.* **2019**, *220*, 375–385, doi:10.1016/j.conbuildmat.2019.05.181.

114. Manjarrez, L.; Zhang, L. Utilization of copper mine tailings as road base construction material through geopolymerization. *J. Mater. Civ. Eng.* **2018**, *30*, doi:10.1061/(ASCE)MT.1943-5533.0002397.

115. Davidovits, R.; Plelegris, C.; Davidovits, J. Standardized Method in Testing Commercial Metakaolins for Geopolymer. *Geopolymer Instute Libr.* **2019**, doi:10.13140/RG.2.2.18109.10727/1.

116. Duxson, P.; Fernández-Jiménez, A.; Provis, J.L.; Lukey, G.C.; Palomo, A.; Van Deventer, J.S.J. Geopolymer technology: The current state of the art. *J. Mater. Sci.* **2007**, *42*, 2917–2933, doi:10.1007/s10853-006-0637-z.

117. Fernández-Jiménez, A.; Palomo, A. Characterisation of fly ashes. Potential reactivity as alkaline cements. *Fuel* **2003**, *82*, 2259–2265, doi:10.1016/S0016-2361(03)00194-7.

118. Davidovits, J.; Izquierdo, M.; Querol, X.; Antennuci, D.; Nugteren, H.; Butselaar-Orthlieb, V.; Fernández-Pereira, C.; Luna, Y. The European research project geoash: Geopolymeric cement based on European fly-ashes. *A Glob. Road Map Ceram. Mater. Technol. Forecast. Futur. Ceram. Int. Ceram. Fed. -*

2nd Int. Congr. Ceram. ICC 2008, Final Program. **2008**, *4*, 0–10.

119. Salihoglu, N.K.; Salihoglu, G. Marble sludge recycling by using geopolymerization technology. *J. Hazardous, Toxic, Radioact. Waste* **2018**, *22*, doi:10.1061/(ASCE)HZ.2153-5515.0000415.

120. Yliniemi; Paiva; Ferreira; Tiainen; Illikainen Development and incorporation of lightweight waste-based geopolymer aggregates in mortar and concrete. *Constr. Build. Mater.* **2017**, *131*, 784–792, doi:10.1016/j.conbuildmat.2016.11.017.

121. Alanazi, H.; Hu, J.; Kim, Y.R. Effect of slag, silica fume, and metakaolin on properties and performance of alkali-activated fly ash cured at ambient temperature. *Constr. Build. Mater.* **2019**, *197*, 747–756, doi:10.1016/j.conbuildmat.2018.11.172.

122. Moukannaa, S.; Nazari, A.; Bagheri, A.; Loutou, M.; Sanjayan, J.G.; Hakkou, R. Alkaline fused phosphate mine tailings for geopolymer mortar synthesis: Thermal stability, mechanical and microstructural properties. *J. Non. Cryst. Solids* **2019**, *511*, 76–85, doi:10.1016/j.jnoncrysol.2018.12.031.

123. Komnitsas, K.; Zaharaki, D. Geopolymerisation: A review and prospects for the minerals industry. *Miner. Eng.* **2007**, *20*, 1261–1277, doi:10.1016/j.mineng.2007.07.011.

124. Kastiukas, G.; Zhou, X.; Castro-Gomes, J. Preparation conditions for the synthesis of alkali-activated binders using tungsten mining waste. *J. Mater. Civ. Eng.* **2017**, *29*, doi:10.1061/(ASCE)MT.1943-5533.0002029.

125. Zhang, M.; El-Korchi, T.; Zhang, G.; Liang, J.; Tao, M. Synthesis factors affecting mechanical properties, microstructure, and chemical composition of red mud-fly ash based geopolymers. *Fuel* **2014**, *134*, 315–325, doi:10.1016/j.fuel.2014.05.058.

126. Rakhimova, N.R.; Rakhimov, R.Z. Alkali-activated cements and mortars based on blast furnace slag and red clay brick waste. *Mater. Des.* **2015**, *85*, 324–331, doi:10.1016/j.matdes.2015.06.182.

127. Ahmari, S.; Zhang, L.; Zhang, J. Effects of activator type/concentration and curing temperature on alkali-activated binder based on copper mine tailings. *J. Mater. Sci.* **2012**, *47*, 5933–5945, doi:10.1007/s10853-012-6497-9.

128. Kastiukas, G.; Zhou, X. Effects of waste glass on alkali-activated tungsten mining waste: composition and mechanical properties. *Mater. Struct. Constr.* **2017**, *50*, doi:10.1617/s11527-017-1062-2.

129. Komljenović, M.; Baščarević, Z.; Bradić, V. Mechanical and microstructural properties of alkali-activated fly ash geopolymers. *J. Hazard. Mater.* **2010**, *181*, 35–42, doi:10.1016/j.jhazmat.2010.04.064.

130. Duxson, P.; Provis, J.L.; Lukey, G.C.; Mallicoat, S.W.; Kriven, W.M.; Van Deventer, J.S.J. Understanding the relationship between geopolymer composition, microstructure and mechanical properties. *Colloids Surfaces A Physicochem. Eng. Asp.* **2005**, *269*, 47–58, doi:10.1016/j.colsurfa.2005.06.060.

131. Indiana Department of Transportation *Certified aggregate producer program - Procedures and policy manual*; Indiana State, 2019;

132. Wang, A.; Liu, H.; Hao, X.; Wang, Y.; Liu, X.; Li, Z. Geopolymer synthesis using garnet tailings from molybdenum mines. *Minerals* **2019**, *9*, doi:10.3390/min9010048.

133. Lampris, C.; Lupo, R.; Cheeseman, C.R. Geopolymerisation of silt generated from construction and demolition waste washing plants. *Waste Manag.* **2009**, *29*, 368–373, doi:10.1016/j.wasman.2008.04.007.

134. Arulrajah, A.; Yaghoubi, M.; Disfani, M.M.; Horpibulsuk, S.; Bo, M.W.; Leong, M. Evaluation of fly ash- and slag-based geopolymers for the improvement of a soft marine clay by deep soil mixing. *Soils Found.* **2018**, *58*, 1358–1370, doi:10.1016/j.sandf.2018.07.005.

135. Wang, B.; Li, G.; Han, J.; Zheng, Y.; Liu, H.; Song, W. Study on the properties of artificial flood-prevention stone made by Yellow River silt. *Constr. Build. Mater.* **2017**, *144*, 484–492, doi:10.1016/j.conbuildmat.2017.03.206.

195

136. Molino, B.; De Vincenzo, A.; Ferone, C.; Messina, F.; Colangelo, F.; Cioffi, R. Recycling of clay sediments for geopolymer binder production. A new perspective for reservoir management in the framework of Italian Legislation: The Occhito reservoir case study. *Materials (Basel).* **2014**, *7*, 5603–5616, doi:10.3390/ma7085603.

137. Pacheco-Torgal, F.; Jalali, S. Influence of sodium carbonate addition on the thermal reactivity of tungsten mine waste mud based binders. *Constr. Build. Mater.* **2010**, *24*, 56–60, doi:10.1016/j.conbuildmat.2009.08.018.

138. Fernando, P.-T.; João, C.-G.; Said, J. Durability and environmental performance of alkali-activated tungsten mine waste mud mortars. *J. Mater. Civ. Eng.* **2010**, *22*, 897–904, doi:10.1061/(ASCE)MT.1943-5533.0000092.

139. Fernando, P.-T.; Said, J. Resistance to acid attack, abrasion and leaching behavior of alkali-activated mine waste binders. *Mater. Struct. Constr.* **2011**, *44*, 487–498, doi:10.1617/s11527-010-9643-3.

140. Afonso, M.L.; Dinis-Almeida, M.; Pereira-De-Oliveira, L.A.; Castro-Gomes, J.; Zoorob, S.E. Development of a semi-flexible heavy duty pavement surfacing incorporating recycled and waste aggregates - Preliminary study. *Constr. Build. Mater.* **2016**, *102*, 155–161, doi:10.1016/j.conbuildmat.2015.10.165.

141. Silva, I.; Castro-Gomes, J.; Albuquerque, A. Mineral Waste Geopolymeric Artificial Aggregates as Alternative Materials for Wastewater-Treatment Processes: Study of Structural Stability and pH Variation in Water. *J. Mater. Civ. Eng.* **2012**, *24*, 623–628, doi:10.1061/(ASCE)MT.1943-5533.0000429.

142. Wei, B.; Zhang, Y.; Bao, S. Preparation of geopolymers from vanadium tailings by mechanical activation. *Constr. Build. Mater.* **2017**, *145*, 236–242, doi:10.1016/j.conbuildmat.2017.03.234.

143. Thakur, A.K.; Pappu, A.; Thakur, V.K. Synthesis and characterization of new class of geopolymer hybrid composite materials from industrial wastes. *J. Clean. Prod.* **2019**, *230*, 11–20, doi:10.1016/j.jclepro.2019.05.081.

144. Sharath, B.P.; Shivaprasad, K.N.; Athikkal, M.M.; Das, B.B. Some Studies on Sustainable Utilization of Iron Ore Tailing (IOT) as Fine Aggregates in Fly Ash Based Geopolymer Mortar. In Proceedings of the IOP Conference Series: Materials Science and Engineering; 2018; Vol. 431.

145. Kuranchie, F.A.; Shukla, S.K.; Habibi, D. Utilisation of iron ore mine tailings for the production of geopolymer bricks. *Int. J. Mining, Reclam. Environ.* **2016**, *30*, 92–114, doi:10.1080/17480930.2014.993834.

146. Ge, S.T.; Bi, Y.B.; Wang, J.K.; Li, S.S.; Zhang, G.; Zhang, H.J. Effect of alkali activator on preparation, and mechanical and thermal properties of iron mine tailing-based lightweight materials. *Solid State Phenom.* 2018, *281 SSP*, 940–945.

147. Duan, P.; Yan, C.; Zhou, W.; Ren, D. Fresh properties, compressive strength and microstructure of fly ash geopolymer paste blended with iron ore tailing under thermal cycle. *Constr. Build. Mater.* **2016**, *118*, 76–88, doi:10.1016/j.conbuildmat.2016.05.059.

148. Lancellotti, I.; Kiventerä, J.; Catauro, M.; Poggetto, F.D.; Illikainen, M. Inertization of mine tailing via cold consolidation in geopolymer matrix. *Key Eng. Mater.* 2018, *761 KEM*, 31–34.

149. Kiventerä, J.; Golek, L.; Yliniemi, J.; Ferreira, V.; Deja, J.; Illikainen, M. Utilization of sulphidic tailings from gold mine as a raw material in geopolymerization. *Int. J. Miner. Process.* **2016**, *149*, 104–110, doi:10.1016/j.minpro.2016.02.012.

150. Gitari, M.W.; Akinyemi, S.A.; Thobakgale, R.; Ngoejana, P.C.; Ramugondo, L.; Matidza, M.; Mhlongo, S.E.; Dacosta, F.A.; Nemapate, N. Physicochemical and mineralogical characterization of Musina mine copper and New Union gold mine tailings: Implications for fabrication of beneficial geopolymeric construction materials. *J. African Earth Sci.* **2018**, *137*, 218–228, doi:10.1016/j.jafrearsci.2017.10.016.

151. Kiventerä, J.; Lancellotti, I.; Catauro, M.; Poggetto, F.D.; Leonelli, C.; Illikainen, M. Alkali activation as new option for gold mine tailings inertization. *J. Clean. Prod.* **2018**, *187*, 76–84, doi:10.1016/j.jclepro.2018.03.182.

152. Demir, F.; Derun, E.M. Modelling and optimization of gold mine tailings based geopolymer by using response surface method and its application in Pb2+ removal. *J. Clean. Prod.* **2019**, *237*, doi:10.1016/j.jclepro.2019.117766.

153. Ahmari, S.; Chen, R.; Zhang, L. Utilization of mine tailings as road base material. In Proceedings of the Geotechnical Special Publication; 2012; pp. 3654–3661.

154. Ahmari, S.; Zhang, L. Utilization of cement kiln dust (CKD) to enhance mine tailings-based geopolymer bricks. *Constr. Build. Mater.* **2013**, *40*, 1002–1011, doi:10.1016/j.conbuildmat.2012.11.069.

155. Ren, X.; Zhang, L.; Ramey, D.; Waterman, B.; Ormsby, S. Utilization of aluminum sludge (AS) to enhance mine tailings-based geopolymer. *J. Mater. Sci.* **2015**, *50*, 1370–1381, doi:10.1007/s10853-014-8697-y.

156. Perumal, P.; Piekkari, K.; Sreenivasan, H.; Kinnunen, P.; Illikainen, M. One-part geopolymers from mining residues – Effect of thermal treatment on three different tailings. *Miner. Eng.* **2019**, *144*, doi:10.1016/j.mineng.2019.106026.

157. Moukannaa, S.; Loutou, M.; Benzaazoua, M.; Vitola, L.; Alami, J.; Hakkou, R. Recycling of phosphate mine tailings for the production of geopolymers. *J. Clean. Prod.* **2018**, *185*, 891–903, doi:10.1016/j.jclepro.2018.03.094.

158. Jamshaid, H.; Mishra, R. A green material from rock: basalt fiber – a review. *J. Text. Inst.* **2016**, *107*, 923–937, doi:10.1080/00405000.2015.1071940.

159. Esaifan, M.; Hourani, M.; Khoury, H.; Rahier, H.; Wastiels, J. Synthesis of hydroxysodalite zeolite by alkali-activation of basalt powder rich in calc-plagioclase. *Adv. Powder Technol.* **2017**, *28*, 473–480, doi:10.1016/j.apt.2016.11.002.

160. Ye, J.; Zhang, W.; Shi, D. Properties of an aged geopolymer synthesized from

calcined ore-dressing tailing of bauxite and slag. *Cem. Concr. Res.* **2017**, *100*, 23–31, doi:10.1016/j.cemconres.2017.05.017.

161. Ye, J.; Zhang, W.; Shi, D. Performance evolutions of tailing-slag-based geopolymer under severe conditions. *J. Sustain. Cem. Mater.* **2015**, *4*, 101–115, doi:10.1080/21650373.2015.1030000.

162. Ferone, C.; Liguori, B.; Capasso, I.; Colangelo, F.; Cioffi, R.; Cappelletto, E.; Di Maggio, R. Thermally treated clay sediments as geopolymer source material. *Appl. Clay Sci.* **2015**, *107*, 195–204, doi:10.1016/j.clay.2015.01.027.

163. San Nicolas, R.; Cyr, M.; Escadeillas, G. Characteristics and applications of flash metakaolins. *Appl. Clay Sci.* **2013**, *83–84*, 253–262, doi:10.1016/j.clay.2013.08.036.

164. Ferone, C.; Colangelo, F.; Cioffi, R.; Montagnaro, F.; Santoro, L. Use of reservoir clay sediments as raw materials for geopolymer binders. *Adv. Appl. Ceram.* **2013**, *112*, 184–189, doi:10.1179/1743676112Y.0000000064.

165. Peirce, S.; Santoro, L.; Andini, S.; Montagnaro, F.; Ferone, C.; Cioffi, R. Clay sediment geopolymerization by means of alkali metal aluminate activation. *RSC Adv.* **2015**, *5*, 107662–107669, doi:10.1039/c5ra22140d.

166. Messina, F.; Ferone, C.; Molino, A.; Roviello, G.; Colangelo, F.; Molino, B.; Cioffi, R. Synergistic recycling of calcined clayey sediments and water potabilization sludge as geopolymer precursors: Upscaling from binders to precast paving cement-free bricks. *Constr. Build. Mater.* **2017**, *133*, 14–26, doi:10.1016/j.conbuildmat.2016.12.039.

167. Yu, L.; Zhang, Z.; Huang, X.; Jiao, B.; Li, D. Enhancement experiment on cementitious activity of copper-mine tailings in a geopolymer system. *Fibers* **2017**, *5*, doi:10.3390/fib5040047.

168. Chen, T.J.; Zhang, Y.M.; Jiao, X.K.; Liu, T. Research on preparation and performance of vandium tailings-based geopolymer. In Proceedings of the 26th International Mineral Processing Congress, IMPC 2012: Innovative Processing

for Sustainable Growth - Conference Proceedings; 2012; pp. 830–838.

169.   Silva, I.; Castro-Gomes, J.P.; Albuquerque, A. Effect of immersion in water partially alkali-activated materials obtained of tungsten mine waste mud. *Constr. Build. Mater.* **2012**, *35*, 117–124, doi:10.1016/j.conbuildmat.2012.02.069.

170.   Hardjito, D.; Rangan, B.V. Development and properties of low-calcium fly ash-based geopolymer concrete. *Res. Rep. GC* **2005**, 94.

171.   Falah, M.; Obenaus-Emler, R.; Kinnunen, P.; Illikainen, M. Effects of Activator Properties and Curing Conditions on Alkali-Activation of Low-Alumina Mine Tailings. *Waste and Biomass Valorization* **2019**, doi:10.1007/s12649-019-00781-z.

172.   Tekin, I. Properties of NaOH activated geopolymer with marble, travertine and volcanic tuff wastes. *Constr. Build. Mater.* **2016**, *127*, 607–617, doi:10.1016/j.conbuildmat.2016.10.038.

173.   Yaghoubi, M.; Arulrajah, A.; Disfani, M.M.; Horpibulsuk, S.; Bo, M.W.; Darmawan, S. Effects of industrial by-product based geopolymers on the strength development of a soft soil. *Soils Found.* **2018**, *58*, 716–728, doi:10.1016/j.sandf.2018.03.005.

174.   Sedira, N.; Castro-Gomes, J. Strength and microstructure of tungsten mining waste-based hybrid alkaline material: Effect of activators. In Proceedings of the Proceedings of the 12th fib International PhD Symposium in Civil Engineering; 2018; pp. 145–152.

175.   Falayi, T.; Mashifana, T.; Ntuli, F. Silicon and aluminium leaching kinetics from acidic gold mine tailings. In Proceedings of the IOP Conference Series: Materials Science and Engineering; 2019; Vol. 652.

176.   Wan, Q.; Rao, F.; Song, S.; García, R.E.; Estrella, R.M.; Patiño, C.L.; Zhang, Y. Geopolymerization reaction, microstructure and simulation of metakaolin-based geopolymers at extended Si/Al ratios. *Cem. Concr. Compos.* **2017**, *79*, 45–52, doi:10.1016/j.cemconcomp.2017.01.014.

177. Kalinkina, E. V; Gurevich, B.I.; Kalinkin, A.M. Alkali-activated binder based on milled antigorite. *Minerals* **2018**, *8*, doi:10.3390/min8110503.

178. Onyelowe, K.; Igboayaka, C.; Orji, F.; Ugwuanyi, H.; Van, D.B. Triaxial and density behaviour of quarry dust based geopolymer cement treated expansive soil with crushed waste glasses for pavement foundation purposes. *Int. J. Pavement Res. Technol.* **2019**, *12*, 78–87, doi:10.1007/s42947-019-0010-7.

179. Ahmari, S.; Zhang, L. Durability and leaching behavior of mine tailings-based geopolymer bricks. *Constr. Build. Mater.* **2013**, *44*, 743–750, doi:10.1016/j.conbuildmat.2013.03.075.

180. Ahmari, S.; Zhang, L. The properties and durability of mine tailings-based geopolymeric masonry blocks. In *Eco-Efficient Masonry Bricks and Blocks*; Elsevier: Amsterdam, The Netherlands, 2015; pp. 289–309 ISBN 9781782423188.

181. Aydln, S.; Klzlltepe, C.Ç. Valorization of Boron Mine Tailings in Alkali-Activated Mortars. *J. Mater. Civ. Eng.* **2019**, *31*, 1–12, doi:10.1061/(ASCE)MT.1943-5533.0002871.

182. Ahmari, S.; Parameswaran, K.; Zhang, L. Alkali activation of copper mine tailings and low-calcium flash-furnace copper smelter slag. *J. Mater. Civ. Eng.* **2015**, *27*, doi:10.1061/(ASCE)MT.1943-5533.0001159.

183. Ahmari, S.; Zhang, L. Production of eco-friendly bricks from copper mine tailings through geopolymerization. *Constr. Build. Mater.* **2012**, *29*, 323–331, doi:10.1016/j.conbuildmat.2011.10.048.

184. Falayi, T. Effect of potassium silicate and aluminate on the stabilisation of gold mine tailings. *Proc. Inst. Civ. Eng. Waste Resour. Manag.* **2019**, *172*, 56–63, doi:10.1680/jwarm.18.00015.

185. Cheng, T.-W.; Ding, Y.-C.; Lee, W.-H.; Lu, P. A Study on Marble-Based Geopolymer. *MATEC Web Conf.* **2017**, *97*, 01004, doi:10.1051/matecconf/20179701004.

186. Adesanya, E.; Ohenoja, K.; Yliniemi, J.; Illikainen, M. Mechanical transformation of phyllite mineralogy toward its use as alkali-activated binder precursor. *Miner. Eng.* **2020**, *145*, doi:10.1016/j.mineng.2019.106093.

187. Bonet-Martínez, E.; Pérez-Villarejo, L.; Eliche-Quesada, D.; Carrasco-Hurtado, B.; Bueno-Rodríguez, S.; Castro-Galiano, E. Inorganic polymers synthesized using biomass ashes-red mud as precursors based on clay-kaolinite system. *Mater. Lett.* **2018**, *225*, 161–166, doi:10.1016/j.matlet.2018.05.012.

188. Song, M.; Jiaping, L.; Qian, J.; Jianzhong, L.; Liang, S. Experimental Study on Utilization of Quartz Mill Tailings as a Filler to Prepare Geopolymer. *Miner. Process. Extr. Metall. Rev.* **2016**, *37*, 311–322, doi:10.1080/08827508.2016.1218867.

189. Muñoz, J.F.; Easton, T.; Dahmen, J. Using alkali-activated natural aluminosilicate minerals to produce compressed masonry construction materials. *Constr. Build. Mater.* **2015**, *95*, 86–95, doi:10.1016/j.conbuildmat.2015.07.144.

190. Chen, T.; Zhang, Y.; Jiao, X.; Zhao, J. Research on Preparation and Performance of Vandium Tailings-based Geopolymer. *MRS Proc.* **2012**, *1380*, imrc2011-1380-s21-full014, doi:10.1557/opl.2012.412.

191. Wan, Q.; Rao, F.; Song, S.; Zhang, Y. Immobilization forms of ZnO in thesolidification/stabilization (S/S) of a zinc minetailing through geopolymerization. *J. Mater. Res. Technol.* **2019**, 6–13, doi:10.1016/j.jmrt.2019.09.040.

192. Prokopski, G.; Marchuk, V.; Huts, A. The effect of using granite dust as a component of concrete mixture. *Case Stud. Constr. Mater.* **2020**, *13*, e00349, doi:10.1016/j.cscm.2020.e00349.

193. Singhal, A.; Goel, S.; Sengupta, D. Physicochemical and elemental analyses of sandstone quarrying wastes to assess their impact on soil properties. *J. Environ. Manage.* **2020**, *271*, 111011, doi:10.1016/j.jenvman.2020.111011.

194. Gautam, P.K.; Kalla, P.; Nagar, R.; Jethoo, A.S. Laboratory investigation on use of quarry waste in open graded friction course. *Resour. Policy* **2018**, *59*, 62–67, doi:10.1016/j.resourpol.2018.02.009.

195. De Rezende, L.R.; De Carvalho, J.C. The use of quarry waste in pavement construction. *Resour. Conserv. Recycl.* **2003**, *39*, 91–105, doi:10.1016/S0921-3449(02)00123-4.

196. Amran, Y.H.M.; Alyousef, R.; Alabduljabbar, H.; El-Zeadani, M. Clean production and properties of geopolymer concrete; A review. *J. Clean. Prod.* 2020, *251*, 119679.

197. Nawaz, M.; Heitor, A.; Sivakumar, M. Geopolymers in construction - recent developments. *Constr. Build. Mater.* 2020, *260*, 120472.

198. Mabroum, S.; Moukannaa, S.; El Machi, A.; Taha, Y.; Benzaazoua, M.; Hakkou, R. Mine wastes based geopolymers: A critical review. *Clean. Eng. Technol.* **2020**, *1*, 100014, doi:10.1016/j.clet.2020.100014.

199. Iftikhar, S.; Rashid, K.; Ul Haq, E.; Zafar, I.; Alqahtani, F.K.; Iqbal Khan, M. Synthesis and characterization of sustainable geopolymer green clay bricks: An alternative to burnt clay brick. *Constr. Build. Mater.* **2020**, *259*, 119659, doi:10.1016/j.conbuildmat.2020.119659.

200. Tammam, Y.; Uysal, M.; Canpolat, O. Effects of alternative ecological fillers on the mechanical, durability, and microstructure of fly ash-based geopolymer mortar. *Eur. J. Environ. Civ. Eng.* **2021**, 1–24, doi:10.1080/19648189.2021.1925157.

201. Buchwald, A.; Vicent, M.; Kriegel, R.; Kaps, C.; Monzó, M.; Barba, A. Geopolymeric binders with different fine fillers - Phase transformations at high temperatures. *Appl. Clay Sci.* **2009**, *46*, 190–195, doi:10.1016/j.clay.2009.08.002.

202. Kohout, J.; Koutník, P. Effect of Filler Type on the Thermo-Mechanical Properties of Metakaolinite-Based Geopolymer Composites. *Materials (Basel).*

2020, *13*, 2395, doi:10.3390/ma13102395.

203. Tahmasebi Yamchelou, M.; Law, D.; Brkljača, R.; Gunasekara, C.; Li, J.; Patnaikuni, I. Geopolymer synthesis using low-grade clays. *Constr. Build. Mater.* **2021**, *268*, 121066, doi:10.1016/j.conbuildmat.2020.121066.

204. Bandow, N.; Gartiser, S.; Ilvonen, O.; Schoknecht, U. Evaluation of the impact of construction products on the environment by leaching of possibly hazardous substances. *Environ. Sci. Eur.* 2018.

205. Müller, A.; Österlund, H.; Marsalek, J.; Viklander, M. The pollution conveyed by urban runoff: A review of sources. *Sci. Total Environ.* 2020.

206. Fathollahi, A.; Coupe, S.J.; El-Sheikh, A.H.; Nnadi, E.O. Cu(II) biosorption by living biofilms: Isothermal, chemical, physical and biological evaluation. *J. Environ. Manage.* **2021**, doi:10.1016/j.jenvman.2021.111950.

207. de Zwart, D.; Adams, W.; Galay Burgos, M.; Hollender, J.; Junghans, M.; Merrington, G.; Muir, D.; Parkerton, T.; De Schamphelaere, K.A.C.; Whale, G.; et al. Aquatic exposures of chemical mixtures in urban environments: Approaches to impact assessment. *Environ. Toxicol. Chem.* **2018**, doi:10.1002/etc.3975.

208. Földvari, M. *Handbook of thermogravimetric system of minerals and its use in geological practice*; Geological Institute of Hungary: Budapest, 2011; ISBN 9789636712884 9636712883.

209. Zhao, Y.; Qiu, J.; Xing, J.; Sun, X. Recycling of quarry dust for supplementary cementitious materials in low carbon cement. *Constr. Build. Mater.* **2020**, *237*, doi:10.1016/j.conbuildmat.2019.117608.

210. Ukrainczyk, N. Simple model for alkali leaching from geopolymers: Effects of raw materials and acetic acid concentration on apparent diffusion coefficient. *Materials (Basel).* **2021**, doi:10.3390/ma14061425.

211. Longhi, M.A.; Rodríguez, E.D.; Walkley, B.; Zhang, Z.; Kirchheim, A.P. Metakaolin-based geopolymers: Relation between formulation,

physicochemical properties and efflorescence formation. *Compos. Part B Eng.* **2020**, doi:10.1016/j.compositesb.2019.107671.

212. Mehta, A.; Siddique, R. Sulfuric acid resistance of fly ash based geopolymer concrete. *Constr. Build. Mater.* **2017**, doi:10.1016/j.conbuildmat.2017.04.077.

213. Wambugu, C.W.; Rene, E.R.; van de Vossenberg, J.; Dupont, C.; van Hullebusch, E.D. Role of biochar in anaerobic digestion based biorefinery for food waste. *Front. Energy Res.* **2019**, doi:10.3389/fenrg.2019.00014.

214. Longhi, M.A.; Zhang, Z.; Rodríguez, E.D.; Kirchheim, A.P.; Wang, H. Efflorescence of alkali-activated cements (geopolymers) and the impacts on material structures: A critical analysis. *Front. Mater.* **2019**, doi:10.3389/fmats.2019.00089.

215. Fathollahi, A.; Coupe, S.J.; El-Sheikh, A.H.; Sañudo-Fontaneda, L.A. The biosorption of mercury by permeable pavement biofilms in stormwater attenuation. *Sci. Total Environ.* **2020**, doi:10.1016/j.scitotenv.2020.140411.

216. Fathollahi, A.; Coupe, S.J. Effect of environmental and nutritional conditions on the formation of single and mixed-species biofilms and their efficiency in cadmium removal. *Chemosphere* **2021**, doi:10.1016/j.chemosphere.2021.131152.

217. Sun, Z.; Vollpracht, A. Leaching of monolithic geopolymer mortars. *Cem. Concr. Res.* **2020**, doi:10.1016/j.cemconres.2020.106161.

218. Missaoui, A.; Said, I.; Lafhaj, Z.; Daoued, S.; Ali, I.B.H. Laboratory study on recycling of sediments in paving blocks. *Environ. Geotech.* **2016**, *3*, 397–407, doi:10.1680/envgeo.15.00006.

219. Wang, L.; Yeung, T.L.K.; Lau, A.Y.T.; Tsang, D.C.W.; Poon, C.S. Recycling contaminated sediment into eco-friendly paving blocks by a combination of binary cement and carbon dioxide curing. *J. Clean. Prod.* **2017**, *164*, 1279–1288, doi:10.1016/j.jclepro.2017.07.070.

220. K., M.A.; Singaravelu, V.; Jean-Mathieu, P.; Manjusri, M. Composites from

renewable and sustainable resources: Challenges and innovations. *Science (80-.).* **2018**, *362*, 536–542, doi:10.1126/science.aat9072.

221. Kaliyavaradhan, S.K.; Ling, T.-C.; Mo, K.H. Valorization of waste powders from cement-concrete life cycle: A pathway to circular future. *J. Clean. Prod.* **2020**, *268*, 122358, doi:https://doi.org/10.1016/j.jclepro.2020.122358.

222. Coppola, B.; Tulliani, J.-M.; Antonaci, P.; Palmero, P. Role of Natural Stone Wastes and Minerals in the Alkali Activation Process: A Review. *Mater.* 2020, *13*.

223. Agrawal, Y.; Gupta, T.; Siddique, S.; Sharma, R.K. Potential of dolomite industrial waste as construction material: a review. *Innov. Infrastruct. Solut.* **2021**, *6*, 205, doi:10.1007/s41062-021-00570-5.

224. Sharma, A.; Singh, P.; Kapoor, K. Utilization of recycled fine powder as an activator in fly ash based geopolymer mortar. *Constr. Build. Mater.* **2022**, *323*, 126581, doi:https://doi.org/10.1016/j.conbuildmat.2022.126581.

225. Hu, Y.; Tang, Z.; Li, W.; Li, Y.; Tam, V.W.Y. Physical-mechanical properties of fly ash/GGBFS geopolymer composites with recycled aggregates. *Constr. Build. Mater.* **2019**, *226*, 139–151, doi:https://doi.org/10.1016/j.conbuildmat.2019.07.211.

226. Ye, T.; Xiao, J.; Duan, Z.; Li, S. Geopolymers made of recycled brick and concrete powder – A critical review. *Constr. Build. Mater.* **2022**, *330*, 127232, doi:https://doi.org/10.1016/j.conbuildmat.2022.127232.

227. Tan, J.; Cai, J.; Li, J. Recycling of unseparated construction and demolition waste (UCDW) through geopolymer technology. *Constr. Build. Mater.* **2022**, *341*, 127771, doi:https://doi.org/10.1016/j.conbuildmat.2022.127771.

228. Albidah, A.; Alsaif, A.; Abadel, A.; Abbas, H.; Al-Salloum, Y. Role of recycled vehicle tires quantity and size on the properties of metakaolin-based geopolymer rubberized concrete. *J. Mater. Res. Technol.* **2022**, *18*, 2593–2607, doi:https://doi.org/10.1016/j.jmrt.2022.03.103.

229. Long, W.-J.; Zhang, X.; Xie, J.; Kou, S.; Luo, Q.; Wei, J.; Lin, C.; Feng, G.-L. Recycling of waste cathode ray tube glass through fly ash-slag geopolymer mortar. *Constr. Build. Mater.* **2022**, *322*, 126454, doi:https://doi.org/10.1016/j.conbuildmat.2022.126454.

230. Şahin, F.; Uysal, M.; Canpolat, O.; Aygörmez, Y.; Cosgun, T.; Dehghanpour, H. Effect of basalt fiber on metakaolin-based geopolymer mortars containing rilem, basalt and recycled waste concrete aggregates. *Constr. Build. Mater.* **2021**, *301*, 124113, doi:https://doi.org/10.1016/j.conbuildmat.2021.124113.

231. Singh, S.; Aswath, M.U.; Ranganath, R. V. Performance assessment of bricks and prisms: Red mud based geopolymer composite. *J. Build. Eng.* **2020**, *32*, 101462, doi:10.1016/j.jobe.2020.101462.

232. Pan, Z.; Sanjayan, J.G.; Rangan, B. V. An investigation of the mechanisms for strength gain or loss of geopolymer mortar after exposure to elevated temperature. *J. Mater. Sci.* **2009**, *44*, 1873–1880, doi:10.1007/s10853-009-3243-z.

233. Kong, D.L.Y.; Sanjayan, J.G.; Sagoe-Crentsil, K. Factors affecting the performance of metakaolin geopolymers exposed to elevated temperatures. *J. Mater. Sci.* **2008**, *43*, 824–831, doi:10.1007/s10853-007-2205-6.

234. Zhang, L. Production of bricks from waste materials – A review. *Constr. Build. Mater.* **2013**, *47*, 643–655, doi:https://doi.org/10.1016/j.conbuildmat.2013.05.043.

235. Khalil, W.; Frayyeh, Q.; Ahmed, M. Characteristics of Eco-Friendly Metakaolin Based Geopolymer Concrete Pavement Bricks. *Eng. Technol. J.* **2020**, *38*, 1706–1716, doi:10.30684/etj.v38i11a.1699.

236. Sukmak, P.; Horpibulsuk, S.; Shen, S.-L. Strength development in clay–fly ash geopolymer. *Constr. Build. Mater.* **2013**, *40*, 566–574, doi:https://doi.org/10.1016/j.conbuildmat.2012.11.015.

237. Perera, D.S.; Uchida, O.; Vance, E.R.; Finnie, K.S. Influence of curing schedule

on the integrity of geopolymers. *J. Mater. Sci.* **2007**, *42*, 3099–3106.

238. Liew, Y.M.; Heah, C.Y.; Mohd Mustafa, A.B.; Kamarudin, H. Structure and properties of clay-based geopolymer cements: A review. *Prog. Mater. Sci.* **2016**, *83*, 595–629, doi:10.1016/j.pmatsci.2016.08.002.

239. Wang, H.; Li, H.; Yan, F. Synthesis and mechanical properties of metakaolinite-based geopolymer. *Colloids Surfaces A Physicochem. Eng. Asp.* **2005**, *268*, 1–6, doi:10.1016/j.colsurfa.2005.01.016.

240. Ghani, U.; Hussain, S.; Noor-ul-Amin; Imtiaz, M.; Khan, S.A. Role of calcination on geopolymerization of lateritic clay by alkali treatment. *J. Saudi Chem. Soc.* **2021**, *25*, 101198, doi:10.1016/j.jscs.2021.101198.

241. Solouki, A.; Tataranni, P. Mixture Optimization of Concrete Paving Blocks Containing Waste Silt. **2022**, 1–15.

242. Choudhary, J.; Kumar, B.; Gupta, A. Potential utilization of construction wastes in asphalt pavements as fillers using ranking framework. *Constr. Build. Mater.* **2021**, *277*, 122262, doi:https://doi.org/10.1016/j.conbuildmat.2021.122262.

243. Tian, Y.; Sun, L.; Li, H.; Zhang, H.; Harvey, J.; Yang, B.; Zhu, Y.; Yu, B.; Fu, K. Laboratory investigation on effects of solid waste filler on mechanical properties of porous asphalt mixture. *Constr. Build. Mater.* **2021**, *279*, 122436, doi:https://doi.org/10.1016/j.conbuildmat.2021.122436.

244. Ma, Y.; Zhou, H.; Jiang, X.; Polaczyk, P.; Xiao, R.; Zhang, M.; Huang, B. The utilization of waste plastics in asphalt pavements: A review. *Clean. Mater.* **2021**, *2*, 100031, doi:https://doi.org/10.1016/j.clema.2021.100031.

245. Li, H.; Feng, Z.; Ahmed, A.T.; Yombah, M.; Cui, C.; Zhao, G.; Guo, P.; Sheng, Y. Repurposing waste oils into cleaner aged asphalt pavement materials: A critical review. *J. Clean. Prod.* **2022**, *334*, 130230, doi:https://doi.org/10.1016/j.jclepro.2021.130230.

246. Jamshidi, A.; White, G. Evaluation of performance and challenges of use of waste materials in pavement construction: A critical review. *Appl. Sci.* **2020**, *10*,

doi:10.3390/app10010226.

247. Antunes, V.; Freire, A.C.; Quaresma, L.; Micaelo, R. Evaluation of waste materials as alternative sources of filler in asphalt mixtures. *Mater. Struct.* **2017**, *50*, 254, doi:10.1617/s11527-017-1126-3.

248. Eisa, M.S.; Basiouny, M.E.; Youssef, A.M. Effect of using various waste materials as mineral filler on the properties of asphalt mix. *Innov. Infrastruct. Solut.* **2018**, *3*, 27, doi:10.1007/s41062-018-0129-4.

249. Tarbay, E.W.; Azam, A.M.; El-Badawy, S.M. Waste materials and by-products as mineral fillers in asphalt mixtures. *Innov. Infrastruct. Solut.* **2018**, *4*, 5, doi:10.1007/s41062-018-0190-z.

250. Shamsaei, M.; Khafajeh, R.; Ghasemzadeh Tehrani, H.; Aghayan, I. Experimental evaluation of ceramic waste as filler in hot mix asphalt. *Clean Technol. Environ. Policy* **2020**, *22*, 535–543, doi:10.1007/s10098-019-01788-9.

251. Choudhary, J.; Kumar, B.; Gupta, A. Utilization of solid waste materials as alternative fillers in asphalt mixes: A review. *Constr. Build. Mater.* **2020**, *234*, 117271, doi:10.1016/j.conbuildmat.2019.117271.

252. Aljassar, A.H.; Metwali, S.; Ali, M.A. Effect of filler types on Marshall stability and retained strength of asphalt concrete. *Int. J. Pavement Eng.* **2004**, *5*, 47–51.

253. Huang, B.; Shu, X.; Chen, X. Effects of mineral fillers on hot-mix asphalt laboratory-measured properties. *Int. J. Pavement Eng.* **2007**, *8*, 1–9, doi:10.1080/10298430600819170.

254. Diab, A.; Enieb, M. Investigating influence of mineral filler at asphalt mixture and mastic scales. *Int. J. Pavement Res. Technol.* **2018**, *11*, 213–224, doi:10.1016/j.ijprt.2017.10.008.

255. Sakanlou, F.; Shirmohammadi, H.; Hamedi, G.H. Investigating the effect of filler types on thermodynamic parameters and their relationship with moisture sensitivity of asphalt mixes. *Mater. Struct. Constr.* **2018**, *51*, 1–16, doi:10.1617/s11527-018-1166-3.

256. European Commission Final Implementation Report for Directive 86/278/EEC on Sewage Sludge : 2013 – 2015. *Eur. Comm.* 2018, 2013–2015.

257. Wu, W.; Jiang, W.; Yuan, D.; Lu, R.; Shan, J.; Xiao, J.; Ogbon, A.W. A review of asphalt-filler interaction: Mechanisms, evaluation methods, and influencing factors. *Constr. Build. Mater.* **2021**, *299*, 124279, doi:10.1016/j.conbuildmat.2021.124279.

258. Lesueur, D.; Petit, J.; Ritter, H.J. The mechanisms of hydrated lime modification of asphalt mixtures: A state-of-the-art review. *Road Mater. Pavement Des.* **2013**, *14*, 1–16, doi:10.1080/14680629.2012.743669.

259. Bani Baker, M.I.; Abendeh, R.M.; Obaidat, T.A.S. Employing Natural Bentonite Clay as Partial Replacement of Mineral Filler in Asphalt Mixtures. *J. Mater. Civ. Eng.* **2018**, *30*, 04018167, doi:10.1061/(asce)mt.1943-5533.0002375.

260. Rondón-Quintana, H.A.; Ruge-Cárdenas, J.C.; Bastidas-Martínez, J.G.; Velandia-Castelblanco, M.Y.; Muniz de Farias, M. Use of Thermally Treated Bentonite as Filler in Hot Mix Asphalt. *J. Mater. Civ. Eng.* **2020**, *32*, 04020070, doi:10.1061/(asce)mt.1943-5533.0003127.

261. Marín-García, B.F.; Jiménez-Jiménez, O.J.; Rondón-Quintana, H.A. Behavior of thermally treated kaolin filler in an asphalt concrete mixture. *Rev. Logos, Cienc. Tecnol.* **2019**, *11*, 10–17, doi:10.22335/rlct.v11i3.861.

262. Acharya, B.; Dutta, A.; Basu, P. Study of calcination-carbonation of calcium carbonate in different fluidizing mediums for chemical looping gasification is circulating fluidized beds. In Proceedings of the "10th International Conference on Circulating Fluidized Beds and Fluidization Technology - CFB-10; 2013.

263. Hassani, A.; Taghipoor, M.; Karimi, M.M. A state of the art of semi-flexible pavements: Introduction, design, and performance. *Constr. Build. Mater.* **2020**, *253*, 119196, doi:10.1016/j.conbuildmat.2020.119196.

264. Thao, A.; Magee, B.; Woodward, D. A preliminary characterisation of innovative semi-flexible composite pavement comprising geopolymer grout and

reclaimed   asphalt   planings.   *Materials   (Basel).*   **2020**,   *13*, doi:10.3390/MA13163644.

265.   Hamid Abed, M.; Sabbar Abbas, I.; Hamed, M.; Canakci, H. Rheological, fresh, and mechanical properties of mechanochemically activated geopolymer grout: A comparative study with conventionally activated geopolymer grout. *Constr. Build. Mater.* **2022**, *322*, 126338, doi:10.1016/j.conbuildmat.2022.126338.

266.   Afonso, M.L.; Dinis-Almeida, M.; Pereira-De-Oliveira, L.A.; Castro-Gomes, J.; Zoorob, S.E. Development of a semi-flexible heavy duty pavement surfacing incorporating recycled and waste aggregates - Preliminary study. *Constr. Build. Mater.* **2016**, *102*, 155–161, doi:10.1016/j.conbuildmat.2015.10.165.

267.   Zhang, Y.; Wang, Y.; Wu, Z.G.; Lu, Y.M.; Kang, A.H.; Xiao, P. Optimal design of geopolymer grouting material for semi-flexible pavement based on response surface   methodology.   *Constr.   Build.   Mater.*   **2021**,   *306*,   124779, doi:10.1016/j.conbuildmat.2021.124779.

268.   Tian, Y.; Sun, L.; Li, H.; Zhang, H.; Harvey, J.; Yang, B.; Zhu, Y.; Yu, B.; Fu, K. Laboratory investigation on effects of solid waste filler on mechanical properties of porous asphalt mixture. *Constr. Build. Mater.* **2021**, *279*, doi:10.1016/j.conbuildmat.2021.122436.

269.   Zhang, H.; Li, H.; Zhang, Y.; Wang, D.; Harvey, J.; Wang, H. Performance enhancement of porous asphalt pavement using red mud as alternative filler. *Constr.   Build.   Mater.*   **2018**,   *160*,   707–713, doi:10.1016/j.conbuildmat.2017.11.105.

270.   Yang, B.; Li, H.; Zhang, H.; Sun, L.; Harvey, J.; Tian, Y.; Zhu, Y.; Zhang, X.; Han, D.; Liu, L. Environmental impact of solid waste filler in porous asphalt mixture.   *Constr.   Build.   Mater.*   **2021**,   *303*,   124447, doi:10.1016/j.conbuildmat.2021.124447.

271.   Chen, M.; Lin, J.; Wu, S. Potential of recycled fine aggregates powder as filler in   asphalt   mixture.   *Constr.   Build.   Mater.*   **2011**,   *25*,   3909–3914,

doi:https://doi.org/10.1016/j.conbuildmat.2011.04.022.

272. Wang, H.; Al-Qadi, I.L.; Faheem, A.F.; Bahia, H.U.; Yang, S.-H.; Reinke, G.H. Effect of Mineral Filler Characteristics on Asphalt Mastic and Mixture Rutting Potential. *Transp. Res. Rec.* **2011**, *2208*, 33–39, doi:10.3141/2208-05.